Title
Redefining Druggability Using Chemoproteomic Platforms

Author
Ward, Carl Cori

Publication Date
2020

Redefining Druggability Using Chemoproteomic Platforms

By

Carl C Ward

A dissertation submitted in partial satisfaction of the
requirements for the degree of
Doctor of Philosophy
in
Molecular and Cell Biology
in the
Graduate Division
of the
University of California, Berkeley

Committee in charge:

Professor Daniel Nomura, Chair
Professor Christopher Chang
Professor Roberto Zoncu
Professor Matthew Francis

Summer 2020

Abstract

Redefining Druggability Using Chemoproteomic Platforms

by

Carl Cori Ward

Doctor of Philosophy in Molecular and Cell Biology

University of California, Berkeley

Professor Daniel Nomura, Chair

The Undruggable Proteome – those proteins which do not have a canonical small molecule binding pocket – poses one of the largest problems in modern drug discovery. The genomics revolution linked the function of thousands of proteins to corresponding diseases, but many of these disease-causing proteins are difficult or seemingly impossible to target or study with traditional small-molecule based approaches. Recently, chemoproteomics – the combination of chemical-biology methods with proteomics – has given us new tools to approach this undruggable proteome, especially in combination with covalently-acting probes or ligands. Using these emerging technologies this work shows three examples of how chemoproteomics can enable both tool development for better understanding of undruggable proteins and also allow direct engagement with such proteins for drug development.

Firstly, we show that NHS-esters are viable chemoproteomic probes, allowing the profiling of the reactivity of thousands of lysines in complex proteomes. Furthermore, scaffolds bearing an NHS-ester have surprising specificity, opening the door for covalent ligand discovery around the NHS-ester warhead. Secondly, we further highlight the efficacy of covalent molecules in targeting undruggable proteins by mapping the anti-cancer targets of Withaferin A, a natural product, with chemoproteomic methods. We show the primary target is a traditionally undruggable site on a traditionally undruggable protein, cysteine 377 on the scaffolding subunit of the phosphatase PP2A (PPP2R1A). We are then able to screen simple covalent fragments against this target, to find a small, synthetically-accessible fragment which binds same site and recapitulates the biochemical activity of Withaferin A. Lastly, we leverage similar covalent fragment screening approaches to discover a non-functional ligand against the E3 ligase RNF4. We use this ligand with success in targeted protein degradation applications, demonstrating the synergy between chemoproteomics and other emerging approaches to tackle to undruggable proteome.

Acknowledgements

Thank you to my family - mom, dad, Fred, and Alice – my friends, my labmates and colleagues in the Nomura Lab and throughout Berkeley, and Dan Nomura for all the support the past five years. It's been a lot of fun.

Table of Contents

Chapter 1: Introduction to Activity-Based Protein Profiling for Mapping and Pharmacologically Interrogating Proteome-Wide Ligandable Hotspots*

1.1 Abstract

Despite the completion of human genome sequencing efforts nearly 15 years ago and the promise of genome-based discoveries that would cure human diseases, most protein targets that control human diseases have remained largely untranslated in-part because the majority of these protein targets are considered "undruggable." Developing small-molecule modulators of many of these protein targets that lack screening assays or accessible binding pockets has remained challenging. Here, we discuss modern methods for activity-based protein profiling-based chemoproteomic strategies to map "ligandable" hotspots in proteomes using activity-based and reactivity-based chemical probes to enable the pharmacological interrogation of these hotspots. We will showcase several recent examples of how these technologies have been used to develop highly selective small-molecule inhibitors against disease-related protein targets.

1.2 Introduction

While many disease-modifying protein targets have been discovered, most of these targets have remained untranslated as many of these proteins are considered to be "undruggable" or difficult to target with small-molecule drugs. Indeed, most of the proteome is devoid of pharmacological tools, hindering and oftentimes paralyzing both basic and translational research efforts. Studies have convincingly demonstrated that the development of high-quality chemical tools for proteins catalyzes research into the function and therapeutic exploitation of those proteins, thus correlating the development of chemical tools for specific proteins with their associated research activity [1]. As Scott Dixon and Brent Stockwell pointed out in their review, only ~2 % of all predicted human gene products are currently targeted with small-molecule drugs and only 10-15 % of all human genes are thought to be "druggable," with only a 25 % overlap between druggable protein targets and known disease-modifying targets [2]. Thus, developing approaches that enable the discovery of pharmacological tools for every protein in the proteome would radically expand our ability to understand protein function and accelerate the drug discovery process to cure complex diseases. Here, we will discuss established, emerging, and potential applications of activity-based protein profiling (ABPP) as a powerful chemoproteomic strategy to map "ligandable" hotspots or sites within proteins that can be pharmacologically interrogated for drug discovery. We will also discuss the advantages of coupling ABPP platforms with the development of irreversible small-molecule modulators of protein targets to facilitate drug discovery efforts.

1.3 ABPP with active-site directed probes to develop active-site directed inhibitors

With the completion of human genome sequencing efforts over a decade ago, there has been a widening gap between the number of promising genes and their encoded proteins that

*Part of the work presented in this chapter has been previously published in the following manuscript: Roberts, A. M., Ward, C. C. & Nomura, D. K. Activity-based protein profiling for mapping and pharmacologically interrogating proteome-wide ligandable hotspots. *Current Opinion in Biotechnology* **43**, 25–33 (2017).

have been linked to health and disease and pharmacological tools and drugs to interrogate these targets for biological characterization and disease therapy [2,3]. This widening gap has formed in-part because many of these disease-relevant protein targets are considered "undruggable," in which these proteins may not have obvious binding pockets that can be pharmacologically interrogated or do not possess high-throughput screening amenable functional assays for identifying small-molecule modulators against these targets. Compounding upon these challenges, many targets that may be linked to disease may also be uncharacterized in their biochemical roles, thus hindering both their mechanistic characterization as well as the ability to assay for inhibitors against these targets.

Chemical proteomics or chemoproteomics has arisen as a powerful technology to broadly assess protein functionality, and through doing so, has enabled strategies to not only assay protein function for even uncharacterized protein targets, but also to develop inhibitors against these targets [4–6]. Among these chemoproteomic strategies, activity-based protein profiling (ABPP) has been particularly useful for coupling the assessment of protein activities with inhibitor development. ABPP uses active site-directed or reactivity-based chemical probes to map protein functionality directly in complex proteomes. In addition to their chemical warhead that binds to functional sites within proteins, these probes also bear chemical handles, such as fluorophores, biotin, or alkynes for subsequent fluorescent visualization, avidin-enrichment and mass-spectrometry (MS)-based quantification, or biorthogonal conjugation of handles for subsequent analysis of protein activities, respectively [7]. Because these probes bind to functional sites within protein targets, small-molecule inhibitors can be competed against probe binding, enabling a universal assay strategy for identifying inhibitors against any protein that can be assayed with ABPP methods [3]. ABPP is amenable to many assay formats including gel-based formats measuring in-gel fluorescence, quantitative proteomic methods, high-throughput fluorescence polarization-based technologies, or imaging probes in living systems [8–12]. Additionally, because activity-based probes not only assess the activity of the protein target of interest, but also activities across an entire enzyme class when performed in complex biological samples, selectivity of inhibitors can be assessed on a proteome-wide scale. Subsequently, lead selective inhibitors can also be turned into probes through the development of a biorthogonal analogs to further assess inhibitor selectivity [6]. From bench science to pre-clinical and clinical perspectives, developing covalent inhibitors of targets using ABPP has also been particularly advantageous. Target engagement and selectivity of covalent inhibitors can be assessed *ex vivo* using ABPP methods, which is not only valuable for biological characterization, but also for confirmation of target engagement in pre-clinical and clinical testing paradigms in animal models and humans [3]. In this section, we will initially focus on the original application of ABPP using activity-based probes to map protein activity and develop active-site directed inhibitors. There have been many activity-based probes developed over the past two decades including fluorophosphonate (FP)-based probes, vinyl sulfone or epoxide-based probes, diphenyl phosphonates, β-lactams and β-lactones, 4-(2-aminoethyl) benzenesulfonyl fluoride (AEBSF), carbamates and heterocyclic ureas for serine hydrolases and proteases [13,14]. Additional probes have been developed for cysteine proteases, glycosidases, serine, threonine, and tyrosine phosphatases, glycosidases, cytochrome P450s, ubiquitin-modifying enzymes, proteasomes, oxidoreductases, lysine acetyltransferases, and ATP-binding enzymes [14–16]. There have been many previous reviews on ABPP which have described activity-based probes and their utility so we will focus here on recent examples using this technology for inhibitor development.

Among the most successful application of ABPP has been in pharmacologically interrogating the serine hydrolase superfamily of enzymes that constitutes activities such as esterases, lipases, thioesterases, proteases, and peptidases, many of which have been linked to important (patho)physiological roles [17]. There have been many prior successes with ABPP in developing small-molecule inhibitors include the development of highly selective inhibitors against serine hydrolases such as fatty acid amide hydrolase (FAAH), monoacylglycerol lipase (MAGL), and diacylglycerol lipase (DAGL) involved in endocannabinoid and eicosanoid biology, KIAA1363 involved in ether lipid metabolism and cancer pathogenicity, and many others [17–21].

There have been many more recent examples in the past few years of using ABPP to develop inhibitors against both characterized and uncharacterized serine hydrolases. A selective and reversible platelet activating factor acetyl hydrolase 1B2 and 1B3 (PAFAH1B2 and PAFAH1B3) inhibitor P11 was identified through fluorescence-polarization based ABPP methods and was used to show that PAFAH1B2 and 1B3 were important metabolic drivers of cancer pathogenicity in multiple types of aggressive human cancer cells [22,23]. A highly selective inhibitor against the uncharacterized serine hydrolase DDHD2, KLH45, was developed using ABPP methods and was used in mouse models to aid in characterizing DDHD2 as an enzyme that hydrolyzes triacylglycerols in the brain. Inloes et al showed that inactivation of DDHD2 led to a debilitating neurodegenerative disease known as hereditary spastic paraplegia which results in lower limb spasticity and weakness and intellectual disability, due to the accumulation of triacylglycerols and lipid droplets in the brain [24]. Carboxylesterase 3 (Ces3) inhibitors were also discovered through chemical genetic screening coupled with ABPP as agents that ameliorate multiple features of the metabolic syndrome [25]. Inhibitors were also developed against previously uncharacterized hydrolase ABHD16A, KC01, using ABPP methods. Using subsequent metabolomic approaches, Kamat et al discovered that ABHD16A is a phosphatidylserine hydrolase that releases lysophosphatidylserine which in-turn is further hydrolyzed by ABHD12. Previous studies had shown that ABHD12 loss of function led to a neurodegenerative disease known as polyneuropathy, hearing loss, ataxia, retinitis pigmentosa and cataract (PHARC) due to an accumulation of pro-inflammatory lysophosphatidylserine levels. The authors showed that inhibition of ABHD16A could reduce lysophosphatidylserine levels and subsequently attenuate neuroinflammatory responses [26]. In another study, Xu et al used a substrate-competitive ABPP approach to identify carboxylesterase 1 as an oseltamivir-activating enzyme in intestinal cell homogenates [27]. In a study by Wolf et al., the authors used competitive ABPP methods to screen a library of 50 small-molecule inhibitors consisting of known serine hydrolase-inhibiting scaffolds such as isocoumarins, phosphonates, and □-lactones against 13 different rhomboid serine proteases and identified both pan rhomboid inhibitors as well as several that displayed selectivity for certain rhomboids over others [28].

Examples of using competitive ABPP platforms for inhibitor discovery outside of the serine hydrolase family include a recent report of inhibitors against two atypical integral membrane hydrolases AIG1 and ADTRP that degrade bioactive fatty acid esters of hydroxyl fatty acids (FAHFAs). Interestingly, AIG1 was identified through ABPP profiling using a serine hydrolase probe, but the probe reacted instead with a conserved threonine, and ADTRP was identified due to its homology to AIG1. Nonetheless, the authors were able to develop inhibitors KC01 and JJH260 for AIG1 using competitive ABPP [29].

Competitive ABPP methods using activity-based probes have also been used to identify off-target effects of environmental chemicals. Medina-Cleghorn et al used ABPP platforms to

map off-target profiles of multiple widely used organophosphorus pesticides and showed that MAGL and FAAH as well as many other serine hydrolases were inhibited by these agents *in vivo* in mice [30]. The authors further showed that inhibition of these targets led to downstream biochemical changes in substrate and product levels of the inhibited enzymes.

1.4 ABPP with reactivity-based probes to map new proteome-wide druggable hotspots

ABPP approaches using active-site directed activity-based probes have led to the development of many inhibitors for both characterized and uncharacterized enzymes and have led to their biological characterization and translation of these inhibitors into clinical development. While many activity-based probes have been developed by the chemical biology field over the last decade, there are still many different enzyme classes and more important much more types of protein functionalities that are not detectable with the current arsenal of active-site directed probes. More recent efforts in using ABPP have employed generally reactive electrophilic probes to more globally map protein functionality through the quantitative peptide-level mapping of hyper-reactive hotspots in complex proteomes using isotopic tandem orthogonal proteolysis–activity-based protein profiling (isoTOP-ABPP) [31]. These reactivity-based probes that more generally react with nucleophilic hotspots within proteomes, such as cysteines and lysines, are not only restricted to catalytic sites within enzymes, but also solvent-accessible binding pockets, post-translational modification sites, cysteine oxidation sites, protein-protein interaction sites, and other types of regulatory or functional domains across the entirety of the proteome [15,16,32,33]. When coupled with isoTOP-ABPP platforms to quantitatively map reactivities of specific sites of probe-modification, this overall approach enables a much broader and global mapping of protein functionality and more importantly, facilitates the identification of ligandable and eventually druggable hotspots within protein targets that may have previously been considered to be undruggable.

Among these reactivity-based probes, the cysteine-reactive iodoacetamide (IA)-alkyne probe, has been particularly versatile in mapping hyper-reactive and functional cysteines in proteomes [31]. Additional cysteine reactive probes have also been developed for chemoproteomic profiling. IA-alkyne is a versatile cysteine-reactive probe, but cannot be used on living cells due to its high level of reactivity. To be able to profile cysteine reactivity in living cells, Abo and Weerapana developed a caged bromomethylketone electrophilic probe that can be spatially and temporally activated within living cells through irradiation to map cysteine reactivity in live cells [34]. Abegg et al developed an ethynyl benziodoxolone reagent to further expand the accessible cysteine landscape [35]. Different states of cysteine oxidation have also been targeted for isoTOP-ABPP profiling. Yang et al. used the dimedone-based probe for selective labeling of S-sulfenic acids in intact cells and isoTOP-ABPP to map proteome-wide specific sites of S-sulfenylation [36]. In another study, Majmudar et al. showed that sulfinate-linked probes could be used to enrich and annotate hundreds of endogenous S-nitrosated proteins [37]. Conversely, these authors also showed that *S*-nitrosothiol-linked probes could be used to enable enrichment and detection of endogenous *S*-sulfinated proteins. Using these probes, the authors demonstrated that hydrogen peroxide increased *S*-sulfination of human DJ-1 at Cys106, but that Cys46 and Cys53 underwent full oxidation to sulfonic acids [37].

There have also been considerable efforts in developing reactivity-based probes that target other important nucleophilic amino acid residues in biology. Irreversible acetylation of serines on cyclooxygenase enzymes has long been understood as the mechanism for acetylsalicylic acid's (aspirin) anti-inflammatory and antipyretic effects. Both Bateman *et al.* and

Wang *et al.* developed an aspirin-alkyne probe to map the targets of aspirin acylation and surprisingly revealed that this probe could be used to broadly label lysine, serine, arginine, histidine, threonine, tyrosine, tryptophan and cysteine, thus revealing the potential diverse mechanisms underlying the anti-inflammatory actions of aspirin, but also showing the potentially versatility of this scaffold in expanding our future mapping of hyper-reactive and functional hotspots using isoTOP-ABPP platforms [38,39]. In another study, Lewallen et al. developed a biotin-conjugated phenylglyoxal probe to map global protein citrullination, a post-translational modification that is particularly heightened in rheumatoid arthritis, and identified >50 intracellular citrullinated proteins, of which more than 20 of these were involved in RNA spicing, suggesting a role for citrullination in linking RNA biology to inflammatory disorders [40]. Shannon et al. investigated the differences in reactivity of aryl halides by developing alkyne-tagged probes and using isoTOP-ABPP and showed that *p*-chloronitrobenzene was highly cysteine reactive, whereas the dichlorotriazine scaffold favored reactivity with lysines [13].

1.5 ABPP with reactivity-based probes to map the proteome-wide targets of endogenous and exogenous electrophiles

Beyond global mapping of hyper-reactive and functional sites, reactivity-based probes have also been used in a competitive manner to map specific cysteines on particular protein targets or off-targets that are susceptible to modification by endogenously-derived electrophiles as well as pesticides and pharmaceutical agents. The IA-alkyne probe has been used to map cysteine-reactivity of endogenously-derived lipid aldehydes such as hydroxynonenal and S-nitrosoglutathione [41,42]. Wang et al. showed that 4-hydroxy-2-nonenal shows selective labeling of certain cysteines on specific protein targets, such as an active-site proximal cysteine on ZAK kinase which results in enzyme inhibition and creates a negative feedback mechanisms that suppresses the activation of JNK pathways normally induced by oxidation stress [42]. Zhou et al. recently performed competitive isoTOP-ABPP profiling of S-nitrosoglutathione against IA-alkyne labeling to quantitatively map particularly sensitive transnitrosation sites, and discovered that S-nitrosation of a cysteine residue distal to the HADH2 active site and a catalytic cysteine in the lysosomal aspartyl protease cathepsin D (CTSD) impaired catalytic activity or proteolytic activation of these proteins, respectively [41].

Reactivity-based probes have also been used to map the cysteine reactivity of both agrochemical and pharmaceutical agents as well. Medina-Cleghorn et al. used the IA-alkyne probe to competitively profile the *in vitro* and *in vivo* reactivity of various cysteine-reactive pesticides and showed in-particular that the widely used fungicide chlorothalonil targets the catalytic cysteines of several enzymes involved in fatty acid oxidation and metabolism, thus identifying a novel mechanisms of toxicity for these pesticides [43]. Abegg et al. used their ethynyl benziodoxolone cysteine-reactive probe to reveal that the anti-cancer agent curcumin covalently modified cysteines on several key players of cellular signaling and metabolism, including casein kinase I gamma, showing potential mechanisms of action of this drug [35].

1.6 ABPP with reactivity-based probes or reactive chemical scaffolds to develop small-molecule inhibitors against ligandable hotspots in proteins

The coupled usage of reactivity-based chemoproteomic probes and isoTOP-ABPP platforms has led to the discovery of hundreds to thousands of potentially novel functional sites within proteins that may represent not only catalytic sites, but also regulatory or functional sites of post-translational modification, sites of oxidation, protein-protein interactions, metal binding,

and allosteric regulation [13,31,35,39]. These methods have mostly been used for identification of these sites, or competitive studies to map reactivity of endogenous and exogenous electrophilic agents. However, the isoTOP-ABPP technology has much broader potential applications in the area of drug discovery, in which the sites of probe-labeling by reactivity-based probes each constitute potential ligandable sites within these proteins that can be pharmacologically interrogated for drug discovery efforts.

Crawford and Weerapana, for example, recently developed a library of functionalized dichlorotriazines and found that the L-leucine methyl ester functionalized DCT variant (LAS-17) proved to be a highly selective covalent modifier of GSTP1 through reacting with a tyrosine 108 which in-turn inhibits GSTP1 activity [44]. This inhibitor was subsequently used in another study where the dichlorotriazine-alkyne probe was used to discover that GSTP1 was heightened selectively in triple-negative breast cancer cells and that LAS17 treatment and GSTP1 blockade attenuated triple-negative breast cancer pathogenicity through impairing breast cancer metabolism and signaling [45]. In another example, Wang et al. showed that chloromethyltriazoles were a promising cysteine-reactive scaffold and that its reactivity could be tempered to confer selectivity for certain cysteines over others. The authors showcase a cloromethyltriazole AA-CW236 as the first potent, selective, non-pseudosubstrate inhibitor of the O(6)-alkyguanine DNA methyltransferase (MGMT) [46].

More recently, this method was used in concert with chemoproteomic screening of a cysteine-reactive chloroacetamide and acrylamide fragment library to identify pharmacological ligands against over 700 cysteines across 637 unique protein targets or sites within protein targets classically considered to be undruggable [47]. The authors able to identify ligands against many protein-targets in parallel through the isoTOP-ABPP screening of cysteine-reactive fragments directly in complex proteomes or living cells. More importantly 82% of these protein did not have a small molecule modulator or probe annotated within the DrugBank database, indicating the promise of this type of approach for massively expanding upon the druggability of the proteome. Among these interactions, Backus et al focused on one particular example where they identified a cysteine-reactive fragment that preferentially reacts with pro-caspases [47].

1.7 Conclusions

Over the past nearly two decades since ABPP was introduced, ABPP platforms have shown great versatility in their applications, including identifying new disease-relevant targets, developing small-molecule inhibitors against these targets, assessing proteome-wide selectivity of drugs or revealing off-targets of pharmaceutical or environmental chemicals, and revealing novel functional sites in the proteome. Perhaps the most exciting application moving forward is using ABPP coupled with modern quantitative proteomic methods and newer active-site directed, reactivity-based, or other types of probes to comprehensively and globally map all ligandable hotspots or binding pockets in the proteome towards greatly expanding our scope of pharmacological tool-chest and drugs for the largely pharmacologically-devoid and undruggable proteome. This review primarily covers how this can be potentially achieved with active-site targeted or reactivity-based probes, but these types of approaches can be even further advanced with reversibly-acting molecules that are made to act covalently with photoaffinity tags to even further broaden our scope of ligandable sites. For example, this has been recently accomplished with a fatty acid probe bearing a biorthogonal handle and photoaffinity tag to reveal the lipid interaction proteome. Niphakis et al. used this approach to not only show that the lipid interaction proteome is rich in potential drug targets, but also identified a lipid binding protein

nucleobindin-1 that perturbs the metabolism of endocannabinoids and used the lipid probe to develop a selective chemical modulator for this protein [48].

Furthermore, while covalent inhibitors have been historically frowned upon due to their potential non-selective reactivity, coupling the development of inhibitors with chemoproteomic platforms such as ABPP enables the synthesis of potent and selective covalent inhibitors against protein targets through ABPP driving the medicinal chemistry and vice versa [7,47,49]. The future focus of using chemoproteomics and ABPP towards expanding our scope of the druggable proteome will not only lead to potential new cures for diseases but will be an engine for discovery that will rival the promise seen with emerging gene editing methods.

1.8 Acknowledgements

We thank the members of the Nomura Research Group for critical reading of the manuscript. This work was supported by grants from the National Institutes of Health (R01CA172667), American Cancer Society Research Scholar Award (RSG14-242-01-TBE), and DOD Breakthroughs Award (CDMRP W81XWH-15-1-0050).

1.9 Figures

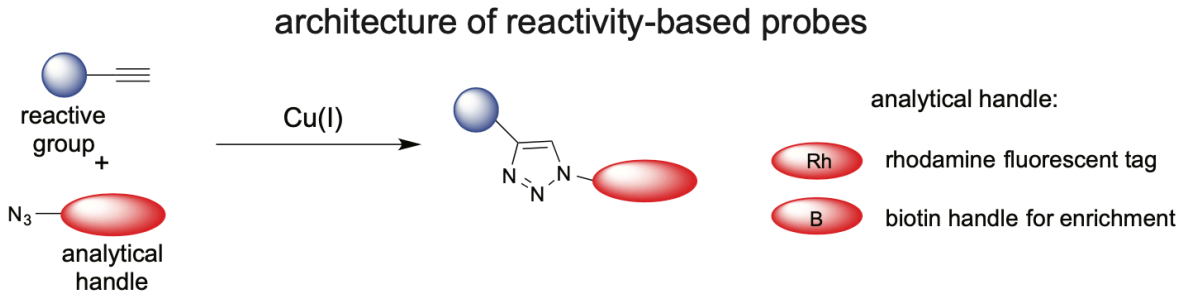

Figure 1.1: Design of activity-based and reactivity-based chemoproteomic probes

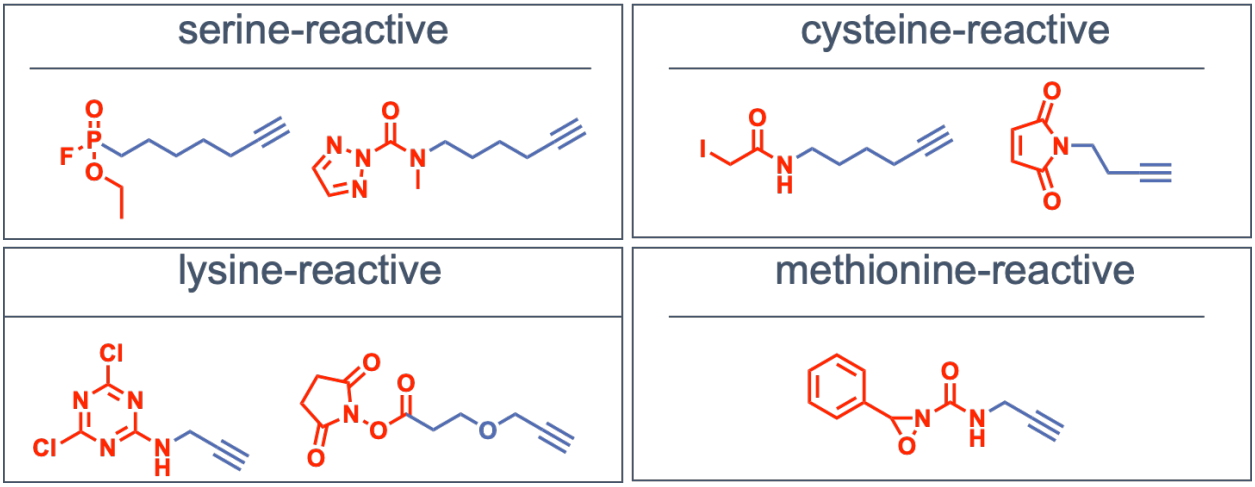

Figure 1.2: Examples of current reactivity-based warheads for various nucleophilic amino-acids.

Chapter 2: NHS-Esters as Versatile Reactivity-Based Probes for Mapping Proteome-Wide Ligandable Hotspots*

2.1 Abstract

Most of the proteome is considered undruggable oftentimes hindering translational efforts for drug discovery. Identifying previously unknown druggable hotspots in proteins would enable strategies for pharmacologically interrogating these sites with small-molecules. Activity-based protein profiling (ABPP) has arisen as a powerful chemoproteomic strategy that uses reactivity-based chemical probes to map reactive, functional, and ligandable hotspots in complex proteomes, which has enabled inhibitor discovery against various therapeutic protein targets. Here, we report an alkyne-functionalized N-hydroxysuccinimide-ester (NHS-ester) as a versatile reactivity-based probe for mapping the reactivity of a wide range of nucleophilic ligandable hotspots, including lysines, serines, threonines, and tyrosines encompassing active sites, allosteric sites, post-translational modification sites, protein interaction sites, and previously uncharacterized potential binding sites. Surprisingly, we also show that fragment-based NHS-ester ligands can be made to confer selectivity for specific lysine hotspots on specific targets including Dpyd, Aldh2, and Gstt1. We thus put forth NHS-esters as promising reactivity-based probes and chemical scaffolds for covalent ligand discovery.

2.2 Introduction

Even with the discovery of thousands of proteins implicated in human disease, translating these potential therapeutic targets into drugs remain difficult, in-part because most protein targets are considered "undruggable" or difficult to target with small-molecules. Most of the proteome is devoid of pharmacological tools, hindering both basic and translational research efforts. Only ~2% of all predicted human gene products are currently targeted with small-molecule drugs and 85-90% of the proteome is considered undruggable [2]. A major limiting factor in defining the druggability of a target is the lack of apparent binding pockets that can be targeted with small molecules to modulate protein function; such pockets can be difficult to predict based on sequence or structures. Identifying ligandable binding pockets within the proteome would thus potentially enable us to identify sites that can be pharmacologically interrogated for drug discovery.

Activity-based protein profiling (ABPP) has arisen as a powerful chemoproteomic strategy to identify ligandable hotspots in complex proteomes, enabling inhibitor discovery [47,50,51]. ABPP uses reactivity-based chemical probes to map reactive, functional, and ligandable hotspots in complex proteomes. When used in a competitive manner, covalently acting small-molecules can be competed against binding of reactivity-based probes to enable pharmacological interrogation of druggable hotspots [6,47,50]. Previous studies have used ABPP platforms to identify irreversible small-molecule inhibitors against many different enzymes [21,47,52,53]. Recently, covalent ligand discovery has also been coupled with isotopic tandem orthogonal proteolysis-enabled ABPP (isoTOP-ABPP) platforms to map covalent ligands against many ligandable cysteine hotspots in complex proteomes [47,54,55].

*Part of the work presented in this chapter has previously been published in the following manuscript: Ward, C. C., Kleinman, J. I. & Nomura, D. K. NHS-Esters As Versatile Reactivity-Based Probes for Mapping Proteome-Wide Ligandable Hotspots. *ACS Chem. Biol.* **12**, 1478–1483 (2017).

Cysteines within proteins have been particularly targeted for pharmacological tool and drug development due to well-established chemical scaffolds that exhibit high reactivity and specificity towards thiols, including haloacetamides, acrylamides, and maleamides [15,47,56,57]. Thanks to these reactive scaffolds, there are many examples of cysteine-reactive small-molecules targeting various druggable and undruggable protein targets [47,57–59]. There have also been more recent efforts to develop reactivity-based probes and covalently-acting small-molecules for chemoproteomic studies targeting other nucleophilic residues, such as lysines, serines, threonines, and tyrosines. For example, Shannon et al. found that dichlorotriazines show lysine-selective reactivity and can be used for chemoproteomic applications [13]. Identifying additional broadly reactive probes and scaffolds that can target these other nucleophilic hotspots beyond cysteines would drastically expand our ability to profile reactivity throughout the proteome and provide new handles for pharmacological interrogation of functional sites.

N-hydroxysuccinimide-esters (NHS-esters) are used extensively as functional groups in bioconjugation reactions, forming an amide bond with amines, such as lysines or N-termini. Other studies have also shown that NHS-esters can also react with other nucleophilic amino acids including serines, threonines, and tyrosines [60,61]. We were thus intrigued as to whether NHS-esters could be used as reactivity-based probes to broadly map reactivity across these and other nucleophilic amino acid hotspots and whether, despite their high reactivity, small fragments designed containing an NHS-ester could target specific sites within the proteome.

2.3 Results and Discussion

2.3.1 NHS-ester-alkyne is Broadly Reactive and Forms MS Stable Adducts

To determine whether NHS-esters can be used as reactivity-based probes for chemoproteomic profiling, we used a commercially available alkyne-functionalized NHS-ester (Propargyl-*N*-hydroxysuccinimidyl ester) (NHS-ester-alkyne) to label mouse liver proteomes. We labeled proteomes with either high (500 μM) or low (100 μM) concentration of NHS-ester-alkyne to map the relative reactivity of probe labeled sites using the isoTOP-ABPP platform **(Fig. 2.1; Table A.2.1, 3, 5, 7, 9 ,11; Fig. A.3.1)**. We then interpreted the quantitative ratios of those probe-modified peptides that were identified in two out of four biological replicates.

Through this effort, we identified over 3000 probe-modified peptides in mouse liver proteome. Nearly half of these sites (1639 sites) were lysines, consistent with the known preference of NHS-esters for amines. However, serines and threonines also represented ~17-18% each of total modified peptides. In addition, we also observed labeling of tyrosines and arginines, and to a lesser extent, cysteines **(Fig. 2.1A)**. Thus, we show that NHS-ester-alkyne is a versatile reactivity-based chemoproteomic probe for mapping the reactivity of proteome-wide accessible nucleophilic amino acids in complex proteomes. Most probe-modified peptides exhibited light (500 μM) to heavy (100 μM) ratios of 5 or greater **(Fig. A.3.1; Table A.2.1, 3, 5, 7, 9 ,11),** while a subset of these peptides demonstrated ratios less than 5. Previous studies using isoTOP-ABPP to quantitatively map cysteine-reactivity showed that those peptides with ratios less than 2 were considered hyper-reactive and enriched in functional residues [31]. A subset of probe-labeled peptides also showed light to heavy ratios less than 2, suggesting that these sites exhibited saturable binding at lower concentrations of probe and may possibly represent sites of preferential reactivity, potentially due to conditions in their local protein microenvironment **(Fig. A.3.1; Table A.2.1, 3, 5, 7, 9 ,11)**. In contrast, we interpret those probe-modified peptides that show a light to heavy ratio much greater than 5 as essentially showing little to no labeling at 100

μM compared to 500 μM. We also performed a parallel study with the dichlorotriazine-alkyne lysine-reactive probe reported in Shannon et al. in mouse liver proteome and report 85 probe-modified lysines **(Table A.2.13)**, which is on-par with the number of probe-labeled lysines reported previously [13]. Overall, these data indicate that NHS-ester-alkyne is a promising reactivity-based probe that can be used in chemoproteomic experiments to map the reactivity of lysines and many other nucleophilic amino acids.

2.3.2 NHS-ester-alkyne Modified A Diverse Array of Functional Sites

Further characterization of these NHS-ester-alkyne probe-modified peptides using the Uniprot database showed significant overlap with annotated functional sites **(Fig. 2.1B; Table A.2.2, 4, 6 ,8, 10, 12)**. Among probe-modified lysines, 31 % of these sites were annotated. Among these annotated residues, most were known sites of post-translational modifications such as lysine acetylation, succinylation, and malonylation. The remaining annotated lysine residues included active sites, binding sites, calcium binding regions, and nucleotide phosphate-binding regions **(Fig. 2.1B; A.2.2, 4, 6 ,8, 10, 12)**. While most probe-modified amino acids that we identified across the other nucleophilic residues were unannotated, the annotated sites included active sites, binding sites, post-translational modification sites, and metabolite and metal binding regions **(Fig. 2.1B; A.2.2, 4, 6 ,8, 10, 12).**

We provide structural examples of both annotated sites as well as unannotated sites that may be functional, highlighting both the diversity of nucleophiles labeled as well as the variety of roles these nucleophiles possess. In the cases where solved crystal structures of mouse proteins were not available, the closest human homolog was used after confirming the labeled residue was conserved. Consistent with the role of lysines in enzyme catalysis, we observed several lysines in metabolic enzymes labeled with the NHS-ester-alkyne probe. First, in our isoTOP-ABPP data, we showed the active-site K230 labeled by our NHS-ester-alkyne probe in fructose bisphosphonate aldolase B (Aldob) (shown in red), a glycolytic enzyme that catalyzes the reversible cleavage of fructose 1,6-bisphosphate to glyceraldehyde-3-phosphate and dihydroxyacetone phosphate [62]. K230 forms a Schiff-base with dihydroxyacetonephosphate **(Fig. 2.2A, PDB: 1QO5)** [63]. Consistent with the functional role of K230 in the catalytic mechanism of Aldob, we showed that the isotopic light to heavy ratio of this lysine is significantly less than 2, indicating this site is hyper-reactive **(Table A.2.1).** Our data also revealed labeling of an active site tyrosine, Y55 in estradiol 17 beta-dehydrogenase 5 (Akr1c6), which acts as the proton donor during Akr1c6 catalyzed reduction of various androgens and estrogens **(Fig. 2.2B, PDB: 1J96)** [64]. Beyond catalytic residues, we also demonstrated labeling of residues within enzyme active sites that are involved in substrate or cofactor binding, including K12 (shown in red) and R105 (shown in orange) labeled by our probe in nucleoside diphosphate kinase A (Nme1)—an enzyme that catalyzes the generation of nucleotide triphosphates [65]. Both K12 and R105 interact with the α and β phosphates of the bound nucleoside diphosphate **(Fig. 2.2C, PDB: 2HVD)**. In addition to active-site lysines, we also observed labeling of post-translational modification sites within enzymes as well. K46 in glycine N-methyltransferase (Gnmt) was as another site of probe labeling (shown in red). Gnmt catalyzes the conversion of S-adenosyl-L-methionine to S-adenosyl-L-homocysteine and sarcosine [66]. K46 is a known lysine succinylation site **(Fig. 2.2D, PDB: 1R8X)** [67].

Beyond metabolic enzymes, our isoTOP-ABPP data also uncovered labeling of lysines in other non-enzyme protein classes. Our isoTOP-ABPP data showed an unannotated K91 on profilin-1 (Pfn1) as a probe-labeled site (shown in red) [68]. Profilin is an actin-binding protein

involved in restructuring the actin cytoskeleton and maintaining actin monomer homeostasis. Solved structures of human profilin-1 bound to actin show K91 is forms salt bridges with D288 and D286 on actin, sitting ~3 Å from each Asp. Disruption of this interaction would likely destabilize that profilin-1-actin interface **(Fig. 2.2E, PDB: 1FIL, 2PBD)**. Another example of an unannotated site is T31 on annexin A5 that is labeled by our probe. Annexin A5 is a protein that binds to phosphatidylserine in a calcium-dependent manner [69]. Structural analysis shows that T31 sits very closely (~4 Å) to the calcium binding site within Annexin A5, suggesting that covalent modification of T31 could disrupt calcium binding and play a direct role in annexin A5 activity **(Fig. 2.2F, PDB: 1ANW).**

Thus, by structurally examining sites of NHS-ester-alkyne probe labeling using isoTOP-ABPP, we demonstrate the versatility of NHS-ester-alkyne to provide a reactivity readout on a wide variety of functional and putatively ligandable sites, enabling both biological study and ligand discovery against these sites.

2.3.3 Fragments Bearing NHS-esters can be Engineered for Selectivity and Potency

Following up on these data, we next sought to investigate whether NHS-esters could be used as scaffolds for covalent ligand discovery against specific nucleophilic hotspots targeted by the NHS-ester-alkyne probe. We synthesized two compounds CW 1-26 and CW 1-33, with varied structure around the NHS-ester reactive moiety **(Fig. 2.3)**. The starting carboxylic acid precursors for synthesizing CW 1-26 and CW 1-33 were chosen due to their commercial availability, price, and structural variety. While there were thousands of available carboxylic acids, the high reactivity of NHS esters led us to select relatively large structures that had a higher chance of possessing selectivity.

First, we demonstrated that neither of these compounds broadly impair NHS-ester-alkyne labeling of mouse liver proteomes, indicating already that these compounds are not reacting non-specifically across the proteome **(Fig. A.3.2)**. We next performed competitive isoTOP-ABPP studies to identify the specific targets of these NHS-ester based covalent ligands in which we competed vehicle or CW 1-26 or CW 1-33 against the binding of NHS-ester-alkyne in mouse liver proteome followed by conjugation of isotopically light (for vehicle-treated) or heavy (for NHS-ester ligand-treated) biotin-enrichment handles bearing a TEV protease recognition sequence, followed by combining control and treated proteomes in a 1:1 ratio, avidin-enrichment and tryptic digestion of probe-modified proteins, and subsequent isolation and TEV protease release of probe-modified tryptic peptides for proteomic analysis **(Fig. 2.3).** We then only interpreted the light to heavy isotopic ratios of probe-modified tryptic peptides for those peptides that were present in at least two out of three biological replicates. Among >600 probe-modified peptides profiled, we demonstrated that CW 1-26 selectively interacted with six targets, showing a light to heavy ratio of >5. These targets include included R53 of Bpifb5, K497 and T489 of dihydropyrimidine dehydrogenase (Dpyd), S69 on Hba5, K55 on Atp5l, and K48 on Slc25a42 that possess an isotopically light to heavy probe-modified peptide ratio of >5 **(Fig. 2.3A, 3B; Table A.2.14)**. We further validated one of these interactions showing competition of CW 1-26 against NHS-ester-alkyne labeling of pure human DPYD protein with a 50 % inhibitory concentration (IC50) of 40 μM **(Fig. 2.3C)**. Dpyd is the initial and rate-limiting enzyme in uracil and thymidine catabolism. Examining a previously solved structure of human DPYD revealed that K497 is within 3 Å of D119 and is located where a strand from the other half of the DPYD homodimer crosses the protein surface. Disruption of this electrostatic interaction or addition by a bulky ligand could destabilize the DPYD dimer and affect enzyme function **(Fig. 2.3D)**.

The second ligand we tested, CW 1-33, also showed relatively selective interactions with 4 targets showing ratios of >5. These targets included S151 of Rpl6, K639 of Zfp318, K211 of aldehyde dehydrogenase 2 (Aldh2), and K71 of glutathione transferase t1 (Gstt1) **(Fig. 2.3F; Table A.2.15)**. We validated interaction of CW 1-33 with some of these targets and showed competition of CW 1-33 against NHS-ester-alkyne labeling of human ALDH2 and GSTT1, and mapped the labeled sites in solved structures of these enzymes **(Fig. 2.3G-3J).** CW 1-33 showed more potent interactions with ALDH2 compared to GSTT1 with IC50 values of 4.1 and 100 μM, respectively **(Fig. 2.3G, 3I).** Interestingly, both lysines targeted by CW 1-33 on ALDH2 and GSTT1 appear to be surface lysines with no obviously evident binding pocket **(Fig. 2.3H, 3J)**. These data may indicate that either there are subtle ligandable binding pockets, pockets that are formed by protein-protein interactions or conformational changes, or that these structures may dynamically form binding pockets upon interactions with CW 1-33 which may not be evident in these static structures. IC50 dose-response studies were performed by pre-incubating ligands with pure protein for 30 min followed by 1 h labeling with NHS-ester-alkyne and thus these reported IC50 values are relative potency values that can only be compared between the two probes under the same conditions. Most surprisingly, both CW 1-26 and CW 1-33 selectively interact with a only handful of targets out of hundreds of sites profiled, despite bearing their highly reactive NHS-ester core, as evidenced by most probe-modified peptides showing isotopic ratios of ~1 **(Fig. 2.3B, 3F)**. While these covalent ligands are clearly not selective enough for the reported targets, these data suggest that fragment-based NHS-ester covalent ligands can be potentially used to develop selective lead small-molecule modulators against specific nucleophilic hotspots targeted by the NHS-ester-alkyne probe. CW 1-33 does not inhibit ALDH2 activity based on a substrate activity assay in mouse liver proteome (data not shown). However, one could envision combining selective covalent ligands with small-molecule "degraders" that recruit E3 ubiquitin ligases for subsequent proteosomal degradation of specific protein targets [70–72] as a means of leveraging this specificity for biological or therapeutic function.

2.3.4 Conclusion

Overall, our study demonstrates that the NHS-ester-alkyne probe is as a versatile reactivity-based probe for mapping the reactivity of a wide range of nucleophilic ligandable hotspots, including lysines, serines, threonines, and tyrosines encompassing active sites, allosteric sites, post-translational modification sites, protein interaction sites, and previously uncharacterized potential binding sites using chemoproteomic approaches. This commercially available probe can thus serve as a complementary tool to other previously-developed reactivity-based probes that target lysines, such as with the dichlorotriazine-alkyne probe, as well as other nucleophilic residues [13–15,73]. Surprisingly, we also demonstrate that selectivity for specific nucleophilic hotspots can be conferred with NHS-ester scaffolds lending its future potential applicability for covalent ligand discovery against specific druggable hotspots targeted by reactivity-based probes.

2.4 Methods

Materials: 2,5-dioxopyrrolidin-1-yl-3-(prop-2-ynyloxy)propanoate (NHS-ester-alkyne) was obtained from Sigma-Aldrich. The dichlorotriazine-alkyne probe was synthesized according to the methods reported in Shannon et al [13]. The synthesis of CW 1-26 and CW 1-33 is reported in Supporting Information.

2.4.1 IsoTOP-ABPP.

IsoTOP-ABPP studies were done as previously reported [31,47]. Proteome samples were derived from mouse livers, which were previously partitioned into 3 pieces, homogenized in PBS with a bead-blaster, and cleared of debris via high speed centrifugation. For isoTOP-ABPP studies, liver proteomes were diluted in PBS to 2 mg/ml and were labeled with NHS-ester-alkyne for 1 h at room temperature. CuAAC was used by sequential addition of tris(2-carboxyethyl)phosphine (1 mM, Sigma), tris[(1-benzyl-1H-1,2,3-triazol-4-yl)methyl]amine (34 μM, Sigma), copper (II) sulfate (1 mM, Sigma), and biotin-linker-azide, the linker functionalized with a TEV protease recognition sequence along with an isotopically light or heavy valine for treatment of control or treated proteome, respectively. Subsequent isoTOP-ABPP procedures and MS analysis were performed as previously reported [31,47,74,75]. Cysteine residues were searched with a static modification for carboxyaminomethylation (+57.02146) and probe-modification of peptides was searched with up to two differential modifications for methionine oxidation and either the light or heavy TEV tags (m/z +550.22797 for light and +556.24178 for heavy for lysines, serines, threonines, arginines, and tyrosines and +493.20647 light and +499.22028 for heavy for cysteine to account for the static modification). Peptides were required to have at least one tryptic end and to contain the TEV modification. ProLUCID data was filtered through DTASelect to achieve a peptide false-positive rate below 1%. For studies, with covalent ligands, proteomes were pre-incubated with DMSO or ligand for 30 min at room temperature prior to probe-labeling. The isoTOP-ABPP study with dichlorotriazine-alkyne was performed as described above, but the differential modifications for probe-modified lysines were m/z +550.22797 for light and +556.24178 for heavy. We note that the total numbers of NHS-ester-alkyne probe-modified peptides differ between the first run compared with the competitive isoTOP-ABPP runs with ligands. This may be due to running four biological replicates in **Fig 2.1** compared to three biological replicates in **Fig. 2.3**, differences in mass spectrometry sensitivity at the time of running the samples, or instability of the probe with longer periods of storage.

2.4.2 Peptide Computational Analysis

Quantified light:heavy ratios from each experiment that corresponded to the same peptide (including truncations) and labeling site were averaged, as long as the peptide had appeared in >= 2 experiments. These averages yielded a master list of labeled sites in the proteome for each residue of interest. The “feature” list from the uniprot records that each peptide mapped to was downloaded and all features that overlapped with the labeled site in the protein, were shorter than 30 amino acids, and were not in a list of ambigious/poorly annotated features (e.g. “strand,” “domain,” “site”) were kept as annotations for the peptide.

2.4.3 Gel-Based ABPP.

Gel-based ABPP methods were performed as previously described [43]. Recombinant pure human proteins were either purified or purchased from Origene. Whole liver lysates were generated as previously described. Both samples were pre-treated with DMSO or fragment in an incubation volume of 50 μL PBS for 30 min at room temperature, and were subsequently treated with NHS-ester-alkyne (10 μM final concentration) for 60 min at room temperature. CuAAC was performed to append rhodamine-azide onto probe-labeled proteins. The samples were separated by SDS/PAGE and scanned using a ChemiDoc MP (Bio-Rad Laboratories, Inc).

2.5 Acknowledgements.
We thank the members of the Nomura Research Group for critical reading of the manuscript. This work was supported by grants from the National Institutes of Health (R01CA172667 and Chemical Biology Training Grant T32 GM066698), American Cancer Society Research Scholar Award (RSG14-242-01-TBE), and Department of Defense Breakthroughs Award (CDMRP W81XWH-15-1-0050).

2.6 Figures

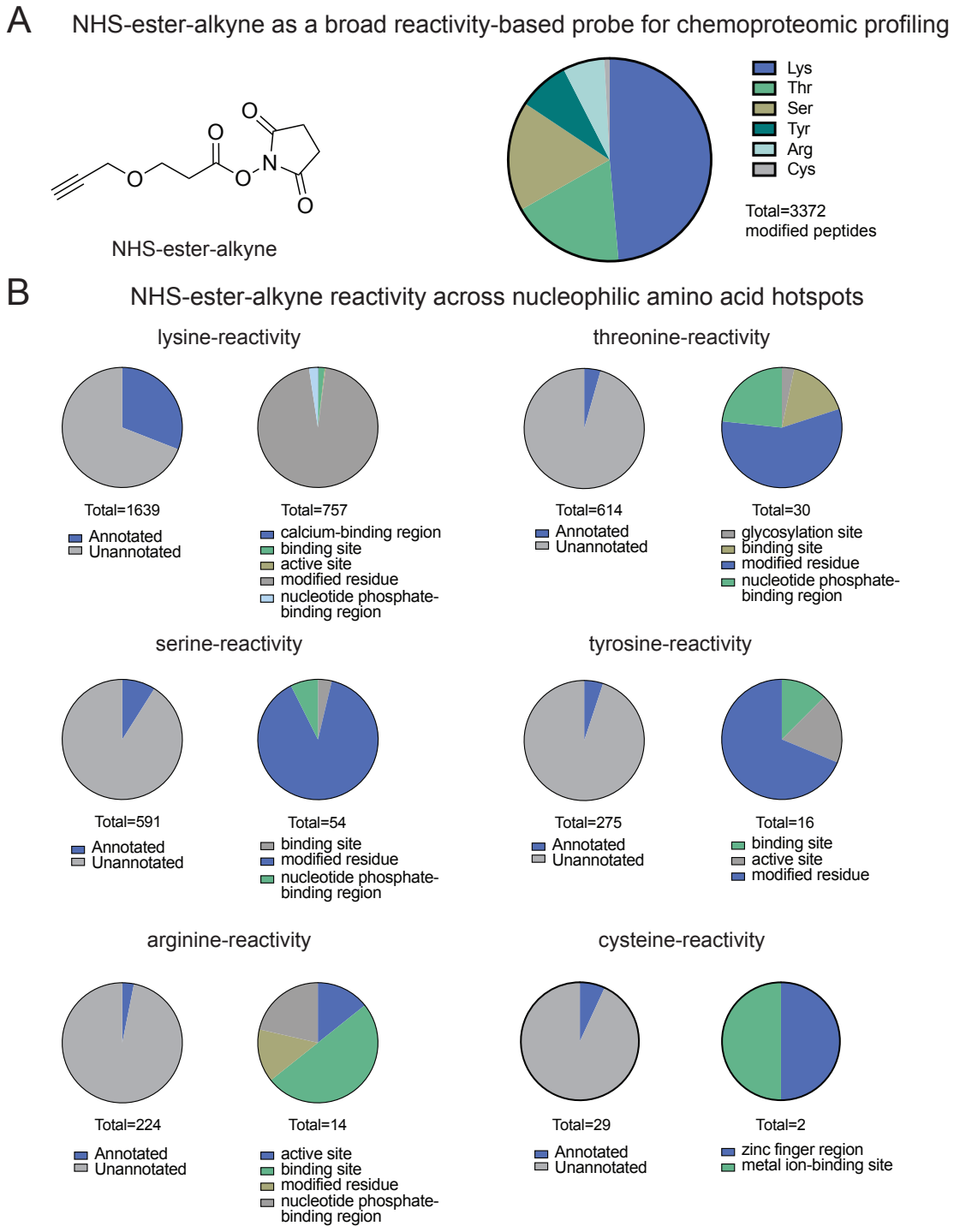

Figure 1.1: IsoTOP-ABPP of NHS-ester-alkyne reactivity in mouse liver proteome.
(A) Structure of NHS-ester-alkyne (NHSyne) and distribution of probe-modified peptides in mouse liver proteome assessed by isoTOP-ABPP. Mouse liver proteomes were labeled with NHS-ester-alkyne (500 or 100 μM), followed by copper-catalyzed azide-alkyne cycloaddition (CuAAC) conjugation of a biotin-azide tag bearing an isotopically light (for 500 μM) or heavy (100 μM) mass tag to probe-labeled proteins. Probe-labeled proteins were subsequently avidin-enriched, digested with trypsin, and probe-modified tryptic peptides were isolated and eluted by TEV

protease for subsequent LC-LC/MS/MS proteomic analysis. Raw data and ratiometric analysis of heavy to light peptides can be found in **Fig. S1, Table S1.** NHS-ester-alkyne predominantly reacted with lysines, showed significant reactivity with threonines and serines, and showed minor reactivity with tyrosines, arginines, and cysteines. **(B)** Breakdown of probe-labeled sites compared against annotated UniProt functional sites. While the majority of labeled residues are unannotated, the annotated sites were predominantly post-translationally modified or involved in ligand binding. Data shown in **(A)** and **(B)** are representative of probe-modified peptides found in two out of four biological replicates.

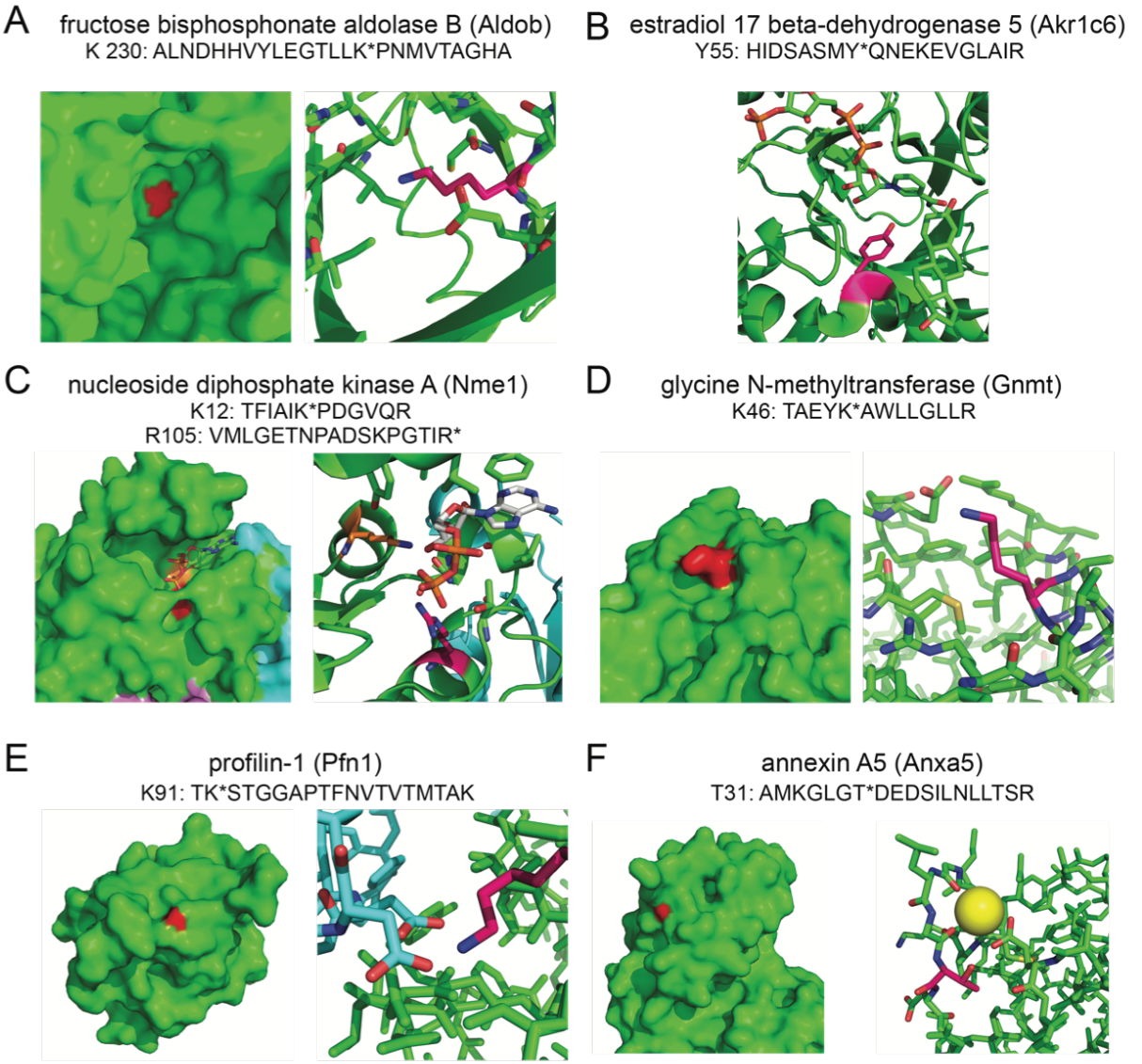

Figure 2.2: Examples of various types of nucleophilic residues targeted by NHS-ester-alkyne.
(A) K230 on Aldob, a catalytic residue within the active site. **(B)** Y55 on Akr1c6, the catalytic proton donor within the active site. Specific structures are all from human counterparts. **(C)** K12 and R105 on Nme1, two positively charged residues involved in binding nucleoside diphosphates. **(D)** K46 on Gnmt, a surface lysine and known succinylation site. **(E)** K91 on Pfn1, a surface lysine which forms two salt bridges with aspartate residues at the actin – Pfn1 interface. **(F)** T31 on Anxa5, a surface threonine near the calcium binding site. PDB file designations are listed in the text.

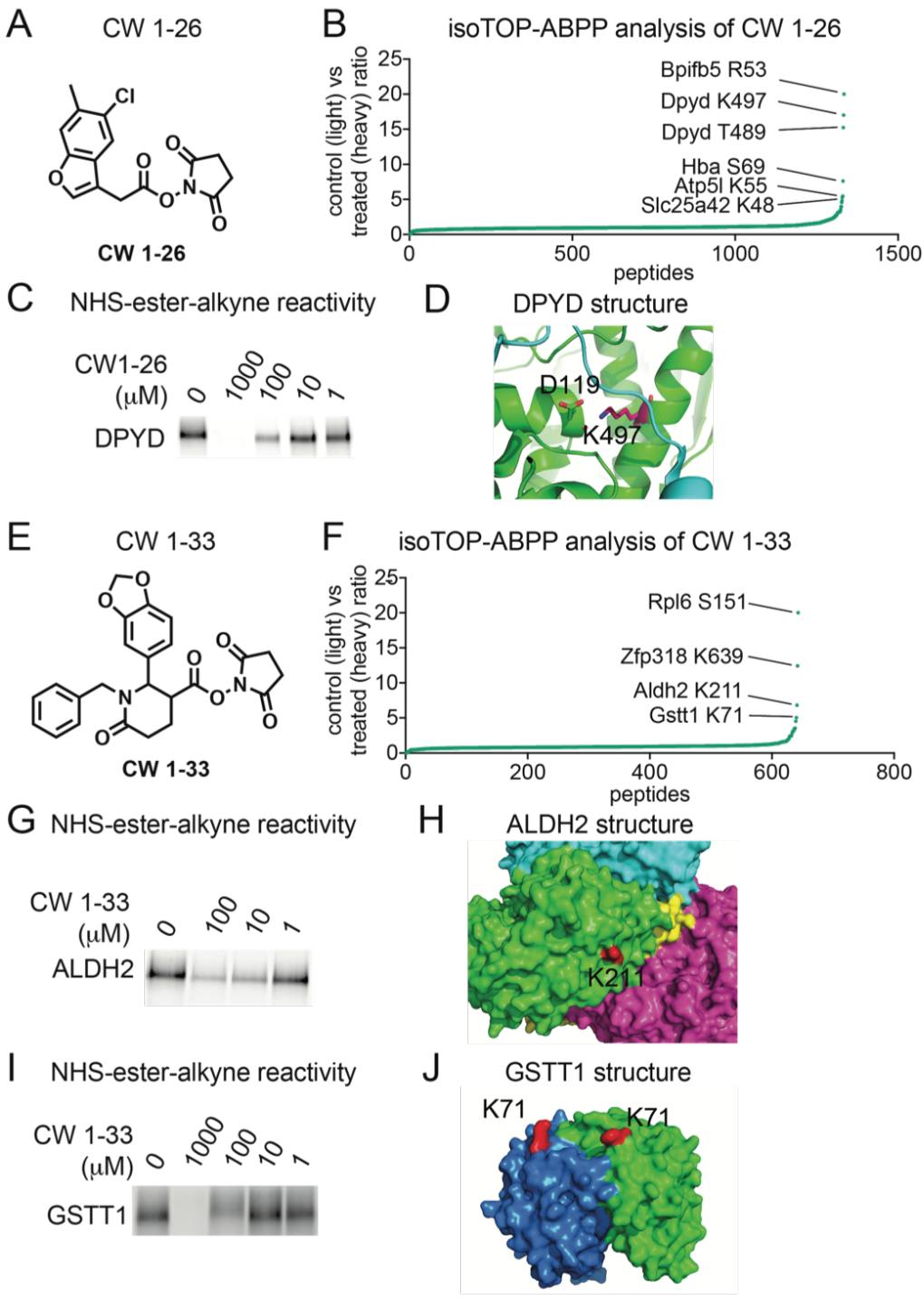

Figure 2.3: NHS-ester based covalent ligands confer selectivity for lysines on specific protein targets. **(A)** Structure of NHS-ester fragment CW 1-26. **(B)** Competitive isoTOP-ABPP analysis of CW 1-26 lysine reactivity in mouse liver proteomes. DMSO vehicle or CW 1-26 (100 μM) was pre-incubated with mouse liver proteomes for 30 min prior to labeling with NHS-ester-alkyne (500 μM) for 1 h. Probe-labeled samples were then taken through the isoTOP-ABPP procedure. Shown are individual isotopically light (vehicle-treated) to heavy (CW-1-26-treated) probe-labeled peptides, showing K497 as the primary target. **(C)** Competition of CW1-26 against NHS-ester-alkyne labeling of recombinant pure human DPYD using gel-based in-gel fluorescence ABPP methods. **(D)** K497 is a surface lysine on DPYD which forms a salt bridge with D119 and resides at an interface between

DPYD dimeric partners. **(E)** A second NHS-ester fragment CW1-33. **(F)** Competitive isoTOP-ABPP analysis of CW1-33 using the same approach described in **(B)** yielded three targets, K639 on Zfp318, K211 on Aldh2, and K71 Gstt1. **(G-J)** Validation of CW 1-33 competition against NHS-ester-alkyne labeling of pure human ALDH2 **(G)** and GSTT1 **(I)** protein and locations of lysines targeted by CW 1-33 on ALDH2 **(H)** and GSTT1 **(J)** structures. Data in **(B, D)** show average ratios for probe-labeled peptides identified in at least two out of three biological replicates. Gels shown in **(C, G,** and **I**) are representative gels from n=3.

Chapter 3: Covalent Ligand Discovery Against Druggable Hotspots Targeted by Anti-Cancer Natural Products*

3.1 Abstract

While there are countless covalently-acting natural products that have been shown to possess anti-cancer activity, the direct protein targets for most of these natural products are not well understood. Furthermore, many of these natural products are oftentimes difficult to synthesize or isolate, hindering their development as drugs. Identifying potential druggable hotspots targeted by covalently-acting anti-cancer natural products can enable pharmacological interrogation of these sites using more synthetically tractable compounds. Here, we used isotopic tandem orthogonal proteolysis-enabled activity-based protein profiling (isoTOP-ABPP) to map proteome-wide targets of withaferin A, a covalently-acting natural product with anti-cancer activity, directly in breast cancer proteomes. We showed that withaferin A targets C377 on the regulatory subunit PPP2R1A of the tumor suppressor protein phosphatase 2A (PP2A) complex leading to activation of PP2A, inactivation of AKT signaling, and impairments in breast cancer cell proliferation. Covalent ligand screening in breast cancer cells revealed a cysteine-reactive chloroacetamide that modifies the same cysteine on PPP2R1A. Further optimization of this covalent ligand led to the generation of JNS 1-40, which selectively targets C377 of PPP2R1A to also activate PP2A and recapitulate the signaling and pathogenic impairments observed with withaferin A in breast cancer cells. Our study highlights the utility of using chemoproteomic strategies for mapping druggable hotspots targeted by complex natural products and subsequently interrogating these sites with more synthetically tractable covalent ligands for potential cancer therapy.

3.2 Introduction

There are countless natural products that have been isolated from microbes, plants, and other living organisms that demonstrate diverse biological action, including antibiotic, anti-inflammatory, and anti-cancer activities [76]. Among these natural products are agents that contain potential reactive electrophilic centers that can covalently react with nucleophilic amino acid hotspots on proteins to modulate their biological action [76]. Examples include natural product scaffolds such as β-lactones and β -lactams, many of which show antibiotic activity through covalent modification and inhibition of the catalytic serines of transpeptidases. However, there are many more reactive natural products that bear other reactive moieties such as Michael acceptors, epoxides, and aldehydes which may react with other nucleophilic side chains such as cysteines and lysines [76]. However, the reactivity and direct targets of most of these natural products that bear reactive centers remain poorly understood. Traditional approaches for target identification of natural products entail synthesis or derivatization of the natural products so that they can be appended to enrichment handles or beads for subsequent isolation and chemoproteomic studies. However, many natural products are incredibly complex to synthesize or may not necessarily have appropriate sites for derivatization, hindering the ability to develop natural product analogs to allow traditional chemoproteomic target identification.

---

* Part of the work presented in this chapter has been previously published in the following manuscript: Grossman, E. A.[$], Ward, C.C.[$], *et al*. Covalent Ligand Discovery against Druggable Hotspots Targeted by Anti-cancer Natural Products. *Cell Chemical Biology* **24**, 1368-1376.e4 (2017).

[$]These authors contributed equally to this work.

Isotopic tandem orthogonal proteolysis-enabled activity-based protein profiling (isoTOP-ABPP) has arisen as a complementary chemoproteomic approach for target discovery of covalently-acting small-molecules. IsoTOP-ABPP uses reactivity-based chemical probes to map proteome-wide reactive, functional, and ligandable hotspots directly in complex proteomes. When used in a competitive manner, covalently-acting small-molecules can be competed against the binding of reactivity-based probes directly in complex proteomes to map its proteome-wide reactivity and targets [6,42,47,50]. While the disadvantages of this isoTOP-ABPP strategy include biasing oneself to profiling of sites targeted by reactivity-based probes and the indirect nature of the assay inherent to competing small-molecules against probe binding, a major advantage of this method is that it enables identification of the specific amino acids targeted by covalently-acting small-molecules. Furthermore, this type of competitive isoTOP-ABPP strategy can be performed with the original parent molecule without having to synthesize analogs or derivatize the molecule. Several recent studies have used ABPP strategies to identify direct targets of reactive natural products such as licochalcone A, celastrol, and curcumin [35,77,78].

The advantage of identifying the direct targets and druggable hotspots targeted by covalently-acting anti-cancer natural products is that these sites can subsequently be deconvoluted to identify the specific target(s) responsible for the specific bioactivity; the identified targets can then be further pharmacologically interrogated with other types of chemical scaffolds to advance drug discovery efforts. This method contrasts with having to perform medicinal chemistry efforts on natural product scaffolds that are oftentimes synthetically challenging, with readouts based on their bioactivity rather than affinity to specific protein targets. Furthermore, identifying the nucleophilic amino acid hotspots targeted by reactive natural products enables covalent ligand discovery against these sites toward developing more potent and selective covalent inhibitors; these targets may also be more synthetically accessible compared to the oftentimes more complex structures of natural products. Recent studies have shown that covalent ligand discovery can be used to identify selective lead ligands against unique nucleophilic druggable hotspots in proteins [47,79,80].

Here, we have used the isoTOP-ABPP platform to couple target identification of a covalently-acting anti-cancer natural product with covalent ligand screening to identify a lead ligand that selectively interacts with the same target of interest. For this study, we have chosen to investigate the proteome-wide reactivity and targets of the natural product withaferin A, a steroidal lactone from the Ayurvedic plant Withania somnifera, which has been shown to possess anti-inflammatory, anti-diabetic, and anti-cancer activity [81–84]. Withaferin A bears a Michael acceptor that may react with cysteine nucleophilic hotspots in protein targets **(Fig. 1A)**. Previous studies have shown that withaferin A binds to functional cysteines in targets such as vimentin and NF-KB which have been postulated to account for its cancer and anti-inflammatory activities, respectively [85,86]. However, these studies either used a derivatized form of withaferin A, which could have missed targets that did not interact with this derivatized form, or performed experiments with specific proteins. Thus, withaferin A may potentially interact with additional targets that may be responsible for its anti-cancer activity. We have determined that withaferin A targets a particular cysteine on a regulatory subunit of the tumor suppressor protein phosphatase 2A (PP2A) to activate PP2A activity and inactivate multiple oncogenic signaling pathways which contributes to impairments in breast cancer pathogenicity and metabolism. We have also identified a significantly more synthetically tractable covalent ligand that selectively targets this same site to recapitulate the effects observed with withaferin A.

3.3 Results and Discussion

3.3.1 Anti-Cancer Activity of Withaferin A in Breast Cancer Cells

We first tested the anti-cancer activity of withaferin A across several breast cancer cell lines including the receptor-positive MCF7 cells and triple-negative breast cancer (TNBC) cells 231MFP and HCC38 devoid in estrogen, progesterone, and HER2 receptors. TNBCs are highly aggressive breast cancers that show the worst prognosis with little to no targeted therapies [87]. Identifying agents and new druggable hotspots in anti-cancer targets that are capable of impairing TNBC pathogenicity would contribute significantly towards combatting breast cancer. Consistent with previous studies, we show that withaferin A impairs serum-free cell survival and proliferation in MCF7, 231MFP, and HCC38 breast cancer cells **(Fig. 3.1B-1D)**. We show that withaferin A impairs 231MFP cell proliferation in a dose-dependent manner with a 50 % effective concentration (EC50) of 7.5 μM **(Fig. B.3.1A)**.

3.3.2 Mapping Withaferin A Targets with IsoTOP-ABPP

We next used competitive isoTOP-ABPP platforms to map the proteome-wide cysteine-reactivity of withaferin A in 231MFP breast cancer cell proteomes. While previous studies have demonstrated biological effects of withaferin A at lower concentrations [85], in this study, we used the minimum concentration of withaferin A (10 μM) that yielded the maximal anti-proliferative effect. To ascertain the direct targets of withaferin A without potential confounding effects from protein expression changes, we initially performed isoTOP-ABPP studies *in vitro*, in which we competed withaferin A against the reactivity of a broadly cysteine-reactive iodoacetamide-alkyne (IAyne) probe in 231MFP breast cancer cell proteomes. We subsequently appended isotopically light (for vehicle-treated) or heavy (for withaferin A-treated) enrichment handles by copper-catalyzed azide-alkyne cycloaddition (CuAAC), followed by combining vehicle and withaferin A-treated proteomes in a 1:1 ratio, and enrichment and isolation of probe-modified tryptic peptides for quantitative proteomic analysis **(Fig. 3.2A)**. Out of the >3000 total probe-modified peptides identified; we only interpreted those peptides that were present in at least 2 out of 3 biological replicates. Through this analysis, we identified C377 of PPP2R1A, a regulatory subunit of PP2A, as the primary and only target that showed a light to heavy ratio >5 across all three biological replicates **(Fig. 3.2B)**. We also confirmed that C377 of PPP2R1A was the primary *in situ* target of withaferin A in 231MFP cells showing an isotopically light to heavy ratio of 4.0. **(Fig. B.3.1B).**

Previous studies have uncovered several targets of withaferin A, including C328 on vimentin as well as several cysteines on Keap1 [85,88]. In our study, we identified C328 on vimentin as a site of IAyne labeling, but this site was not a target of withaferin A, as evidenced by a light to heavy ratio of 1.0 from *in vitro* treatment of 231MFP breast cancer cell proteomes with withaferin A (10 μM) **(Table B.2.1)** as well as a lack of competition observed between withaferin A and IAyne labeling of pure human vimentin by gel-based ABPP **(Fig. B.3.1C).** While we did not observe IAyne labeled KEAP1 peptides in our isoTOP-ABPP studies, we also showed no competition between withaferin A and IAyne labeling of pure human KEAP1 **(Fig. B.3.1C)**. These results do not negate the possibility that withaferin A may still interact with these targets under other conditions but suggest that these proteins are likely not the primary targets of withaferin A in 231MFP breast cancer cells. We thus focused on further investigating the role of withaferin A interactions with PPP2R1A and its influence on PP2A activity and breast cancer pathogenicity.

3.3.3 Withaferin A Interactions with PPP2R1A

PP2A is a tumor suppressor that dephosphorylates and inactivates oncogenic signaling pathways such as AKT. There has been considerable interest in developing direct or indirect activators of PP2A for cancer therapy [89]. While our IAyne probe labeled both C377 and C390 on PPP2R1A, withaferin A specifically targets C377 but not C390 on PPP2R1A **(Fig. 3.2B).** We confirmed this interaction as demonstrated by competition of withaferin A against IAyne labeling of pure human PPP2R1A protein using gel-based ABPP methods **(Fig. 3.2C)**. In these gel-based studies, we used a lower concentration of IAyne than our isoTOP-ABPP studies, which may explain why we observe full competition of withaferin A against IAyne labeling. C377 sits at an interface between three subunits of the core PP2A complex based on previously solved crystal structures of the PP2A heterotrimeric holoenzyme complex **(Fig. 3.2D)** [90]. We postulated that withaferin A activates PP2A activity through targeting C377 on PPP2R1A to impair 231MFP breast cancer cell proliferation. Consistent with this premise, we showed that withaferin A activated PP2A activity in a reconstituted *in vitro* biochemical assay with purified human wild-type PPP2R1A protein and the regulatory and catalytic subunits PPP2R2A and PPP2CA, respectively, but not with the PPP2R1A C377A mutant protein **(Fig. 3.2E)**. Treatment of 231MFP cells with withaferin A also reduced phosphorylated AKT levels and this effect was rescued by co-treatment with the PP2A-selective inhibitor cantharidin **(Fig. 3.2F)**. Further confirming that targeting of PPP2R1A is involved in withaferin A effects, PPP2R1A knockdown with short interfering RNA (siPPP2R1A) significantly attenuated the anti-proliferative effects observed with withaferin A treatment in 231MFP breast cancer cells **(Fig. B.3.1D, 1E)**. The lack of complete attenuation of withaferin A-induced anti-proliferative effects in siPPP2R1A cells may be due to residual PPP2R1A protein expression in the knockdown cells or the contribution of additional withaferin A targets to the anti-proliferative effects. Nonetheless, our data indicate that withaferin A targeting of C377 of PPP2R1A and activation of PP2A activity is in-part involved in the observed anti-proliferative effects.

3.3.4 Screening Cysteine-Reactive Fragment Libraries to Reveal PPP2R1A Ligands

To identify more synthetically tractable covalent ligands against C377 of PPP2R1A, we next screened a library of cysteine-reactive small-molecule ligands in 231MFP breast cancer cells to identify any compounds that recapitulated the phenotypes of withaferin A in impairing 231MFP cell proliferation **(Fig. 3.3A, 3B)**. The top hit that arose from this screen was the chloroacetamide DKM 2-90 **(Fig. 3.3B-3C, 4A)**.

We next performed competitive isoTOP-ABPP experiments to identify the targets of DKM 2-90 through competition of this lead fragment against IAyne labeling of 231MFP proteomes. While this ligand was not potent, only showing anti-proliferative effects at 100 μM, we found that DKM 2-90 showed considerable selectivity in targeting C377 of PPP2R1A *in vitro* **(Fig. 3.4B; Table B.2.3)**. We also confirmed this through gel-based ABPP methods, showing significant competition of DKM 2-90 against IAyne labeling of pure human PPP2R1A protein with a 50 % inhibitory concentration (IC50) of 10 μM. **(Fig. 3.4C).** IsoTOP-ABPP analysis of DKM 2-90 treatment in 231MFP cells *in situ* also showed targeting of C377 of PPP2R1A with an isotopically light to heavy ratio of 5.9. However, four additional targets were also evident that showed an isotopically light to heavy ratio >5, including TXNDC17 C43, CLIC4 C35, ACAT1 C196, and SCP2 C307 **(Fig. B.3.1F)**. Nonetheless, while DKM 2-90 was a very simple and non-potent covalent ligand, it showed remarkable overall selectivity with only 5 total sites showing

>5 ratio out of >1000 cysteines profiled **(Fig. B.3.1F)**. Despite additional targets of DKM 2-90, we still observed an attenuation of DKM 2-90-mediated anti-proliferative effects in siPPP2R1A 231MFP cells compared to DKM 2-90-treated siControl cells **(Fig. B.3.1G)**. We also recapitulated the reduced levels of phosphorylated AKT and cantharidin rescue with DKM 2-90 treatment in 231MFP cells **(Fig. 3.4D).**

3.3.5 JNS 1-40: An Optimized Covalent Ligand Targeting C377 of PPP2R1A

While DKM 2-90 was not a potent ligand against PPP2R1A, we showed that much simpler covalent ligands could be identified that hit the same druggable hotspots targeted by complex natural products like withaferin A with decent selectivity and cell penetration. We next sought to optimize the potency of DKM 2-90. We found that replacing the benzodioxan ring with a tetralin with JNS 1-37 dramatically reduced potency with an IC50 value of 300 μM **(Fig. B.3.2A)** compared to 10 μM with DKM 2-90**.** Adding an N-benzyl group to DKM 2-90 with JNS 1-40 improved potency towards PPP2R1A by 16-fold with an IC50 of 630 nM **(Fig. 3.5A)**. We thus moved forward with further characterization of JNS 1-40. Both *in vitro* and *in situ* isoTOP-ABPP analysis showed that JNS 1-40 selectively targets C377 of PPP2R1A in both 231MFP complex proteome and cells, and is the only target exhibiting an isotopically light to heavy ratio >5 **(Fig. 3.5B; Fig. B.3.2B)**. Much like withaferin A, we showed that JNS 1-40 activated PP2A activity *in vitro* with purified PP2A complex proteins with wild-type PPP2R1A, but not with the PPP2R1A C377A mutant protein **(Fig. 3.5C)**. Similarly, JNS 1-40 treatment in 231MFP cells significantly reduced phosphorylated AKT levels and impaired proliferation and survival **(Fig. 3.5D)**. We also showed that the anti-proliferative effects observed with JNS 1-40 are attenuated in siPPP2R1A 231MFP cells compared to siControl cells **(Fig. B.3.2C)**. Daily treatment of mice with JNS 1-40 (50 mg/kg ip) *in vivo* initiated 15 days after 231MFP tumor xenograft injection significantly attenuated tumor growth **(Fig. 3.5G)**. Daily treatment with JNS 1-40 for >30 days did not cause any overt toxicity or body weight loss, suggesting that this compound is well tolerated *in vivo* (data not shown).

3.4 Conclusion

In conclusion, we show here that isoTOP-ABPP platforms can be used to identify the druggable hotspots targeted by bioactive covalently-acting natural products, which can in-turn be pharmacologically interrogated with more synthetically tractable covalent ligands. In this study, we reveal a unique and novel druggable hotspot targeted by withaferin A, in which this natural product targets C377 of PPP2R1A, through which withaferin A activates the tumor suppressor PP2A to cause anti-proliferative effects in breast cancer cells. We further show that withaferin A treatment leads to inactivation of AKT signaling, one of the primary substrates of PP2A. We identify DKM 2-90 as an initial covalent ligand lead which we further optimized to generate JNS 1-40, a ligand with nanomolar potency which selectively targets C377 of PPP2R1A both *in vitro* and *in situ* to recapitulate the effects observed with withaferin A in activating PP2A, inactivating AKT signaling, and impairing breast cancer pathogenicity. Previous studies have identified various additional targets of withaferin A, including vimentin, KEAP1, Hsp90, and IKK [85,86,88,91]. Our studies do not rule out that these and other protein targets may also play important roles in the anti-proliferative and pathogenic impairments observed with withaferin A, but instead reveal C377 of PPP2R1A as an additional target of this natural product and a unique druggable hotspot that can be targeted to activate PP2A and impair breast cancer pathogenicity. While we and many other groups have used ABPP platforms to identify targets of covalently-

acting natural products [35,42,77–79,92], we show here that this process can be coupled with covalent ligand discovery approaches, yielding much more synthetically tractable small-molecules that do not require significant synthetic or isolation efforts, that recapitulate the effects observed with complex natural products. Overall, our study demonstrates the utility of using isoTOP-ABPP platforms to map the reactivity and targets of covalently-acting natural products towards identifying their therapeutic mechanism of action and discovering druggable hotspots that can be interrogated by alternate pharmacological scaffolds for future drug discovery efforts.

3.5 Methods

3.5.1 Chemicals.

Withaferin A was obtained from Sigma. IAyne was obtained from CHESS Gmbh. Heavy and light TEV-biotin tags were synthesized per previously described methods [31]. The synthesis for most of our cysteine-reactive ligand library has been described previously [93]. New ligands screened in this paper that were not previously described are in **Supplemental Methods**. All compounds in our library were confirmed to be >95 % pure.

3.5.2 Cell Culture.

The 231MFP cells were obtained from Prof. Benjamin Cravatt and were generated from explanted tumor xenografts of MDA-MB-231 cells. These cells have been previously characterized as a more aggressive variant of the MDA-MB-231 cells [94,95]. HCC38 and MCF7 cells were obtained from the American Type Culture Collection. 231MFP cells were cultured in L15 medium containing 10% FBS, supplemented with 1% glutamine (200 mM stock), and maintained at 37°C with 0% CO_2. HCC38 and MCF7 cells were cultured in RPMI medium containing 10% FBS, supplemented with 1% glutamine (200 mM stock), and maintained at 37°C with 5% CO_2. Unless otherwise specified, all cell culture materials were purchased from Gibco. Withaferin A, DKM 2-90, JNS 1-40, and all other covalent ligands were dissolved in DMSO and final DMSO concentrations in cells were 0.1%.

3.5.3 Cellular Phenotype Studies.

Cell survival and proliferation assays were performed as previously described using Hoechst 33342 dye (Invitrogen) according to manufacturer's protocol [96]. Cells were seeded into 96-well plates (40,000 for survival and 20,000 for proliferation) in a volume of 150 µl and allowed to adhere overnight. Cells were treated with an additional 50 µL of media containing 1:250 dilution of 1000x compound stock in DMSO. Medium was removed from each well and 100 µl of staining solution containing 10% formalin and Hoechst 33342 dye was added to each well and incubated for 15 min in the dark at room temperature. After incubation, staining solution was removed and wells were washed with PBS before imaging. Studies with HCC38 cells were also performed as above but were seeded with 20,000 cells for survival and 10,000 cells for proliferation.

3.5.4 Western Blotting.

Antibodies to vinculin, phospho-Akt (Ser473), and Akt were obtained from Cell Signaling Technology and proteomes were blotted per recommended manufacturer's' procedure. Cells were lysed in lysis buffer (containing the following: 20 mM Tris pH 7.5, 150 mM NaCl, 1 mM EDTA, 1 mM EGTA, 1% Triton X-100, 2.5 mM pyrophosphate, 50 mM NaF, 5 mM β-glycero-

phosphate, 1 mM Na3VO4, 50 nM calyculin A (EMD Millipore), and protease inhibitors (Roche)). Lysate was incubated on a rotator at 4°C for 30 min, and insoluble material was removed via centrifugation at max speed for 10 min. Proteins were resolved by SDS/PAGE and transferred to nitrocellulose membranes using the iBlot system (Invitrogen). Blots were blocked with 5% nonfat milk in Tris-buffered saline containing Tween 20 (TBST) solution for 1 hour at room temperature, washed in TBST, and probed with primary antibody diluted in recommended diluent per manufacturer overnight at 4°C. Following washes with TBST, the blots were incubated in the dark with secondary antibodies purchased from Rockland and used at 1:10 000 dilution in 5% nonfat milk in TBST at room temperature. Blots were visualized using an Odyssey Li-Cor scanner after additional washes.

3.5.5 Purification of PPP2R1A and PPP2R2A Subunits.
Wild-type mammalian expression plasmids with C-terminal FLAG tag were purchased from Origene (PPP2R1A: RC200056; PPP2R2A, MR207137). The PPP2R1A C337A mutant was generated with Agilent QuickChange Lightning site-directed mutagenesis kit according to manufacturer's instructions. HEK293T cells (ATCC CRL-11268) were grown to 60% confluency in DMEM (Corning) supplemented with 10% FBS (Corning) and 2mM L-glutamine (Life Technologies) and maintained at 37˚C with 5% CO_2. Immediately prior to transfection, media was replaced with DMEM + 5% FBS. Each plate was transfected with 20 μg of overexpression plasmid with 100 μg PEI (Sigma). After 48hrs cells were collected in TBS, lysed by sonication, and batch bound with anti-DYKDDDDK resin (GenScript) for 1hr. Lysate and resin was loaded onto a gravity flow column and washed, followed by elution with 250ng/uL 3xFLAG peptide (ApexBio A6001). Purity and concentration were verified by PAGE, UV/Spectroscopy, and BCA assay.

3.5.6 In Vitro PP2A Activity Assay.
Recombinant PPP2CA (40 nM, Origene TP301334) was combined with pulled-down WT or mutant PPP2R1A (50 nM) as well as PPP2R2A (50 nM) and incubated with 10 μM withaferin A, JS 1-40, or vehicle for 30 min at RT in TBS. Activity was assayed by addition of 60 μM Thr phosphopeptide (KRpTIRR, Millipore, 12-219) at 37° C for 25 min, and free phosphate was detected colorimetrically by malachite green kit (Cayman 10009325) per manufacturer's instructions.

3.5.7 PPP2R1A Knockdown Studies.
PPP2R1A was transiently knocked down with siRNA using previously described methods [97]. siRNA for a scrambled RNA oligonucleotide control and pooled RNA oligonucleotides targeting PPP2R1A were purchased from Dharmacon.

3.5.8 IsoTOP-ABPP.
IsoTOP-ABPP studies were done as previously reported [31,47,79]. Cells were lysed by probe sonication in PBS and protein concentrations were measured by BCA assay. Proteome samples diluted in PBS (4 mg of proteome per biological replicate) were treated with a covalently-acting small-molecule or vehicle for 30 min at 37°C. Then, IAyne labeling (100 mM) was performed for 1 h at room temperature. CuAAC was used by sequential addition of tris(2-carboxyethyl)phosphine (1 mM, Sigma), tris[(1-benzyl-1H-1,2,3-triazol-4-yl)methyl]amine (34 μM, Sigma), copper (II) sulfate (1 mM, Sigma), and biotin-linker-azide, the linker functionalized

with a TEV protease recognition sequence along with an isotopically light or heavy valine for treatment of control or treated proteome, respectively. After click reactions, proteomes were precipitated by centrifugation at 6500 x *g*, washed in ice-cold methanol, combined in a 1:1 control/treated ratio, washed again, then denatured and resolubilized by heating in 1.2% SDS/PBS to 80°C for 5 minutes. Insoluble components were precipitated by centrifugation at 6500 x *g* and soluble proteome was diluted in 5 ml 0.2% SDS/PBS. Labeled proteins were bound to avidin-agarose beads (170 µl resuspended beads/sample, Thermo Pierce) while rotating overnight at 4°C. Bead-linked proteins were enriched by washing three times each in PBS and water, then resuspended in 6 M urea/PBS (Sigma) and reduced in TCEP (1 mM, Sigma), alkylated with iodoacetamide (18 mM, Sigma), then washed and resuspended in 2 M urea and trypsinized overnight with 0.5 µg/µl sequencing grade trypsin (Promega). Tryptic peptides were eluted off. Beads were washed three times each in PBS and water, washed in TEV buffer solution (water, TEV buffer, 100 µM dithiothreitol) and resuspended in buffer with Ac-TEV protease and incubated overnight. Peptides were diluted in water and acidified with formic acid (1.2 M, Spectrum) and prepared for analysis.

3.5.9 MS Analysis.

Peptides from all proteomic experiments were pressure-loaded onto a 250 mm inner diameter fused silica capillary tubing packed with 4 cm of Aqua C18 reverse-phase resin (Phenomenex # 04A-4299) which was previously equilibrated on an Agilent 600 series HPLC using gradient from 100% buffer A to 100% buffer B over 10 min, followed by a 5 min wash with 100% buffer B and a 5 min wash with 100% buffer A. The samples were then attached using a MicroTee PEEK 360 µm fitting (Thermo Fisher Scientific #p-888) to a 13 cm laser pulled column packed with 10 cm Aqua C18 reverse-phase resin and 3 cm of strong-cation exchange resin for isoTOP-ABPP studies. Samples were analyzed using an Q Exactive Plus mass spectrometer (Thermo Fisher Scientific) using a 5-step Multidimensional Protein Identification Technology (MudPIT) program, using 0 %, 25 %, 50 %, 80 %, and 100 % salt bumps of 500 mM aqueous ammonium acetate and using a gradient of 5-55 % buffer B in buffer A (buffer A: 95:5 water:acetonitrile, 0.1 % formic acid; buffer B 80:20 acetonitrile:water, 0.1 % formic acid). Data was collected in data-dependent acquisition mode with dynamic exclusion enabled (60 s). One full MS (MS1) scan (400-1800 m/z) was followed by 15 MS2 scans (ITMS) of the nth most abundant ions. Heated capillary temperature was set to 200º C and the nanospray voltage was set to 2.75 kV.

Data was extracted in the form of MS1 and MS2 files using Raw Extractor 1.9.9.2 (Scripps Research Institute) and searched against the Uniprot mouse database using ProLuCID search methodology in IP2 v.3 (Integrated Proteomics Applications, Inc) [98]. Cysteine residues were searched with a static modification for carboxyaminomethylation (+57.02146) and up to two differential modifications for methionine oxidation and either the light or heavy TEV tags (+464.28596 or +470.29977, respectively). Peptides were required to have at least one tryptic end and to contain the TEV modification. ProLUCID data was filtered through DTASelect to achieve a peptide false-positive rate below 1%. Only those probe-modified peptides that were evident in two out of three biological replicates were interpreted for their isotopic light to heavy ratios. MS1 peak shapes were confirmed to be of good quality for interpreted peptides. Targets of covalently-acting molecules are defined here as targets that showed >4 light to heavy ratios across all three biological replicates.

3.5.10 Gel-Based ABPP.

Gel-based ABPP methods were performed as previously described [43,93]. Recombinant pure human proteins were purchased from Origene. Pure proteins (0.2 mg) were pre-treated with DMSO or covalently-acting small-molecules for 30 min at 37ºC in an incubation volume of 50 µL PBS, and were subsequently treated with IAyne (10 µM final concentration) for 30 min at room temperature. CuAAC was performed to append rhodamine-azide (1 mM final concentration) onto IAyne probe-labeled proteins. The samples were separated by SDS/PAGE and scanned using a ChemiDoc MP (Bio-Rad Laboratories, Inc). Inhibition of target labeling was assessed by densitometry using ImageJ.

3.6 Author Contributions.

EAG and CCW are co-first authors and contributed equally to this paper; EAG, CCW, JNS, JIK, and DKN performed experiments, analyzed and interpreted data, and wrote the paper. JNS, LAB, TRH, DKM synthesized compounds and chemical reagents for this study.

3.7 Acknowledgements

We thank the members of the Nomura Research Group for critical reading of the manuscript. This work was supported by grants from the National Institutes of Health (R01CA172667 and T32 GM066698 Training Grant for CCW and EAG), American Cancer Society Research Scholar Award (RSG14-242-01-TBE), and Department of Defense Breast Cancer Research Program Breakthroughs Award (CDMRP W81XWH-15-1-0050).

3.8 Figures

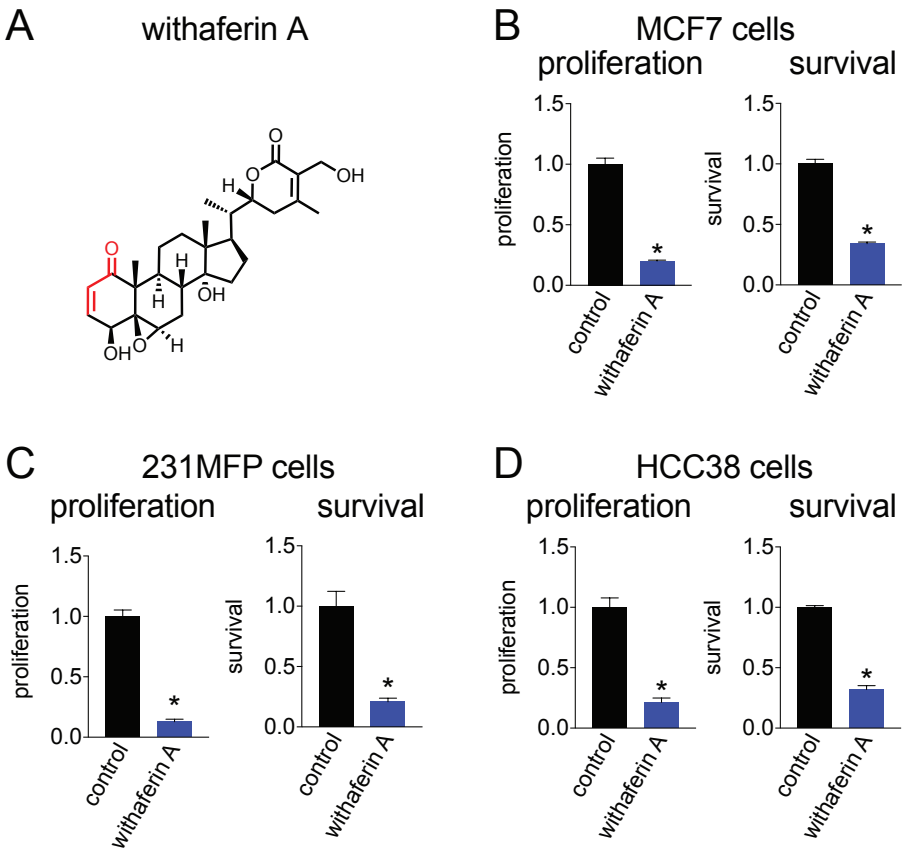

Figure 3.1: Withaferin A impairs breast cancer cell pathogenicity.
(A) Structure of withaferin A. Reactive Michael acceptor is indicated in red. (B) Withaferin A (10 μM) impairs cell proliferation and serum-free cell survival after 48 h in MCF7, 231MFP, and HCC38 cells compared to DMSO-treated controls. Data are presented as mean ± sem, n=5. Significance is shown as *p<0.05 compared to vehicle-treated controls.

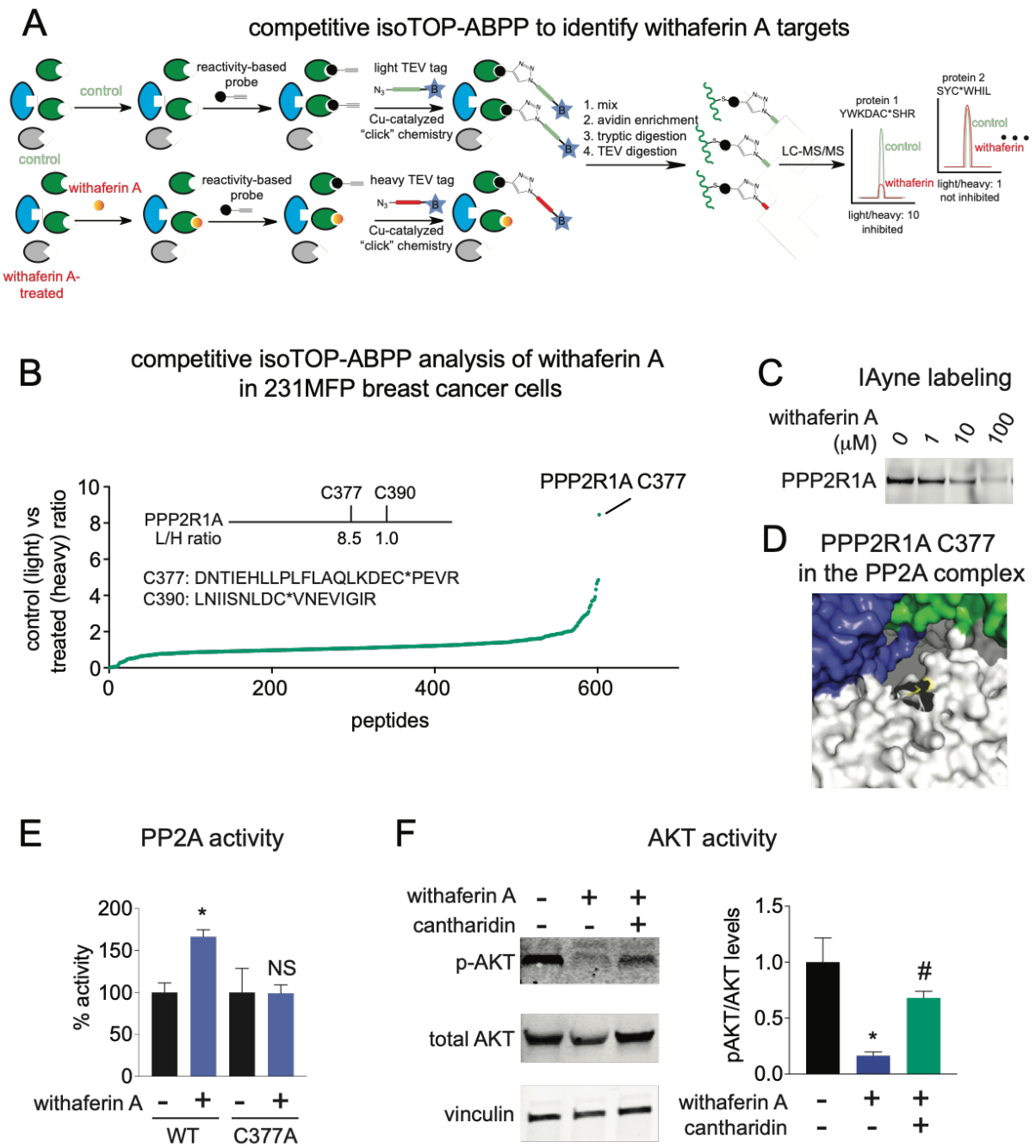

Figure 3.2: Using isoTOP-ABPP platforms to map proteome-wide targets of withaferin A in breast cancer cells.

(A) Competitive isoTOP-ABPP method. We mapped the cysteine-reactivity of withaferin A by pre-incubating withaferin A (10 μM) for 30 min in 231MFP breast cancer cell proteomes, prior to labeling with the cysteine-reactive iodoacetamide-alkyne (IAyne) probe (100 μM, 30 min). Probe labeled proteins were then tagged with an isotopically light (for control) or heavy (for withaferin A-treated) biotin-azide tag bearing a TEV protease recognition site by CuAAC. Control and treated proteomes were then mixed in a 1:1 ratio, probe labeled proteins were avidin-enriched and tryptically digested, probe-labeled tryptic peptides were avidin-enriched again, and released by TEV protease and analyzed by quantitative proteomic methods and light to heavy peptide ratios were quantified. **(B)** Competitive isoTOP-ABPP analysis of withaferin A cysteine-reactivity in 231MFP breast cancer cell proteomes *in vitro*. Light to heavy ratios of ~1 indicate peptides that were labeled by IAyne, but not bound by withaferin A. We designate light to heavy ratios of >5 as targets that were bound by withaferin A. Also shown are

the peptide sequences and sites of modification of probe-modified peptides identified for PPP2R1A and the light to heavy ratios of C377 and C390 on PPP2R1A. **(C)** Validation of PPP2R1A as a target of withaferin A. Withaferin A was pre-incubated with pure human PPP2R1A protein followed by IAyne. Probe-labeled proteins conjugated to rhodamine-azide by CuAAC and analyzed by SDS/PAGE and in-gel fluorescence. **(D)** Crystal structure of PP2A complex showing C377 of PPP2R1A (shown in white), the catalytic subunit shown in blue, and another regulatory subunit shown in green. PDB structure used is 2IAE. **(E)** PP2A activity assay with PP2A complex proteins PPP2R1A wild-type (WT) or C377A mutant and PPP2R2A and PPP2CA subunits measuring phosphate release from a PP2A substrate phosphopeptide. This PP2A complex was treated *in vitro* with DMSO or withaferin A (10 μM) for 30 min prior to initiation of the assay. **(F)** Withaferin A (10 μM, 4 h) treatment significantly reduces phospho-AKT levels in 231MFP breast cancer cells and this reduction is rescued by cotreatment with cantharidin (10 μM, 4 h). Data in **(B)** is average ratios from n=3. Gel in **(C)** is a representative gel from n=3. Data in **(E-F)** are presented as mean ± sem, n=3. Significance expressed as *p<0.05 compared to vehicle-treated controls and #p<0.05 compared to withaferin A-treated control. NS refers to not significant compared to the vehicle-treated C377A PPP2R1A group. Raw isoTOP-ABPP proteomic data can be found in **Table B.2.2** and **B.2.8.** Withaferin A *in situ* isoTOP-ABPP analysis can be found in **Fig B.3.1**. **Fig. 3.2** is associated with **Fig. B.3.1** and **Table B.2.2**

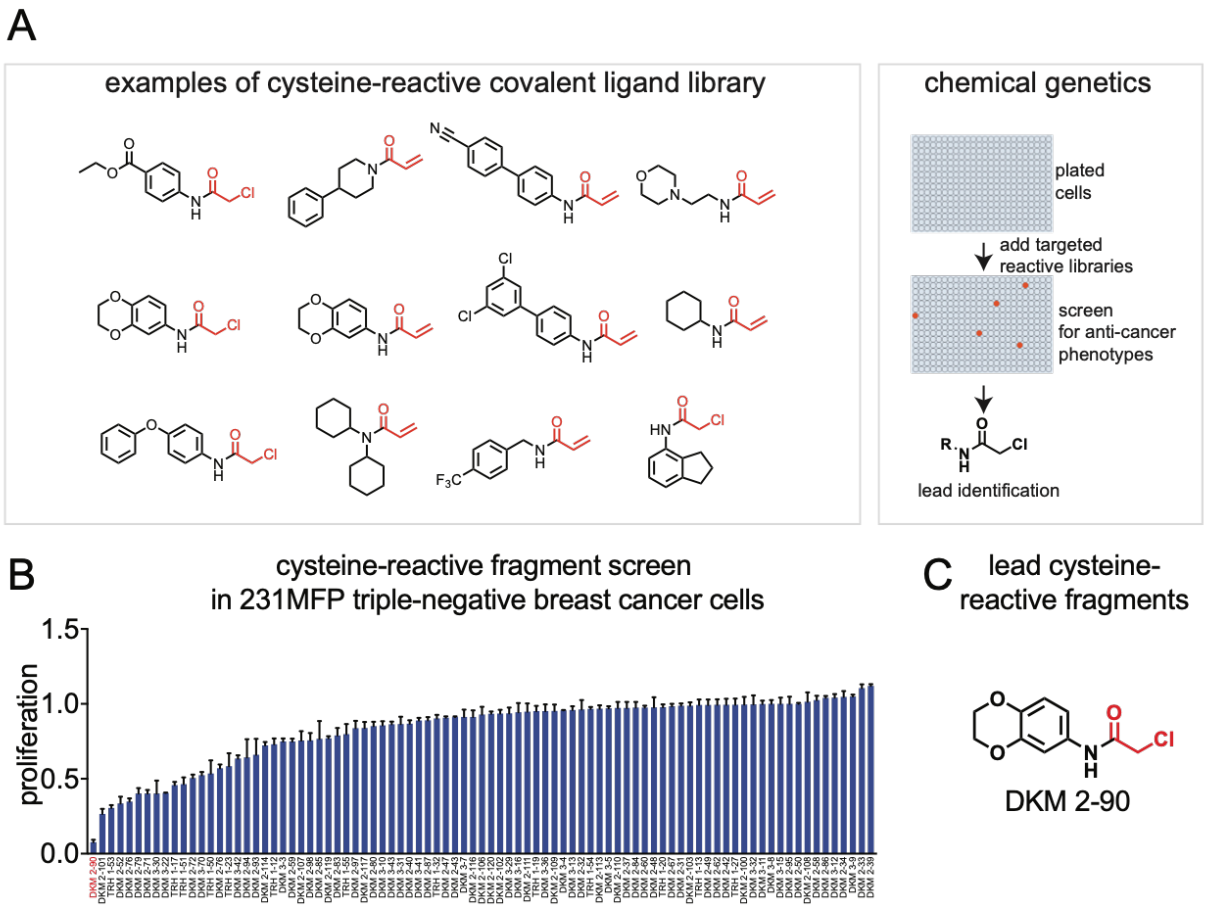

Figure 3.3: Screening of covalent ligand libraries in breast cancer cells.
(A) Coupled screening of a cysteine-reactive covalent ligand library in 231MFP breast cancer cells with competitive isoTOP-ABPP platforms to identify anti-cancer lead compounds, targets, and ligandable hotspots within these targets. **(B)** We screened a cysteine-reactive fragment library consisting of acrylamides and chloroacetamides in 231MFP breast cancer cells (100 μM) to identify any leads that significantly impaired 231MFP breast cancer cell proliferation. Cell viability was assessed 48 h after treatment by Hoescht staining. **(C)** Shown is the structure of the lead covalent ligand DKM 2-90. Reactive chloroacetamide warheads are designated in red. Data in **(B)** are presented as mean ± sem, n=3. Significance expressed as *p<0.05 compared to vehicle-treated controls.

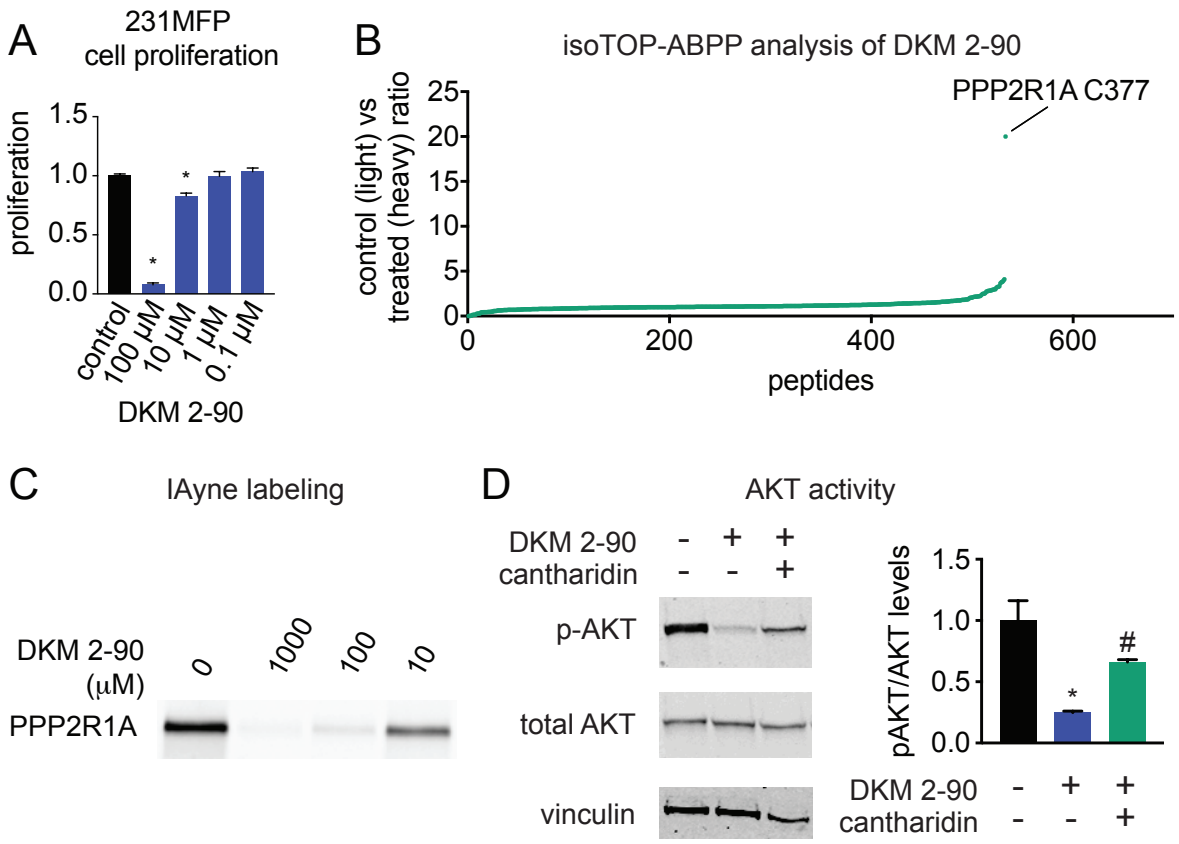

Figure 3.4: Target identification of DKM 2-90 using competitive isoTOP-ABPP platforms.
(A) Dose-responsive effects of DKM 2-90 on cell proliferation in 231MFP breast cancer cells. 231MFP cells were treated with DMSO or DKM 2-90 and proliferation was assessed 48 h after treatment by Hoechst staining. **(B)** IsoTOP-ABPP analysis of DKM 2-90 in 231MFP cell proteomes *in vitro*. 231MFP proteomes were pre-treated with DMSO or DKM 2-90 (100 μM) for 30 min prior to labeling proteomes with IAyne (100 μM) and subjected to the isoTOP-ABPP method. A light to heavy ratio of 1 indicates that the probe-labeled cysteine-bearing peptide was not bound by the covalent ligand, whereas a ratio >5 indicates bound sites. **(C)** Competition of DKM 2-90 against IAyne labeling of pure human PPP2R1A protein. DKM 2-90 was pre-incubated with pure PPP2R1A protein for 30 min prior to labeling with IAyne (100 μM) for 30 min. Rhodamine-azide was appended on by copper-catalyzed azide-alkyne cycloaddition and proteins were separated by SDS/PAGE and analyzed by in-gel fluorescence. **(D)** Levels of total and phosphorylated AKT (p-AKT) and vinculin as a loading control in 231MFP breast cancer cells. 231MFP cells were treated with vehicle, DKM 2-90 (100 μM), or cantharidin (10 μM) and DKM 2-90 (100 μM) for 5 h. Proteins were blotted for p-AKT, total AKT, and vinculin loading control. All data shown represents n=3-5/group. Raw data for **(B)** can be found in **Table B.2.4** and **B.2.10.** IsoTOP-ABPP analysis of DKM 2-90 *in situ* can be found in **Fig. B.3.1. Fig. 3.4** is associated with **Fig. B.3.1** and **Table B.2.4**.

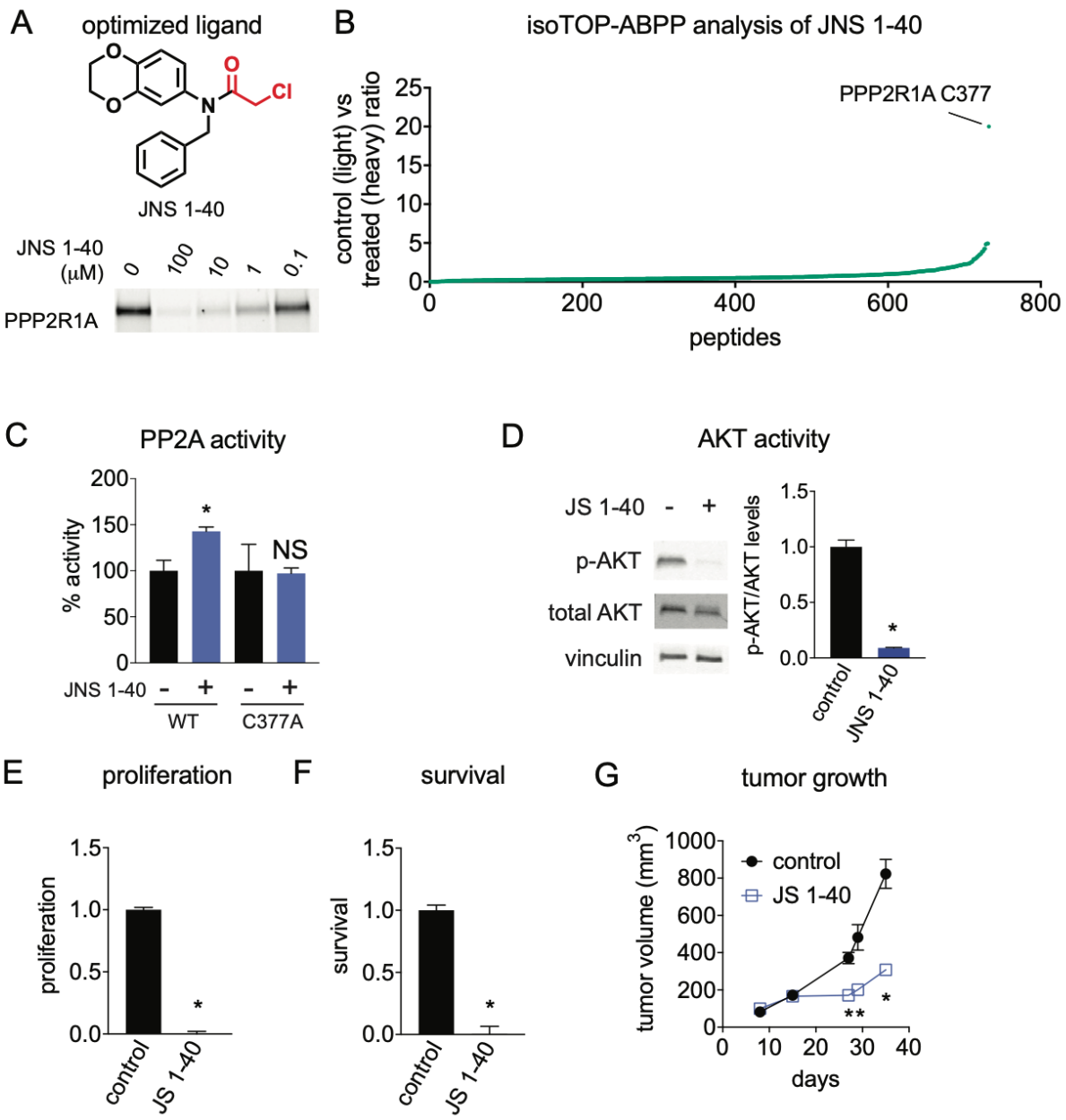

Figure 3.5: Optimized covalent ligand JNS 1-40 selectively targets C377 of PPP2R1A to activate PP2A activity and impair breast cancer pathogenicity.
(A) Structure of JNS 1-40 and gel-based ABPP analysis of its potency against PPP2R1A. Reactive chloroacetamide is shown in red. Pure human PPP2R1A was pre-treated with DMSO or JNS 1-40 for 30 min at 37 ºC prior to IAyne labeling for 30 min at room temperature. Probe-labeled proteins were appended to rhodamine-azide by CuAAC and analyzed by SDS/PAGE and in-gel fluorescence. **(B)** IsoTOP-ABPP analysis of JNS 1-40 treatment in 231MFP cells. 231MFP proteomes were treated *in vitro* with DMSO or JNS 1-40 (100 μM) for 30 min prior to IAyne labeling for 1 h and subjected to the isoTOP-ABPP method. Light to heavy ratios of probe-modified peptides are shown. **(C)** PP2A activity assay with PP2A complex proteins PPP2R1A wild-type (WT) or C377A mutant and PPP2R2A and PPP2CA subunits measuring phosphate release from a PP2A substrate phosphopeptide. This PP2A complex was treated *in vitro* with DMSO or JNS 1-40 (100 μM) for 30 min prior to initiation of the assay. **(D)** Levels of total and phosphorylated AKT (p-AKT) and vinculin as a loading control in 231MFP breast cancer cells. 231MFP cells were treated with vehicle or JNS 1-40 (100 μM) (100 μM) for 75 min. **(E, F)** JS 1-40 (100 μM) impairs cell proliferation and serum-free cell survival after 48 h in 231MFP cells. **(G)** 231MFP tumor xenograft

growth in immune-deficient SCID mice. 231MFP cells were subcutaneously injected into mice. Daily once per day treatment with vehicle or JNS 1-40 (50 mg/kg ip) was initiated 15 days after tumor implantation. Data in **(C-G)** are presented as mean ± sem, n=3-7/group. Data in **(B)** is average ratios from n=3. Significance is shown as *$p<0.05$ compared to vehicle-treated controls. NS indicates not significant ($p>0.05$) compared to the vehicle-treated C377A PPP2R1A group. Raw proteomic data can be found in **Table B.2.6** and **B.2.12**. IsoTOP-ABPP analysis of JNS 1-40 *in situ* can be found in **Fig. B.3.2**. **Fig. 5** is associated with **Fig. B.3.2** and **Table B.2.6.**

Chapter 4: Covalent Ligand Screening Uncovers a RNF4 E3 Ligase Recruiter for Targeted Protein Degradation Applications*

4.1 Abstract

Targeted protein degradation has arisen as a powerful strategy for drug discovery allowing the targeting of undruggable proteins for proteasomal degradation. This approach most often employs heterobifunctional degraders consisting of a protein-targeting ligand linked to an E3 ligase recruiter to ubiquitinate and mark proteins of interest for proteasomal degradation. One challenge with this approach, however, is that only few E3 ligase recruiters currently exist for targeted protein degradation applications, despite the hundreds of known E3 ligases in the human genome. Here, we utilized activity-based protein profiling (ABPP)-based covalent ligand screening approaches to identify cysteine-reactive small-molecules that react with the E3 ubiquitin ligase RNF4 and provide chemical starting points for the design of RNF4-based degraders. The hit covalent ligand from this screen reacted with either of two zinc-coordinating cysteines in the RING domain, C132 and C135, with no effect on RNF4 activity. We further optimized the potency of this hit and incorporated this potential RNF4 recruiter into a bifunctional degrader linked to JQ1, an inhibitor of the BET family of bromodomain proteins. We demonstrate that the resulting compound CCW 28-3 is capable of degrading BRD4 in a proteasome- and RNF4-dependent manner. In this study, we have shown the feasibility of using chemoproteomics-enabled covalent ligand screening platforms to expand the scope of E3 ligase recruiters that can be exploited for targeted protein degradation applications.

4.2 Introduction

Targeted protein degradation is a groundbreaking drug discovery approach for tackling the undruggable proteome by exploiting the cellular protein degradation machinery to selectively eliminate target proteins [99,100]. This technology most often involves the utilization of heterobifunctional degrader molecules consisting of a substrate-targeting ligand linked to an E3 ligase recruiter. These degraders are capable of recruiting E3 ligases to specific protein targets to ubiquitinate and mark targets for degradation in a proteasome-dependent manner. As functional inhibition of the target is not necessary for degrader efficacy, this strategy has the potential to target and degrade any protein in the proteome for which there exists a ligand. However, while there are ~600 different E3 ligases, only a few E3 ligases that have been successfully exploited in such a strategy, including small-molecule recruiters for cereblon, VHL, MDM2, and cIAP [100,101]. Identifying facile strategies for discovering ligands that bind to E3 ligases remains crucial for expanding the set of E3 ligase recruiters that can be utilized for targeted protein degradation of a given target of interest and ultimately expand the applicability of this modality to any protein that can be subjected to proteasomal degradation regardless of subcellular localization or tissue-specific expression.

Activity-based protein profiling (ABPP) has arisen as a powerful platform for ligand discovery against targets of interest, including proteins commonly considered as undruggable [47,102–107]. ABPP utilizes reactivity-based chemical probes to map proteome-wide reactive and ligandable hotspots directly in complex biological systems [31,108]. When used in a competitive

*Part of the work presented in this chapter has been previously published in the following manuscript: Ward, C. C. *et al*. Covalent Ligand Screening Uncovers a RNF4 E3 Ligase Recruiter for Targeted Protein Degradation Applications. *ACS Chem. Biol*. **14**, 2430–2440 (2019).

manner, covalently-acting small-molecule libraries can be screened for competition against the binding of reactivity-based probes to facilitate covalent ligand discovery against proteins of interest [42,47,80,102–104,106,109].

4.3 Results and Discussion

4.3.1 Screening Unveils a Lead RNF4 ligand

In order to discover covalent ligands that may react with E3 ubiquitin ligases, we first investigated whether representative commercially available E3 ligases -- MDM2, RNF4, and UBE3A -- could be labeled by the cysteine-reactive tetramethylrhodamine-5-iodoacetamide dihydroiodide (IA-rhodamine) reactivity-based probe *in vitro*. We observed IA-rhodamine labeling of all three E3 ligases in a dose-responsive manner **(Fig. 1A)**. While previous studies have already uncovered MDM2 and UBE3A small-molecule modulators [110–112], no chemical tools exist for the E3 ubiquitin ligase RNF4, which recognizes SUMOylated proteins and ubiquitinates these proteins for subsequent proteasomal degradation [113,114]. We thus focused our efforts on developing a ligand for RNF4 as E3 ligase recruitment module for heterbifunctional degraders.

In search of RNF4-targeting ligands, we screened a cysteine-reactive covalent ligand library against IA-rhodamine labeling of pure human RNF4 using gel-based ABPP **(Fig. 4.1B; Table C.2.1)**. We identified several potential hits from this screen, including TRH 1-74, YP 1-44, DKM 2-76, TRH 1-23, and TRH 1-163. From these, YP 1-44, TRH 1-163, and TRH 1-23 showed reproducible and dose-responsive inhibition of IA-rhodamine labeling of RNF4 **(Fig. 4.1D, Fig. C.3.1)**. Based on corresponding silver staining of RNF4 in these experiments, we found that TRH 1-163 may be causing protein precipitation. Based on gel-based ABPP analysis of general cysteine-reactivity in 231MFP lysates, YP 1-44 was much less selective compared to TRH 1-23 **(Fig. C.3.1)**. Thus, TRH 1-23 appeared to be the most promising RNF4 hit **(Fig. 4.1D)**.

4.3.2 Optimization of a Nonfunctional RNF4 Recruiter Molecule

We next sought to identify the site-of-modification of TRH 1-23 within RNF4. We performed liquid chromatography-tandem mass spectrometry (LC-MS/MS) analysis of tryptic digests from TRH 1-23-treated purified RNF4 protein and found that TRH 1-23 covalently modified either, but not both, of the two zinc-coordinating cysteines C132 and C135 in the RING domain of RNF4 **(Fig. 4.2A, 2B)**. In support of its utility as a functional RNF4 recruiter, we wanted to see if TRH 1-23 had any effect upon RNF4 autoubiquitination activity, since previous studies had shown that mutation of both cysteines to serines inhibited RNF4 function [115–117]. Surprisingly, TRH 1-23 treatment did not inhibit RNF4 autoubiquitination activity in an *in vitro* reconstituted assay **(Fig. 4.2C)**.

While a promising non-functional ligand against RNF4, we considered the potency of TRH 1-23 with a 50% inhibitory concentration (IC50) in the double digit μM range in competitive ABPP suboptimal for usage as an efficient RNF4 recruiter. We thus synthesized several TRH 1-23 analogs and used gel-based ABPP to test their potency and structure-activity relationships against RNF4 **(Fig. 4.3A).** Among these analogs, we found CCW 16, with an *N*-benzyl and 4-methoxyphenoxyphenyl substitution on the chloroacetamide scaffold, to be among the most potent of the analogs with inhibition of IA-rhodamine labeling of RNF4 observed down to 1 μM. Further confirmatory studies revealed the IC50 for CCW 16 to be 1.8 μM **(Fig. 4.3B)**.

To better understand how CCW 16 was interacting with RNF4, we carried out covalent docking on CCW 16 bound to either C132 or C135 on a publicly available crystal structure of RNF4 (PDB: 4PPE) **(Fig. 4.3C)**. In this model, CCW 16 covalent binding to C132 caused a small portion of the backbone to rotate flipping the C132 sidechain out into a more surface accessible conformation. The CCW 16 ligand occupied a groove on the RNF4 surface consisting of side-chains R125, T129, and S131, with no obvious polar interactions between the ligands and the protein in this model. Interestingly, CCW 16 did not occupy the zinc-binding site, left the other three zinc-coordinating cysteines (C135, C159, and C162) unperturbed (**Fig. 4.3C**). In modeling CCW 16 covalently bound to C135, we observed a similar association with a surface groove of RNF4 occupying a region between Q161, S166, and P174. However, to accommodate the ligand, only a dihedral rotation of Cα & Cβ of C132 was predicted as necessary **(Fig. 4.3C)**. Both models indicate that zinc may still be bound by the three remaining cysteines in the site, while CCW 16 binds outside of the zinc-coordinating site. Since CCW 16 and TRH 1-23 are based on the same scaffold, these results may explain why modification by TRH 1-23 did not inhibit RNF4 autoubiquitination activity while the reported mutation of both cysteines 132 and 135 to serine leads to loss of activity.

4.3.3 Synthesis of a Covalently-acting RNF4-based Bifunctional Degrader – CCW 28-3

Based on the structure-activity relationships observed with TRH 1-23 analogs, the 4-methoxy group on CCW16 presented an ideal position for extending a linker to yield a RNF4-based degrader. To demonstrate that we could use CCW 16 as a potential RNF4 recruiter for targeted protein degradation applications, we synthesized CCW 28-3, a bifunctional degrader linking CCW 16 to the BET bromodomain family inhibitor JQ1 **(Fig. 4.4A)** [118]. CCW 28-3 was prepared in five steps from commercially available materials. Demethylation of 4-(4-methoxyphenoxy)aniline yielded 4-(4-aminophenoxy)phenol, which underwent reductive amination with benzaldehyde using sodium triacetoxyborohydride as the reducing agent to form CCW 22. Alkylation of phenolic moiety of CCW 22 with 4-(Boc-amino)butyl bromide and subsequent reaction with 2-choloracetyl chloride allowed functionalization of the RNF4 recruiter with a linker containing a "latent" reactive handle, a Boc-protected amino group. Boc deprotection by trifluoroacetic acid restored the functional primary amine which could then be reacted with a hydrolyzed free-acid form of JQ1 through amide coupling, yielding the bifunctional degrader CCW 28-3 as the final product **(Appendix C)**. It is noteworthy that the amide coupling reaction should be highly versatile and thus this synthetic scheme should be applicable for conjugating different protein-targeting ligands with carboxylic acid moiety onto our RNF4 recruiter.

4.3.4 Testing and Confirming the Efficacy and Mechanism of CCW 28-3

CCW 28-3 showed higher potency for RNF4 than CCW 16 with an IC50 of 0.54 μM in the competitive ABPP assay **(Fig. 4.4B)**. Compellingly, treatment with CCW 28-3 degraded BRD4 in a dose-responsive manner in 231MFP breast cancer cells **(Fig. 4.4C).** We also confirmed that CCW 28-3 did not inhibit RNF4 autoubiquitination activity **(Fig. 4.4D)**. CCW 28-3-mediated degradation of BRD4 was prevented by pre-treatment of cells with the proteasome inhibitor bortezomib (BTZ), JQ1 alone, as well as the E1 ubiquitin activating enzyme inhibitor TAK-243 **(Fig. 4.4E-4F)**. We next performed tandem mass tagging (TMT)-based quantitative proteomic profiling to determine the selectivity of changes in protein expression from CCW 28-3 treatment. We showed that BRD4 is one of the primary targets

degraded by CCW 28-3 in 231MFP breast cancer cells **(Fig. 4.4G; Table C.2.2)**. We also observed additional downregulated targets such as MT2A, ZC2HC1A, ZNF367, and ENSA, which may represent potential off-targets of JQ1 or transcriptional or post-translationally-driven changes in protein expression stemming from on or off-target effects of our RNF4-targeting ligand in 231MFP cells. Interestingly, CCW 28-3 treatment did not lead to BRD2 and 3 degradation. Previously reported JQ1-based degraders have shown varying levels of degradation of BET bromodomain family members with Cereblon and VHL-recruiting modules [72,119–121]. This study highlights the utility of having additional E3 ligase recruiters for tuning the efficacy and selectivity of degraders targeting a given protein of interest.

We next used isotopic tandem orthogonal proteolysis-enabled ABPP (isoTOP-ABPP) platforms to assess the proteome-wide selectivity of CCW 28-3 [31,47,102,104] **(Fig. C.3.2; Table C.2.3)**. We treated 231MFP cells with vehicle or CCW 28-3 and labeled the resulting proteomes with the cysteine-reactive *N*-hex-5-ynyl-2-iodo-acetamide (IA-alkyne) probe, followed by appendage of isotopically light or heavy TEV protease-cleavable biotin-azide tags onto probe-labeled proteins in vehicle and CCW 28-3-treated groups, respectively. Probe-modified peptides were enriched, eluted, and analyzed using previously described methods for isoTOP-ABPP [31,47,102,104]. Through this analysis, we demonstrated that out of 1114 total quantified probe-modified peptides only 7 potential off-targets of CCW 28-3 showed isotopically light to heavy ratios greater than 4. This ratio >4 indicated that the covalent ligand displaced IA-alkyne probe labeling at the particular site within the protein by >75 %. Most notably, none of these off-targets of CCW 28-3 are part of the ubiquitin-proteasome system indicating that the observed BRD4 degradation can likely be attributed to RNF4-based ubiquitination **(Fig. C.3.2; Table C.2.3).** Unfortunately, we were not able to observe the probe-modified peptide for RNF4 in this experiment likely due to its low abundance or labeling efficiency compared to other IA-alkyne labeled proteins. We were thus not able to confirm the degree of RNF4 occupancy by CCW 28-3 using isoTOP-ABPP.

We thus aimed to confirm engagement of RNF4 by CCW 28-3 *in situ* by other means. Since we had shown that CCW 16 was an optimized covalent ligand against RNF4, we synthesized an alkyne-functionalized derivative of CCW 16—CCW 36 **(Fig. C.3.3).** We then overexpressed RNF4 in HEK293T cells, treated these cells with vehicle or CCW 28-3, enriched for RNF4, and then labeled the enriched RNF4 with CCW 36, followed by CuAAC-mediated appendage of rhodamine-azide to visualize CCW 36 cysteine-reactivity of RNF4 by in-gel fluorescence. Intriguingly, we only observed ~30 % engagement of RNF4 by CCW 28-3 *in situ* at a concentration 10-times higher than the concentration where we observed significant BRD4 degradation **(Fig. C.3.3; Fig 4C, E, F)**. We attribute the low degree of target engagement to poor cell permeability of our yet-unoptimized RNF4-targeting ligand. Nonetheless, our results encouragingly suggest that only a modest degree of engagement of RNF4 is sufficient to facilitate the degradation of BRD4 with CCW 28-3.

Because CCW 28-3 was not completely selective and we were targeting conserved zinc-coordinating cysteines across the RING family of E3 ligases, we next sought to confirm the contributions of RNF4 to CCW 28-3-mediated degradation of BRD4. We compared CCW 28-3-mediated BRD4 degradation in wild-type (WT) and RNF4 knockout (KO) HeLa cells. Convincingly, CCW 28-3-mediated degradation of BRD4 observed in HeLa WT cells was not evident in RNF4 KO cells **(Fig. 4.4H; Fig. C.3.4)**. These data further support our claim that CCW 28-3 degrades BRD4 specifically through RNF4 recruitment.

4.4 Conclusion

In conclusion, our study demonstrates the feasibility of using ABPP-based covalent ligand screening in vitro to rapidly discover chemical entry points for targeting E3 ligases and that these covalent ligand hits can be identified, optimized, and incorporated into degraders for targeted protein degradation applications. While CCW 16 and CCW 28-3 are not yet completely selective for RNF4 and can only achieve fractional target engagement in cells, we demonstrate that we can still degrade BRD4 in a RNF4-dependent manner. We note that CCW 28-3 does not degrade BRD4 as well as other previously reported BRD4 degraders such as MZ1 that utilizes a VHL-recruiter linked to JQ1[119]. Future medicinal chemistry efforts can be employed to optimize the potency, selectivity, and cell permeability of CCW 16 for targeting RNF4 and to improve linker positioning and composition of CCW 28-3 to promote better degradation of protein substrates. Nonetheless, CCW 16 represents a novel, small-molecule E3 ligase recruiter for RNF4, beyond the four other E3 ligase recruiters that have been reported previously, targeting cereblon, VHL, MDM2, and cIAP [100]. Beyond RNF4, our study also highlights zinc-coordinating cysteines as a potential ligandable modality that can be targeted with cysteine-targeting covalent ligands. We believe that the approaches described here, and insights gained in this study can be utilized for future applications in expanding the scope of E3 ligase recruiters or modulators.

4.5 Methods

4.5.1 Covalent Ligand Library used in Initial Screen

The synthesis and characterization of many of the covalent ligands screened against RNF4 have been previously reported [80,102–104]. Synthesis of TRH 1-156, TRH 1-160, TRH 1-167, YP 1-16, YP 1-22, YP 1-26, YP 1-31, YP 1-44 have been previously reported [122–129]. The synthesis and characterization of covalent ligands that have not been reported are described in **Appendix C**

4.5.2 Gel-Based ABPP

Gel-based ABPP methods were performed as previously described [43,96,103,104]. Pure recombinant human RNF4 was purchased from Boston Biochem (K-220). RNF4 (0.25 µg) was diluted into 50 µL of PBS and 1µL of either DMSO (vehicle) or covalently acting small molecule to achieve the desired concentration. After 30 minutes at room temperature, the samples were treated with 250 nM IA-Rhodamine (Setareh Biotech, 6222, prepared in anhydrous DMSO) for 1 h at room temperature. Samples were then diluted with 20 µL of 4x reducing Laemmli SDS sample loading buffer (Alfa Aesar) and heated at 90 °C for 5 min. The samples were separated on precast 4-20% Criterion TGX gels (Bio-Rad Laboratories, Inc.). Fluorescent imaging was performed on a ChemiDoc MP (Bio-Rad Laboratories, Inc) inhibition of target labeling was assessed by densitometry using ImageJ.

4.5.3 LC-MS/MS analysis of RNF4

Purified RNF4 (10 µg) was diluted into 80 µL of PBS and treated for 30 min with DMSO or compound (50 µM). The DMSO control was then treated with light iodoacetamide (IA) while the compound treated sample was incubated with heavy IA for 1 h each at room temperature (100 µM, Sigma-Aldrich, 721328). The samples were precipitated by additional of 20 µL of 100% (w/v) TCA and combined pairwise before cooling to -80 C for one hour. The combined sample was then spun for at max speed for 20 min at 4 °C, supernatant is carefully removed and the sample is washed with ice cold 0.01 M HCl/90 % acetone solution. The sample was then

resuspended in 2.4 M urea containing 0.1 % Protease Max (Promega Corp. V2071) in 100 mM ammonium bicarbonate buffer. The samples were reduced with 10 mM TCEP at 60 °C for 30 min. The samples were then diluted 50% with PBS before sequencing grade trypsin (1 ug per sample, Promega Corp, V5111) was added for an overnight incubation at 37 °C. The next day the sample was centrifuged at 13200 rpm for 30 min. The supernatant was transferred to a new tube and acidified to a final concentration of 5 % formic acid and stored at -80 °C until MS analysis.

4.5.4 RNF4 ubiquitination assay

For *in vitro* auto-ubiquitination assay, 200 nM RNF4 in 15 µL ubiquitination assay buffer (50 mM Tris, 150mM NaCl, 5 mM $MgCl_2$, 5mM DTT, pH 7.4) was pre-incubated with DMSO vehicle or the covalently-acting compound for 30 min at room temperature. Subsequently, UBE1 (50 nM, Boston Biochem, E-305), UBE2D1 (400nM Boston Bichem, E2-615), Flag-ubiquitin (4000 nM, Boston Biochem, U-120) and ATP (200 µM) were added in ubiquitination assay buffer bring the total volume to 30 µL. The mixture was incubated at RT for 30 min before quenching with 10 µL of 4x Laemmli's buffer. Ubiquitination activity was measured by separation on an SDS-PAGE gel and western blotting as previously described.

4.5.5 Synthetic Methods and Characterization of Covalent Ligand Analogs and CCW 28-3 Degrader

Synthetic methods and characterization are detailed in **Appendix C**

4.5.6 Covalent Docking of CCW 16 in RNF4

For covalent docking, a crystal structure of human RNF4 (PDB code: 4PPE) was used [130]. This crystal structure was then prepared for docking utilizing Schrödinger's Maestro (2018-1) protein preparation [131]. Missing loops and side chains were added using PRIME and only A chain was utilized for docking purposes. Protonation was carried out to optimize H-bond assignments (assuming pH 7.0) and all waters were removed. A restrained minimization (<0.3Å) was then carried out to optimize the protein. A Zn coordinated by C132, C135, C159 & C162 was removed for docking purposes.

Prior to docking, CCW16 was prepared via LigPrep. To carry out covalent docking using Schrödinger's covalent docking [132], either C132 or C135 were defined as the center of the binding grid (within 20A). CCW 16 was selected as the ligand and the appropriate reactive residues were selected. A "nucleophilic substitution" was selected as the reaction type and calculations were carried out on a Linux workstation with Intel Xeon 2.4GHz processors running Red Hat 6.8 with 128GB memory.

4.5.7 Cell Culture

The 231MFP cells were obtained from Prof. Benjamin Cravatt and were generated from explanted tumor xenografts of MDA-MB-231 cells as previously described[94]. RNF4 knockout HeLa cells were purchased from EdiGene USA (CL0033025003A). RNF4 wild-type HeLa cells were provided by EdiGene USA or the UC Berkeley Cell Culture Facility. 231MFP cells were cultured in L-15 media (Corning) containing 10% (v/v) fetal bovine serum (FBS) and maintained at 37°C with 0% CO_2. HeLa cells were cultured in DMEM media (Corning) containing 10% (v/v) fetal bovine serum (FBS) and maintained at 37°C with 5% CO_2.

4.5.8 Cell based degrader assays

For assaying degrader activity, cells were seeded (500,000 for 231MFP cells, 300,000 for HeLa cells) into a 6 cm tissue culture dish (Corning) in 2.0 – 2.5 mL of media and allowed to adhere overnight. The following morning, media was replaced with complete media containing the desired concentration of compound diluted from a 1000x stock in DMSO. At the specified timepoint, cells were washed once with PBS on ice, before 150uL of lysis buffer was added to the plate (10 mM sodium phosphate, 150 mM NaCl, 0.1% SDS, 0.5% sodium deoxycholate, 1% Triton X100). The cells were incubated in lysis buffer for 5 min before scraping and transfer to microcentrifuge tubes. The lysates were then frozen at -80C or immediately processed for western blotting. To prepare for western blotting, the lysates were cleared with 20,000 g spin for 10 min and the resulting supernatants quantified via BCA assay. The lysates were normalized by dilution with PBS to match the lowest concentration lysate and appropriate amount of 4x Laemmli's reducing buffer added.

4.5.9 Western blotting

Antibodies to RNF4 (Proteintech, 17810-1-AP, 1:1000), GAPDH (Proteintech, 60004-1-IG, 1:5000), BRD4 (Abcam, Ab128874, 1:1000), and beta-actin (Proteintech Group Inc., 6609-1-IG, 1:7000) were obtained from the specified commercial sources and dilutions were prepared in 5% BSA/TBST at the specified dilutions. Proteins were resolved by SDS/PAGE and transferred to nitrocellulose membranes using the iBlot system (Invitrogen). Blots were blocked with 5 % BSA in Tris-buffered saline containing Tween 20 (TBST) solution for 1 h at room temperature, washed in TBST, and probed with primary antibody diluted in recommended diluent per manufacturer overnight at 4 °C. Following washes with TBST, the blots were incubated in the dark with secondary antibodies purchased from Ly-Cor and used at 1:10,000 dilution in 5 % BSA in TBST at room temperature. Blots were visualized using an Odyssey Li-Cor scanner after additional washes. If additional primary antibody incubations were required the membrane was stripped using ReBlot Plus Strong Antibody Stripping Solution (EMD Millipore, 2504), washed and blocked again before being re-incubated with primary antibody.

4.5.10 IsoTOP-ABPP chemoproteomic studies

IsoTOP-ABPP studies were done as previously reported [31,47,102,104]. Briefly, cells were lysed by probe sonication in PBS and protein concentrations were measured by BCA assay [133]. For *in situ* experiments, cells were treated for 90 min with either DMSO vehicle or covalently-acting small molecule (from 1000X DMSO stock) before cell collection and lysis. For *in vitro* experiments, proteome samples diluted in PBS (4 mg of proteome per biological replicate) were treated with a DMSO vehicle or covalently-acting small molecule for 30 min at room temperature. Proteomes were subsequently treated with IA-alkyne (100 μM, Chess GmbH, 3187) for 1 h at RT. CuAAC was performed by sequential addition of tris(2-carboxyethyl)phosphine (TCEP) (1 mM, Sigma), tris[(1-benzyl-1H-1,2,3-triazol-4-yl)methyl]amine (TBTA) (34 μM, Sigma), copper (II) sulfate (1 mM, Sigma), and biotin-linker-azide—the linker functionalized with a TEV protease recognition sequence as well as an isotopically light or heavy valine for treatment of control or treated proteome, respectively. After CuAAC, proteomes were precipitated by centrifugation at 6500 x g, washed in ice-cold methanol, combined in a 1:1 control/treated ratio, washed again, then denatured and resolubilized by heating in 1.2 % SDS/PBS to 80°C for 5 minutes. Insoluble components were precipitated by centrifugation at 6500 x g and soluble proteome was diluted in 5 ml 0.2% SDS/PBS. Labeled proteins were bound to avidin-agarose beads (170 μl resuspended

beads/sample, Thermo Pierce) while rotating overnight at 4°C. Bead-linked proteins were enriched by washing three times each in PBS and water, then resuspended in 6 M urea/PBS (Sigma) and reduced in TCEP (1 mM, Sigma), alkylated with iodoacetamide (IA) (18 mM, Sigma), then washed and resuspended in 2 M urea and trypsinized overnight with 2 ug/sample sequencing grade trypsin (Promega). Tryptic peptides were eluted off. Beads were washed three times each in PBS and water, washed in TEV buffer solution (water, TEV buffer, 100 μM dithiothreitol) and resuspended in buffer with Ac-TEV protease (Invitrogen) and incubated overnight. Peptides were diluted in water and acidified with formic acid (1.2 M, Spectrum) and prepared for analysis.

4.5.11 IsoTOP-ABPP Mass Spectrometry Analysis

Peptides from all chemoproteomic experiments were pressure-loaded onto a 250 μm inner diameter fused silica capillary tubing packed with 4 cm of Aqua C18 reverse-phase resin (Phenomenex # 04A-4299) which was previously equilibrated on an Agilent 600 series HPLC using gradient from 100% buffer A to 100% buffer B over 10 min, followed by a 5 min wash with 100% buffer B and a 5 min wash with 100% buffer A. The samples were then attached using a MicroTee PEEK 360 μm fitting (Thermo Fisher Scientific #p-888) to a 13 cm laser pulled column packed with 10 cm Aqua C18 reverse-phase resin and 3 cm of strong-cation exchange resin for isoTOP-ABPP studies. Samples were analyzed using an Q Exactive Plus mass spectrometer (Thermo Fisher Scientific) using a 5-step Multidimensional Protein Identification Technology (MudPIT) program, using 0 %, 25 %, 50 %, 80 %, and 100 % salt bumps of 500 mM aqueous ammonium acetate and using a gradient of 5-55 % buffer B in buffer A (buffer A: 95:5 water:acetonitrile, 0.1 % formic acid; buffer B 80:20 acetonitrile:water, 0.1 % formic acid). Data was collected in data-dependent acquisition mode with dynamic exclusion enabled (60 s). One full MS (MS1) scan (400-1800 m/z) was followed by 15 MS2 scans (ITMS) of the nth most abundant ions. Heated capillary temperature was set to 200 °C and the nanospray voltage was set to 2.75 kV.

Data was extracted in the form of MS1 and MS2 files using Raw Extractor 1.9.9.2 (Scripps Research Institute) and searched against the Uniprot human database using ProLuCID search methodology in IP2 v.3 (Integrated Proteomics Applications, Inc) [134]. Cysteine residues were searched with a static modification for carboxyaminomethylation (+57.02146) and up to three differential modifications for methionine oxidation and either the light or heavy TEV tags (+464.28596 or +470.29977, respectively). Peptides were required to have at least one tryptic end and to contain the TEV modification. ProLUCID data was filtered through DTASelect to achieve a peptide false-positive rate below 5%. Only those probe-modified peptides that were evident across all two out of three biological replicates were interpreted for their isotopic light to heavy ratios. Those probe-modified peptides that showed ratios >3 were further analyzed as potential targets of the covalently-acting small-molecule. For modified peptides with ratios >3, we filtered these hits for peptides were present in all three biological replicates. For those probe-modified peptide ratios >3, only those peptides with 3 ratios >3 were interpreted, and otherwise replaced with the lowest ratio. For those probe-modified peptide ratios >4, only those peptides with 3 ratios >4 were interpreted, and otherwise replaced with the lowest ratio. MS1 peak shapes of any resulting probe-modified peptides with ratios >3 were then manually confirmed to be of good quality for interpreted peptides across all biological replicates.

4.5.12 Vectors for RNF4 Overexpression

The pCMV6-Entry-RNF4 (C-term FLAG + Myc tag) vector was purchased from Origene (RC207273). The corresponding pCMV6-Entry-eGFP vector was constructed via Gibson Assembly with primers: GATCTGCCGCCGCGATCGCCatggtgagcaagggcgag, TCGAGCGGCCGCGTACGCGTcttgtacagctcgtccatgcc to amplify the eGFP ORF with desired overlaps, and ACGCGTACGCGGCCG, GGCGATCGCGGCGG to linearize the pCMV6-Entry backbone.

4.5.13 RNF4 Overexpression, Immunoprecipitation, and *in vitro* Probe Labeling Experiments

HEK293T cells were seeded to 30-40 % confluency in 10 cm dishes. The day of transfection, media was replaced with DMEM containing 2.5 % FBS. For transfection, 500 µL of Opti-MEM (Thermo Fisher) containing 10 µg of pCMV6-Entry-RNF4 or eGFP vector and 30 ug of polyethylenimine was added to the plate. Media was replaced 48 h later with identical media containing DMSO or CCW 28-3 (10 µM). After 1.5 h, cells were washed and harvested in PBS, resuspended in 500 µL PBS, and lysed by probe tip sonication at 15 % amplitude for 2 x 10 s. Lysates were cleared by centrifugation at 21,000 g for 20 min, and resulting supernatant was mixed with 30 µL of anti-FLAG resin (Genscript, L00432) and rotated at 4 ºC for 1 h. The beads were washed 3 x with 500 µL PBS containing 300 mM sodium chloride, before elution of FLAG-tagged proteins with 100 µL of 250 ng/µL 3 x FLAG peptide (APExBIO, A6001) in PBS.

For labeling of enriched RNF4 with CCW 36 to monitor *in situ* CCW 28-3 target engagement, 25 µL of eluted protein was treated with 1 µM CCW 36 (alkyne-functionalized probe of CCW 16) for 1 h. A rhodamine ligand was appended with copper catalyzed click chemistry by addition of 1 mM Copper (II) Sulfate, 35 µM Tris(benzyltriazole methylamine) (TBTA), 1 mM TCEP, and 0.1 mM Azide-Fluor 545 (Click Chemistry Tools, AZ109-5). Degree of labeling was assessed SDS/PAGE and measuring in-gel fluorescence using Image J.

4.5.14 TMT-based Quantitative Proteomic Analysis

Cell Lysis, Proteolysis and Isobaric Labeling. Treated cell-pellets were lysed and digested using the commercially available Pierce™ Mass Spec Sample Prep Kit for Cultured Cells (Thermo Fisher Scientific, P/N 84840) following manufacturer's instructions. Briefly, 100 µg protein from each sample was reduced, alkylated, and digested overnight using a combination of Endoproteinase Lys-C and trypsin proteases. Individual samples were then labeled with isobaric tags using commercially available Tandem Mass Tag™ 6-plex (TMTsixplex™) (Thermo Fisher Scientific, P/N 90061) or TMT11plex (TMT11plex™) isobaric labeling reagent (Thermo Fisher Scientific, P/N 23275) kits, in accordance with manufacturer's protocols.

High pH Reversed Phase Separation. Tandem mass tag labeled (TMT) samples were then consolidated, and separated using high-pH reversed phase chromatography (RP-10) with fraction collection as previously described [135]. Fractions were speed-vac dried, then reconstituted to produce 24 fractions for subsequent on-line nanoLC-MS/MS analysis.

Protein Identification and Quantitation by nanoLC-MS/MS. Reconstituted RP-10 fractions were analyzed on a Thermo Orbitrap Fusion Lumos Mass Spectrometer (Xcalibur 4.1, Tune Application 3.0.2041) coupled to an EasyLC 1200 HPLC system (Thermo Fisher Scientific). The EasyLC 1200 was equipped with a 20 µL loop, set-up for 96 well plates. A Kasil-fritted trapping column (75 µm ID) packed with ReproSil-Pur 120 C18-AQ, 5 µm material (15mm bed length) was utilized

together with a 160mm length, 75 μm inner diameter spraying capillary pulled to a tip diameter of approximately 8-10 μm using a P-2000 capillary puller (Sutter Instruments, Novato, CA). The 160mm separation column was packed with ReproSil-Pur 120 C18-AQ, 3 μm material (Dr. Maisch GmbH, Ammerbuch-Entringen, Germany). Mobile phase consisted of A= 0.1% formic acid/2% acetonitrile (v/v), and Mobile phase B= 0.1% formic acid/98% acetonitrile (v/v). Samples (18 μL) were injected on to trapping column using Mobile Phase A at a flow rate of 2.5 μL/min. Peptides were then eluted using an 80 minute gradient (2% Mobile Phase B for 5 min, 2%-40% B from 5-65 min, followed by 70% B from 65-70 minutes, then returning to 2% B from 70-80 min) at a flowrate of 300 nL/min on the capillary separation column with direct spraying into the mass spectrometer. Data was acquired on Orbitrap Fusion Lumos Mass Spectrometer in data-dependent mode using synchronous precursor scanning MS^3 mode (SPS-MS3), with MS^2 triggered for the 12 most intense precursor ions within a mass-to-charge ratio *(m/z)* range of 300-1500 found in the full MS survey scan event. MS scans were acquired at 60,000 mass resolution (*R*) at *m/z* 400, using a target value of 4×10^5 ions, and a maximum fill time of 50 ms. MS^2 scans were acquired as CID ion trap (IT) rapid type scans using a target value of 1×10^4 ions, maximum fill time of 50 ms, and an isolation window of 2 Da. Data-dependent MS^3 spectra were acquired as Orbitrap (OT) scans, using Top 10 MS^2 daughter selection, automatic gain control (AGC) target of 5×10^4 ions, with scan range of *m/z* 100-500. The MS^3 maximum injection time was 86 ms, with HCD collision energy set to 65%. MS^3 mass resolution (*R*) was set to 15,000 at *m/z* 400 for TMT6plex experiments, and 50,000 at *m/z* 400 for TMT11-plex experiments. Dynamic exclusion was set to exclude selected precursors for 60 s with a repeat count of 1. Nanospray voltage was set to 2.2 kV, with heated capillary temperature set to 300 ºC, and an S-lens RF level equal to 30%. No sheath or auxiliary gas flow is applied.

Data Processing and Analysis. Acquired MS data was processed using Proteome Discoverer v. 2.2.0.388 software (Thermo) utilizing Mascot v 2.5.1 search engine (Matrix Science, London, UK) together with Percolator validation node for peptide-spectral match filtering [136]. Data was searched against Uniprot protein database (canonical human and mouse sequences, EBI, Cambridge, UK) supplemented with sequences of common contaminants. Peptide search tolerances were set to 10 ppm for precursors, and 0.8 Da for fragments. Trypsin cleavage specificity (cleavage at K, R except if followed by P) allowed for up to 2 missed cleavages. Carbamidomethylation of cysteine was set as a fixed modification, methionine oxidation, and TMT-modification of N-termini and lysine residues were set as variable modifications. Data validation of peptide and protein identifications was done at the level of the complete dataset consisting of combined Mascot search results for all individual samples per experiment via the Percolator validation node in Proteome Discoverer. Reporter ion ratio calculations were performed using summed abundances with most confident centroid selected from 20 ppm window. Only peptide-to-spectrum matches that are unique assignments to a given identified protein within the total dataset are considered for protein quantitation. High confidence protein identifications were reported using a Percolator estimated <1% false discovery rate (FDR) cut-off. Differential abundance significance was estimated using a background-based ANOVA with Benjamini-Hochberg correction to determine adjusted p-values.

4.6 Acknowledgements

We thank the members of the Nomura Research Group and Novartis Institutes for BioMedical Research for critical reading of the manuscript. This work was supported by Novartis Institutes for BioMedical Research and the Novartis-Berkeley Center for Proteomics and Chemistry

Technologies (NB-CPACT) for all listed authors. This work was also supported by grants from the National Institutes of Health (F31CA225173 for CCW).

4.7 Figures

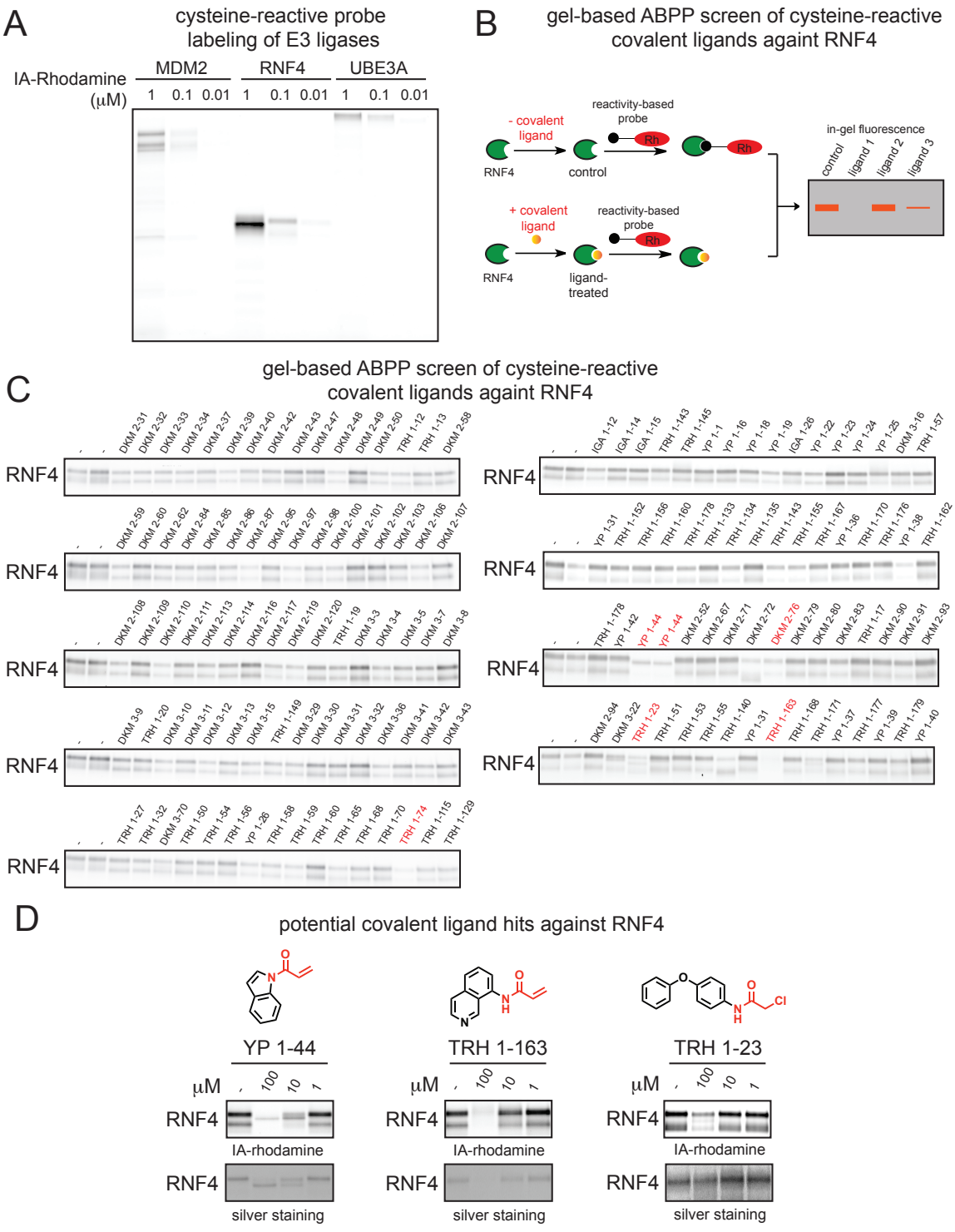

Figure 4.1: Covalent ligand screen against RNF4 using gel-based ABPP.
(A) Gel-based ABPP labeling of E3 ligases MDM2, RNF4, and UBE3A. Purified protein was labeled with IA-rhodamine (IA-Rh) for 30 min at room temperature, followed by SDS/PAGE and visualization by in-gel fluorescence. **(B)** Schematic of gel-based ABPP screen of covalent ligands (50 μM) against IA-rhodamine labeling of pure RNF4; **(C)** Gel-based ABPP screen of cysteine-reactive covalent ligands against IA-rhodamine labeling of RNF4. Covalent ligands were pre-incubated with pure RNF4 protein for 30 min prior to IA-rhodamine labeling (250 nM) for 1 h. Proteins were subjected to SDS/PAGE and visualized by in-gel fluorescence. Highlighted in red were potential hits from this screen. **(D)** Chemical structures and gel-based ABPP confirmation of reproducible RNF4 screening hits, performed as described in **(C)**. Gels were also silver stained to identify compounds that induce protein precipitation.

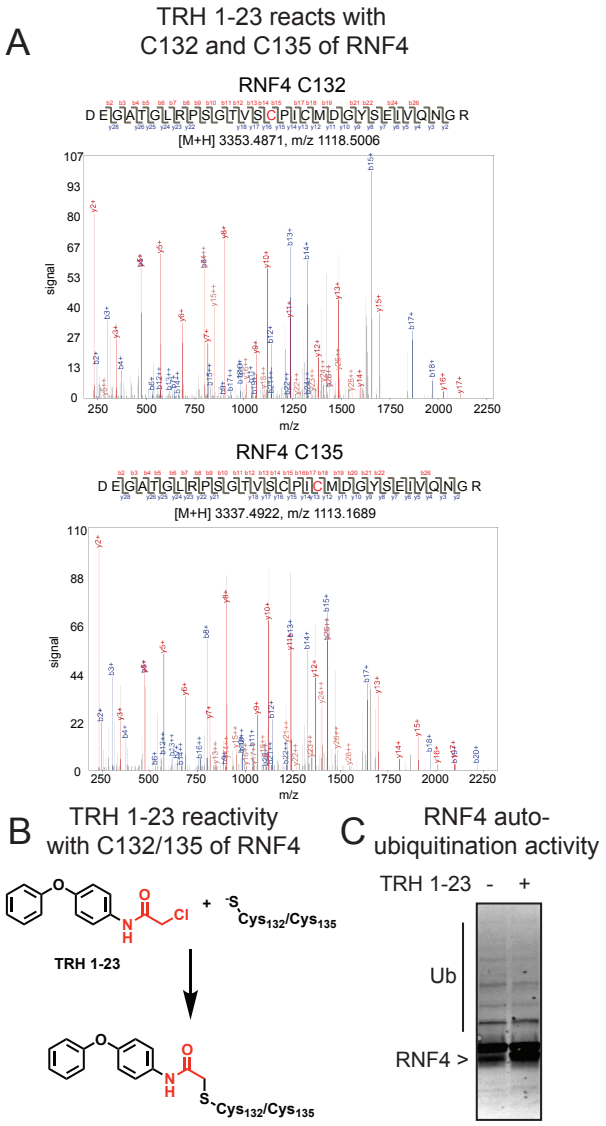

Figure 4.2: TRH 1-23 reacts non-functionally with zinc-coordinating cysteines in RNF4.
(A) LC-MS/MS analysis of TRH 1-23 covalent adduct on RNF4. RNF4 was incubated with TRH 1-23 (50 μM) for 30 min at RT. Tryptic digests of RNF4 were analyzed by LC-MS/MS searched for presence of peptides showing the TRH 1-23 adduct. Shown are the MS/MS spectra of TRH 1-23-modified C132 and C135 RNF4 tryptic peptide. Highlighted in red in the peptide sequence is the cysteine that was modified. **(B)** Schematic of TRH 1-23 reactivity with C132 or C135 of RNF4. **(C)** TRH 1-23 does not inhibit RNF4 autoubiquitination. RNF4 was pre-incubated with TRH 1-23 (100 μM) for 30 min at room temperature followed by addition of UBA1, E2 enzyme, and ATP for

40 min at 37 C. The reaction was quenched and subjected to SDS/PAGE and Western blotting for RNF4. Gel shown in **(C)** is a representative gel from n=3.

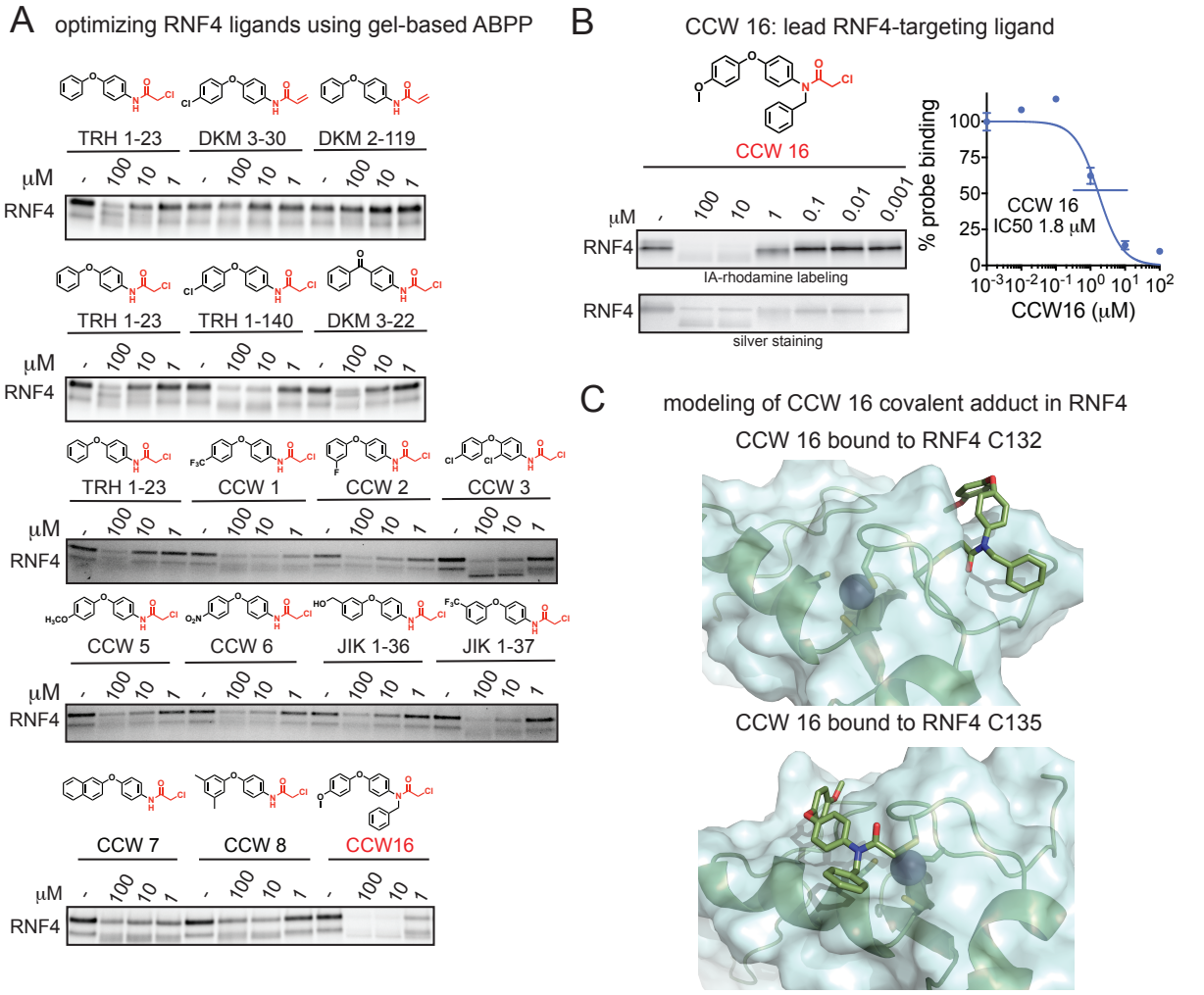

Figure 4.3: Optimizing RNF4 covalent ligands using gel-based ABPP.
(A) Derivatives of TRH 1-23 were tested against IA-rhodamine labeling of RNF4 using gel-based ABPP. Silver stained gels are also shown to visualize total protein content. **(B)** CCW16 was tested against IA-rhodamine labeling of RNF4 using gel-based ABPP. For **(A)** and **(B)**, covalent ligands were pre-incubated with pure RNF4 protein for 30 min prior to IA-rhodamine labeling for 1 h. Proteins were subjected to SDS/PAGE and visualized by in-gel fluorescence. In **(B)**, gels were quantified by densitometry to calculate IC50 values. Gel shown in **(B)** is a representative gel from n=3. **(C)** Covalent docking of CCW 16 bound to either C132 or C135 in RNF4.

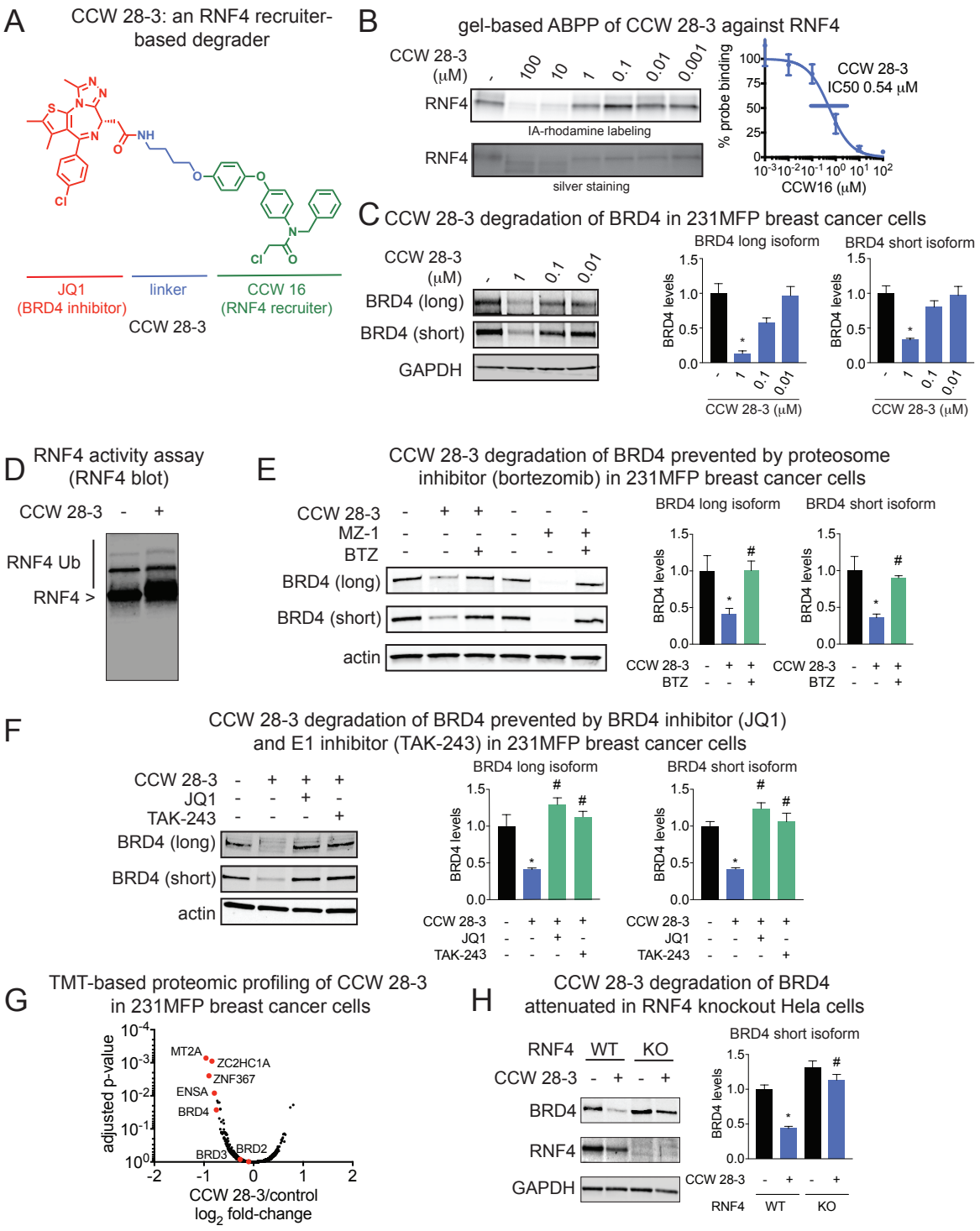

Figure 4.4: RNF4 recruiter-based BRD4 degrader.
(A) Structure of CCW 28-3, an RNF4-recruiter-based degrader linked to BRD4 inhibitor JQ1. **(B)** Gel-based ABPP analysis of CCW 28-3 against pure human RNF4. CCW 28-3 was pre-incubated with pure RNF4 protein for 30 min prior to IA-rhodamine labeling for 1 h. Proteins were subjected to SDS/PAGE and visualized by in-gel fluorescence. Gels were quantified by densitometry to calculate IC50 values. **(C)** CCW 28-3 treatment in 231MFP breast cancer cells leads to BRD4 degradation. 231MFP breast cancer cells were treated with vehicle DMSO or CCW 28-3 for 3 h. Proteins were subjected to SDS/PAGE and Western blotting for BRD4 and GAPDH loading control. **(D)** CCW

28-3 does not inhibit RNF4 autoubiquitination. RNF4 was pre-incubated with CCW 28-3 (10 μM) for 30 min at room temperature followed by addition of UBA1, E2 enzyme, and ATP for 60 min at 37 C. The reaction was quenched and subjected to SDS/PAGE and Western blotting for RNF4. **(E, F)** CCW 28-3 treatment in 231MFP breast cancer cells leads to proteasome-, E1 inhibitor-, and BRD4 inhibitor-dependent BRD4 degradation. Vehicle DMSO or proteasome inhibitor bortezomib (BTZ) (10 μM) **(E)**, E1 inhibitor TAK-243 (10 μM), or BRD4 inhibitor JQ1 (10 μM) **(F)** were pre-incubated for 30 min prior to treatment with MZ1 (1 μM) or CCW 28-3 (1 μM) for 3 h. Proteins were subjected to SDS/PAGE and Western blotting for BRD4 and actin loading control. **(G)** TMT-based quantitative proteomic analysis of protein expression changes from CCW 28-3 (1 μM) treatment for 3 h in 231MFP cells. **(H)** RNF4 wild-type and knockout Hela cells were treated with CCW 28-3 (10 μM) for 5 h and subjected to SDS/PAGE and Western blotting for BRD4, RNF4, and GAPDH. Blots in **(B-F, H)** were quantified by densitometry. Data in **(B-F, H)** are from representative gels from n=3. Bar graphs are average ± sem, n=3-5/group. Significance is expressed as *$p<0.05$ compared to vehicle-treated controls and #$p<0.05$ compared to CCW 28-3 treated groups in **(E-F)** and CCW 28-3 treated wild-type cells in **(H)**. Data in (**G**) represent 6180 protein groups quantified with 2 or more unique peptides in triplicate treatments, see **Table C.2.2** for details.

References

1. Edwards, A. M. *et al.* Too many roads not taken. *Nature* **470**, 163–165 (2011).
2. Dixon, S. J. & Stockwell, B. R. Identifying druggable disease-modifying gene products. *Curr Opin Chem Biol* **13**, 549–555 (2009).
3. Moellering, R. E. & Cravatt, B. F. How chemoproteomics can enable drug discovery and development. *Chem. Biol.* **19**, 11–22 (2012).
4. Boersema, P. J., Kahraman, A. & Picotti, P. Proteomics beyond large-scale protein expression analysis. *Curr. Opin. Biotechnol.* **34**, 162–170 (2015).
5. Medina-Cleghorn, D. & Nomura, D. K. Exploring metabolic pathways and regulation through functional chemoproteomic and metabolomic platforms. *Chem. Biol.* **21**, 1171–1184 (2014).
6. Counihan, J. L., Ford, B. & Nomura, D. K. Mapping proteome-wide interactions of reactive chemicals using chemoproteomic platforms. *Curr Opin Chem Biol* **30**, 68–76 (2016).
7. Counihan, J. L., Ford, B. & Nomura, D. K. Mapping proteome-wide interactions of reactive chemicals using chemoproteomic platforms. *Curr Opin Chem Biol* **30**, 68–76 (2015).
8. Bachovchin, D. A. *et al.* Superfamily-wide portrait of serine hydrolase inhibition achieved by library-versus-library screening. *Proc. Natl. Acad. Sci. U.S.A.* **107**, 20941–20946 (2010).
9. Adibekian, A. *et al.* Click-generated triazole ureas as ultrapotent in vivo-active serine hydrolase inhibitors. *Nat. Chem. Biol.* **7**, 469–478 (2011).
10. Bachovchin, D. A. *et al.* Academic cross-fertilization by public screening yields a remarkable class of protein phosphatase methylesterase-1 inhibitors. *Proc. Natl. Acad. Sci. U.S.A.* **108**, 6811–6816 (2011).
11. Chang, J. W., Moellering, R. E. & Cravatt, B. F. An activity-based imaging probe for the integral membrane hydrolase KIAA1363. *Angew. Chem. Int. Ed. Engl.* **51**, 966–970 (2012).
12. Aron, A. T., Ramos-Torres, K. M., Cotruvo, J. A. & Chang, C. J. Recognition- and reactivity-based fluorescent probes for studying transition metal signaling in living systems. *Acc. Chem. Res.* **48**, 2434–2442 (2015).
13. Shannon, D. A. *et al.* Investigating the proteome reactivity and selectivity of aryl halides. *J. Am. Chem. Soc.* **136**, 3330–3333 (2014).
14. Nomura, D. K., Dix, M. M. & Cravatt, B. F. Activity-based protein profiling for biochemical pathway discovery in cancer. *Nat. Rev. Cancer* **10**, 630–638 (2010).
15. Shannon, D. A. & Weerapana, E. Covalent protein modification: the current landscape of residue-specific electrophiles. *Curr Opin Chem Biol* **24**, 18–26 (2015).
16. Montgomery, D. C. & Meier, J. L. Mapping Lysine Acetyltransferase-Ligand Interactions by Activity-Based Capture. *Meth. Enzymol.* **574**, 105–123 (2016).
17. Bachovchin, D. A. & Cravatt, B. F. The pharmacological landscape and therapeutic potential of serine hydrolases. *Nat Rev Drug Discov* **11**, 52–68 (2012).
18. Long, J. Z. *et al.* Selective blockade of 2-arachidonoylglycerol hydrolysis produces cannabinoid behavioral effects. *Nat. Chem. Biol.* **5**, 37–44 (2009).
19. Hsu, K.-L. *et al.* DAGLβ inhibition perturbs a lipid network involved in macrophage inflammatory responses. *Nat. Chem. Biol.* **8**, 999–1007 (2012).
20. Ahn, K. *et al.* Discovery and characterization of a highly selective FAAH inhibitor that reduces inflammatory pain. *Chem. Biol.* **16**, 411–420 (2009).

21. Chang, J. W., Nomura, D. K. & Cravatt, B. F. A potent and selective inhibitor of KIAA1363/AADACL1 that impairs prostate cancer pathogenesis. *Chem. Biol.* **18**, 476–484 (2011).
22. Chang, J. W. *et al.* A selective inhibitor of platelet-activating factor acetylhydrolases 1b2 and 1b3 that impairs cancer cell survival. *ACS Chem Biol* **10**, 925–932 (2015).
23. Kohnz, R. A. *et al.* Activity-Based Protein Profiling of Oncogene-Driven Changes in Metabolism Reveals Broad Dysregulation of PAFAH1B2 and 1B3 in Cancer. *ACS Chem. Biol.* **10**, 1624–1630 (2015).
24. Inloes, J. M. *et al.* The hereditary spastic paraplegia-related enzyme DDHD2 is a principal brain triglyceride lipase. *Proc. Natl. Acad. Sci. U.S.A.* **111**, 14924–14929 (2014).
25. Dominguez, E. *et al.* Integrated phenotypic and activity-based profiling links Ces3 to obesity and diabetes. *Nat. Chem. Biol.* **10**, 113–121 (2014).
26. Kamat, S. S. *et al.* Immunomodulatory lysophosphatidylserines are regulated by ABHD16A and ABHD12 interplay. *Nat. Chem. Biol.* **11**, 164–171 (2015).
27. Xu, H. *et al.* Substrate-Competitive Activity-Based Profiling of Ester Prodrug Activating Enzymes. *Mol. Pharm.* **12**, 3399–3407 (2015).
28. Wolf, E. V., Zeissler, A. & Verhelst, S. H. L. Inhibitor Fingerprinting of Rhomboid Proteases by Activity-Based Protein Profiling Reveals Inhibitor Selectivity and Rhomboid Autoprocessing. *ACS Chem. Biol.* **10**, 2325–2333 (2015).
29. Parsons, W. H. *et al.* AIG1 and ADTRP are atypical integral membrane hydrolases that degrade bioactive FAHFAs. *Nat. Chem. Biol.* **12**, 367–372 (2016).
30. Medina-Cleghorn, D., Heslin, A., Morris, P. J., Mulvihill, M. M. & Nomura, D. K. Multidimensional Profiling Platforms Reveal Metabolic Dysregulation Caused by Organophosphorus Pesticides. *ACS Chem. Biol.* (2013) doi:10.1021/cb400796c.
31. Weerapana, E. *et al.* Quantitative reactivity profiling predicts functional cysteines in proteomes. *Nature* **468**, 790–795 (2010).
32. Couvertier, S. M., Zhou, Y. & Weerapana, E. Chemical-proteomic strategies to investigate cysteine posttranslational modifications. *Biochim. Biophys. Acta* **1844**, 2315–2330 (2014).
33. Pace, N. J. & Weerapana, E. Diverse functional roles of reactive cysteines. *ACS Chem. Biol.* **8**, 283–296 (2013).
34. Abo, M. & Weerapana, E. A Caged Electrophilic Probe for Global Analysis of Cysteine Reactivity in Living Cells. *J. Am. Chem. Soc.* **137**, 7087–7090 (2015).
35. Abegg, D. *et al.* Proteome-Wide Profiling of Targets of Cysteine reactive Small Molecules by Using Ethynyl Benziodoxolone Reagents. *Angew. Chem. Int. Ed. Engl.* **54**, 10852–10857 (2015).
36. Yang, J. *et al.* Global, in situ, site-specific analysis of protein S-sulfenylation. *Nat Protoc* **10**, 1022–1037 (2015).
37. Majmudar, J. D. *et al.* Harnessing Redox Cross-Reactivity To Profile Distinct Cysteine Modifications. *J. Am. Chem. Soc.* **138**, 1852–1859 (2016).
38. Bateman, L. A., Zaro, B. W., Miller, S. M. & Pratt, M. R. An alkyne-aspirin chemical reporter for the detection of aspirin-dependent protein modification in living cells. *J. Am. Chem. Soc.* **135**, 14568–14573 (2013).
39. Wang, J. *et al.* Mapping sites of aspirin-induced acetylations in live cells by quantitative acid-cleavable activity-based protein profiling (QA-ABPP). *Sci Rep* **5**, 7896 (2015).
40. Lewallen, D. M. *et al.* Chemical Proteomic Platform To Identify Citrullinated Proteins. *ACS Chem. Biol.* **10**, 2520–2528 (2015).

41. Zhou, Y. *et al.* Chemoproteomic Strategy to Quantitatively Monitor Transnitrosation Uncovers Functionally Relevant S-Nitrosation Sites on Cathepsin D and HADH2. *Cell Chem Biol* **23**, 727–737 (2016).
42. Wang, C., Weerapana, E., Blewett, M. M. & Cravatt, B. F. A chemoproteomic platform to quantitatively map targets of lipid-derived electrophiles. *Nat. Methods* **11**, 79–85 (2014).
43. Medina-Cleghorn, D. *et al.* Mapping Proteome-Wide Targets of Environmental Chemicals Using Reactivity-Based Chemoproteomic Platforms. *Chem. Biol.* **22**, 1394–1405 (2015).
44. Crawford, L.A., Weerapana, E. A Tyrosine-Reactive Irreversible Inhibitor for Glutathione S-Transferase Pi (GSTP1). *Submitted*.
45. Louie, S. M. *et al.* GSTP1 is a Driver of Triple-Negative Breast Cancer Cell Metabolism and Pathogenicity. *Cell Chemical Biology* **In press**, (2016).
46. Wang, C., Abegg, D., Hoch, D. G. & Adibekian, A. Chemoproteomics-Enabled Discovery of a Potent and Selective Inhibitor of the DNA Repair Protein MGMT. *Angew. Chem. Int. Ed. Engl.* **55**, 2911–2915 (2016).
47. Backus, K. M. *et al.* Proteome-wide covalent ligand discovery in native biological systems. *Nature* **534**, 570–574 (2016).
48. Niphakis, M. J. *et al.* A Global Map of Lipid-Binding Proteins and Their Ligandability in Cells. *Cell* **161**, 1668–1680 (2015).
49. Johnson, D. S., Weerapana, E. & Cravatt, B. F. Strategies for discovering and derisking covalent, irreversible enzyme inhibitors. *Future Med Chem* **2**, 949–964 (2010).
50. Roberts, A. M., Ward, C. C. & Nomura, D. K. Activity-based protein profiling for mapping and pharmacologically interrogating proteome-wide ligandable hotspots. *Curr. Opin. Biotechnol.* **43**, 25–33 (2016).
51. Evans, M. J. & Cravatt, B. F. Mechanism-based profiling of enzyme families. *Chem. Rev.* **106**, 3279–3301 (2006).
52. Long, J. Z. *et al.* Selective blockade of 2-arachidonoylglycerol hydrolysis produces cannabinoid behavioral effects. *Nat. Chem. Biol.* **5**, 37–44 (2009).
53. Chang, J. W. *et al.* Selective inhibitor of platelet-activating factor acetylhydrolases 1b2 and 1b3 that impairs cancer cell survival. *ACS Chem. Biol.* **10**, 925–932 (2015).
54. Roberts, A. M. *et al.* Chemoproteomic Screening of Covalent Ligands Reveals UBA5 as a Novel Pancreatic Cancer Target. *ACS Chem. Biol.* (2017) doi:10.1021/acschembio.7b00020.
55. Bateman, L. A. *et al.* Chemoproteomics-enabled covalent ligand screen reveals a cysteine hotspot in reticulon 4 that impairs ER morphology and cancer pathogenicity. *Chem. Commun. (Camb.)* (2017) doi:10.1039/c7cc01480e.
56. Pace, N. J. & Weerapana, E. Diverse functional roles of reactive cysteines. *ACS Chem. Biol.* **8**, 283–296 (2013).
57. Liu, Q. *et al.* Developing irreversible inhibitors of the protein kinase cysteinome. *Chem. Biol.* **20**, 146–159 (2013).
58. Ostrem, J. M. L. & Shokat, K. M. Direct small-molecule inhibitors of KRAS: from structural insights to mechanism-based design. *Nat Rev Drug Discov* **15**, 771–785 (2016).
59. London, N. *et al.* Covalent docking of large libraries for the discovery of chemical probes. *Nat. Chem. Biol.* **10**, 1066–1072 (2014).
60. Mädler, S., Bich, C., Touboul, D. & Zenobi, R. Chemical cross-linking with NHS esters: a systematic study on amino acid reactivities. *J Mass Spectrom* **44**, 694–706 (2009).
61. Miller, B. T., Collins, T. J., Rogers, M. E. & Kurosky, A. Peptide Biotinylation with Amine-Reactive Esters: Differential Side Chain Reactivity. *Peptides* **18**, 1585–1595 (1997).

62. Cox, T. M. Aldolase B and fructose intolerance. *FASEB J.* **8**, 62–71 (1994).
63. Lorentzen, E., Siebers, B., Hensel, R. & Pohl, E. Mechanism of the Schiff Base Forming Fructose-1,6-bisphosphate Aldolase: Structural Analysis of Reaction Intermediates. *Biochemistry* **44**, 4222–4229 (2005).
64. Barski, O. A., Tipparaju, S. M. & Bhatnagar, A. The Aldo-Keto Reductase Superfamily and its Role in Drug Metabolism and Detoxification. *Drug Metab Rev* **40**, 553–624 (2008).
65. Attwood, P. V. & Wieland, T. Nucleoside diphosphate kinase as protein histidine kinase. *Naunyn Schmiedebergs Arch. Pharmacol.* **388**, 153–160 (2015).
66. Luka, Z., Mudd, S. H. & Wagner, C. Glycine N-methyltransferase and regulation of S-adenosylmethionine levels. *J. Biol. Chem.* **284**, 22507–22511 (2009).
67. Park, J. *et al.* SIRT5-mediated lysine desuccinylation impacts diverse metabolic pathways. *Mol. Cell* **50**, 919–930 (2013).
68. Alkam, D., Feldman, E. Z., Singh, A. & Kiaei, M. Profilin1 biology and its mutation, actin(g) in disease. *Cell. Mol. Life Sci.* (2016) doi:10.1007/s00018-016-2372-1.
69. Bouter, A. *et al.* Review: Annexin-A5 and cell membrane repair. *Placenta* **36 Suppl 1**, S43-49 (2015).
70. Neklesa, T. K., Winkler, J. D. & Crews, C. M. Targeted protein degradation by PROTACs. *Pharmacol. Ther.* (2017) doi:10.1016/j.pharmthera.2017.02.027.
71. Lai, A. C. *et al.* Modular PROTAC Design for the Degradation of Oncogenic BCR-ABL. *Angew. Chem. Int. Ed. Engl.* **55**, 807–810 (2016).
72. Winter, G. E. *et al.* DRUG DEVELOPMENT. Phthalimide conjugation as a strategy for in vivo target protein degradation. *Science* **348**, 1376–1381 (2015).
73. Weerapana, E., Simon, G. M. & Cravatt, B. F. Disparate proteome reactivity profiles of carbon electrophiles. *Nat. Chem. Biol.* **4**, 405–407 (2008).
74. Ford, B., Bateman, L. A., Gutierrez-Palominos, L., Park, R. & Nomura, D. K. Mapping Proteome-wide Targets of Glyphosate in Mice. *Cell Chemical Biology* **0**, (2017).
75. Counihan, J. L. *et al.* Chemoproteomic Profiling of Acetanilide Herbicides Reveals Their Role in Inhibiting Fatty Acid Oxidation. *ACS Chem. Biol.* (2017) doi:10.1021/acschembio.6b01001.
76. Drahl, C., Cravatt, B. F. & Sorensen, E. J. Protein-reactive natural products. *Angew. Chem. Int. Ed. Engl.* **44**, 5788–5809 (2005).
77. Roberts, L. S., Yan, P., Bateman, L. A. & Nomura, D. K. Mapping Novel Metabolic Nodes Targeted by Anti-Cancer Drugs that Impair Triple-Negative Breast Cancer Pathogenicity. *ACS Chem. Biol.* **12**, 1133–1140 (2017).
78. Zhou, Y. *et al.* Competitive profiling of celastrol targets in human cervical cancer HeLa cells via quantitative chemical proteomics. *Mol Biosyst* **13**, 83–91 (2016).
79. Bateman, L. A. *et al.* Chemoproteomics-enabled covalent ligand screen reveals a cysteine hotspot in reticulon 4 that impairs ER morphology and cancer pathogenicity. *Chem. Commun. (Camb.)* (2017) doi:10.1039/c7cc01480e.
80. Roberts, A. M. *et al.* Chemoproteomic Screening of Covalent Ligands Reveals UBA5 As a Novel Pancreatic Cancer Target. *ACS Chem. Biol.* **12**, 899–904 (2017).
81. Lee, I.-C. & Choi, B. Y. Withaferin-A--A Natural Anticancer Agent with Pleitropic Mechanisms of Action. *Int J Mol Sci* **17**, 290 (2016).
82. Lee, J. *et al.* Withaferin A is a leptin sensitizer with strong antidiabetic properties in mice. *Nat. Med.* **22**, 1023–1032 (2016).

83. Dar, N. J., Hamid, A. & Ahmad, M. Pharmacologic overview of Withania somnifera, the Indian Ginseng. *Cell. Mol. Life Sci.* **72**, 4445–4460 (2015).
84. M, M. *et al.* Evaluating the inhibitory potential of Withania somnifera on platelet aggregation and inflammation enzymes: An in vitro and in silico study. *Pharm Biol* **54**, 1936–1941 (2016).
85. Bargagna-Mohan, P. *et al.* The tumor inhibitor and antiangiogenic agent withaferin A targets the intermediate filament protein vimentin. *Chem. Biol.* **14**, 623–634 (2007).
86. Heyninck, K., Lahtela-Kakkonen, M., Van der Veken, P., Haegeman, G. & Vanden Berghe, W. Withaferin A inhibits NF-kappaB activation by targeting cysteine 179 in IKKβ. *Biochem. Pharmacol.* **91**, 501–509 (2014).
87. Bianchini, G., Balko, J. M., Mayer, I. A., Sanders, M. E. & Gianni, L. Triple-negative breast cancer: challenges and opportunities of a heterogeneous disease. *Nat Rev Clin Oncol* **13**, 674–690 (2016).
88. Heyninck, K. *et al.* Withaferin A induces heme oxygenase (HO-1) expression in endothelial cells via activation of the Keap1/Nrf2 pathway. *Biochem. Pharmacol.* **109**, 48–61 (2016).
89. Sangodkar, J. *et al.* All roads lead to PP2A: exploiting the therapeutic potential of this phosphatase. *FEBS J.* **283**, 1004–1024 (2016).
90. Cho, U. S. & Xu, W. Crystal structure of a protein phosphatase 2A heterotrimeric holoenzyme. *Nature* **445**, 53–57 (2007).
91. Yu, Y. *et al.* Withaferin A targets heat shock protein 90 in pancreatic cancer cells. *Biochem. Pharmacol.* **79**, 542–551 (2010).
92. Blewett, M. M. *et al.* Chemical proteomic map of dimethyl fumarate-sensitive cysteines in primary human T cells. *Sci Signal* **9**, rs10 (2016).
93. Bateman, L. A. *et al.* Covalent Ligand Screening Reveals Cysteine Hotspot within RTN4 that Impairs ER Morphology and Colorectal Cancer Pathogenicity. *Submitted to ACS Chemical Biology* (2017).
94. Jessani, N. *et al.* Carcinoma and stromal enzyme activity profiles associated with breast tumor growth in vivo. *Proc Natl Acad Sci U S A* **101**, 13756–13761 (2004).
95. Jessani, N., Niessen, S., Mueller, B. M. & Cravatt, B. F. Breast cancer cell lines grown in vivo: what goes in isn't always the same as what comes out. *Cell Cycle* **4**, 253–255 (2005).
96. Louie, S. M. *et al.* GSTP1 Is a Driver of Triple-Negative Breast Cancer Cell Metabolism and Pathogenicity. *Cell Chem Biol* **23**, 567–578 (2016).
97. Benjamin, D. I. *et al.* Inositol phosphate recycling regulates glycolytic and lipid metabolism that drives cancer aggressiveness. *ACS Chem. Biol.* **9**, 1340–1350 (2014).
98. Xu, T. *et al.* ProLuCID: An improved SEQUEST-like algorithm with enhanced sensitivity and specificity. *J Proteomics* **129**, 16–24 (2015).
99. Burslem, G. M. & Crews, C. M. Small-Molecule Modulation of Protein Homeostasis. *Chem. Rev.* **117**, 11269–11301 (2017).
100. Lai, A. C. & Crews, C. M. Induced protein degradation: an emerging drug discovery paradigm. *Nat Rev Drug Discov* **16**, 101–114 (2017).
101. Rape, M. Ubiquitylation at the crossroads of development and disease. *Nat. Rev. Mol. Cell Biol.* **19**, 59–70 (2018).
102. Grossman, E. A. *et al.* Covalent Ligand Discovery against Druggable Hotspots Targeted by Anti-cancer Natural Products. *Cell Chem Biol* **24**, 1368-1376.e4 (2017).

103. Counihan, J. L., Wiggenhorn, A. L., Anderson, K. E. & Nomura, D. K. Chemoproteomics-Enabled Covalent Ligand Screening Reveals ALDH3A1 as a Lung Cancer Therapy Target. *ACS Chem. Biol.* (2018) doi:10.1021/acschembio.8b00381.
104. Bateman, L. A. *et al.* Chemoproteomics-enabled covalent ligand screen reveals a cysteine hotspot in reticulon 4 that impairs ER morphology and cancer pathogenicity. *Chem. Commun. (Camb.)* **53**, 7234–7237 (2017).
105. Wang, C., Weerapana, E., Blewett, M. M. & Cravatt, B. F. A chemoproteomic platform to quantitatively map targets of lipid-derived electrophiles. *Nat. Methods* **11**, 79–85 (2014).
106. Hacker, S. M. *et al.* Global profiling of lysine reactivity and ligandability in the human proteome. *Nat Chem* **9**, 1181–1190 (2017).
107. Backus, K. M. Applications of Reactive Cysteine Profiling. *Curr. Top. Microbiol. Immunol.* (2018) doi:10.1007/82_2018_120.
108. Liu, Y., Patricelli, M. P. & Cravatt, B. F. Activity-based protein profiling: the serine hydrolases. *Proc. Natl. Acad. Sci. U.S.A.* **96**, 14694–14699 (1999).
109. Anderson, K. E., To, M., Olzmann, J. A. & Nomura, D. K. Chemoproteomics-Enabled Covalent Ligand Screening Reveals a Thioredoxin-Caspase 3 Interaction Disruptor That Impairs Breast Cancer Pathogenicity. *ACS Chem. Biol.* **12**, 2522–2528 (2017).
110. Vassilev, L. T. *et al.* In vivo activation of the p53 pathway by small-molecule antagonists of MDM2. *Science* **303**, 844–848 (2004).
111. Schneekloth, A. R., Pucheault, M., Tae, H. S. & Crews, C. M. Targeted intracellular protein degradation induced by a small molecule: En route to chemical proteomics. *Bioorg. Med. Chem. Lett.* **18**, 5904–5908 (2008).
112. Malecka, K. A. *et al.* Identification and characterization of small molecule human papillomavirus E6 inhibitors. *ACS Chem. Biol.* **9**, 1603–1612 (2014).
113. Staudinger, J. L. The Molecular Interface Between the SUMO and Ubiquitin Systems. *Adv. Exp. Med. Biol.* **963**, 99–110 (2017).
114. Sriramachandran, A. M. & Dohmen, R. J. SUMO-targeted ubiquitin ligases. *Biochim. Biophys. Acta* **1843**, 75–85 (2014).
115. Tan, B. *et al.* RNF4 negatively regulates NF-κB signaling by down-regulating TAB2. *FEBS Lett.* **589**, 2850–2858 (2015).
116. Fryrear, K. A., Guo, X., Kerscher, O. & Semmes, O. J. The Sumo-targeted ubiquitin ligase RNF4 regulates the localization and function of the HTLV-1 oncoprotein Tax. *Blood* **119**, 1173–1181 (2012).
117. Bilodeau, S., Caron, V., Gagnon, J., Kuftedjian, A. & Tremblay, A. A CK2-RNF4 interplay coordinates non-canonical SUMOylation and degradation of nuclear receptor FXR. *J Mol Cell Biol* **9**, 195–208 (2017).
118. Filippakopoulos, P. *et al.* Selective inhibition of BET bromodomains. *Nature* **468**, 1067–1073 (2010).
119. Zengerle, M., Chan, K.-H. & Ciulli, A. Selective Small Molecule Induced Degradation of the BET Bromodomain Protein BRD4. *ACS Chem. Biol.* **10**, 1770–1777 (2015).
120. Gadd, M. S. *et al.* Structural basis of PROTAC cooperative recognition for selective protein degradation. *Nat. Chem. Biol.* **13**, 514–521 (2017).
121. Nowak, R. P. *et al.* Plasticity in binding confers selectivity in ligand-induced protein degradation. *Nat. Chem. Biol.* (2018) doi:10.1038/s41589-018-0055-y.

122. Kokosza, K., Balzarini, J. & Piotrowska, D. G. Novel 5-Arylcarbamoyl-2-methylisoxazolidin-3-yl-3-phosphonates as Nucleotide Analogues. *Nucleosides, Nucleotides and Nucleic Acids* **33**, 552–582 (2014).
123. Talaty, E. R., Young, S. M., Dain, R. P. & Stipdonk, M. J. V. A study of fragmentation of protonated amides of some acylated amino acids by tandem mass spectrometry: observation of an unusual nitrilium ion. *Rapid Communications in Mass Spectrometry* **25**, 1119–1129 (2011).
124. Timokhin, V. I., Gastaldi, S., Bertrand, M. P. & Chatgilialoglu, C. Rate Constants for the β-Elimination of Tosyl Radical from a Variety of Substituted Carbon-Centered Radicals. *J. Org. Chem.* **68**, 3532–3537 (2003).
125. Cee, V. J. *et al.* Systematic Study of the Glutathione (GSH) Reactivity of N-Arylacrylamides: 1. Effects of Aryl Substitution. *J. Med. Chem.* **58**, 9171–9178 (2015).
126. Le Sann, C., Huddleston, J. & Mann, J. Synthesis and preliminary evaluation of novel analogues of quindolines as potential stabilisers of telomeric G-quadruplex DNA. *Tetrahedron* **63**, 12903–12911 (2007).
127. Ikoma, M., Oikawa, M. & Sasaki, M. Synthesis and domino metathesis of functionalized 7-oxanorbornene analogs toward cis-fused heterocycles. *Tetrahedron* **64**, 2740–2749 (2008).
128. Cho, S.-D. *et al.* A One-Pot Synthesis of Pyrido[2,3-b][1,4]oxazin-2-ones. *J. Org. Chem.* **68**, 7918–7920 (2003).
129. Magolan, J., Carson, C. A. & Kerr, M. A. Total Synthesis of (±)-Mersicarpine. *Org. Lett.* **10**, 1437–1440 (2008).
130. Groocock, L. M. *et al.* RNF4 interacts with both SUMO and nucleosomes to promote the DNA damage response. *EMBO reports* **15**, 601–8 (2014).
131. *Schrödinger Release 2018-1: Maestro, Schrödinger, LLC, New York, NY, 2018.*
132. Zhu, K. *et al.* Docking Covalent Inhibitors: A Parameter Free Approach To Pose Prediction and Scoring. *Journal of Chemical Information and Modeling* **54**, 1932–1940 (2014).
133. Smith, P. K. *et al.* Measurement of protein using bicinchoninic acid. *Anal. Biochem.* **150**, 76–85 (1985).
134. Xu, T. *et al.* ProLuCID: An improved SEQUEST-like algorithm with enhanced sensitivity and specificity. *J Proteomics* **129**, 16–24 (2015).
135. Thomas, J. R. *et al.* A Photoaffinity Labeling-Based Chemoproteomics Strategy for Unbiased Target Deconvolution of Small Molecule Drug Candidates. *Methods Mol. Biol.* **1647**, 1–18 (2017).
136. Käll, L., Canterbury, J. D., Weston, J., Noble, W. S. & MacCoss, M. J. Semi-supervised learning for peptide identification from shotgun proteomics datasets. *Nat. Methods* **4**, 923–925 (2007).

Appendix A

A.1 Supplemental Methods

A.1.1 Synthesis of CW 1-26 and CW 1-33

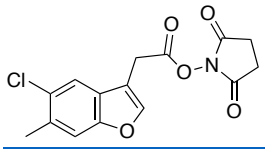

Synthesis of 2,5-dioxopyrrolidin-1-yl 2-(5-chloro-6-methylbenzofuran-3-yl)acetate, CW 1-26: 35.6 mg (160 µmol) of (5-chloro-6-methyl-1-benzofuran-3-yl)acetic acid (Sigma) were dissolved in anhydrous DCM. 1.3 equivalents of NHS (23.9 mg, 208 µmol, Sigma) and EDC-HCl (39.7 mg, 208 µmol, Acros) were added and the mixture was stirred overnight under nitrogen. TLC (70% EtOAc/Hex) showed > 90% conversion. The crude mixture was filtered, concentrated and applied directly to a silica gel column and purified with a mobile phase of 50% EtOAc/Hex, which yielded 28.7 mg of product (56% yield).
^{1}H NMR (600MHz, $CDCl_3$): δ 7.66 (s, 1H), 7.58 (s, 1H), 7.35 (s, 1H), 3.97 (s, 1H), 2.00 (s, 2H), 2.84 (s, 4H), 2.46 (s, 3H).
^{13}C NMR (125MHz, $CDCl_3$): δ 168.8, 165.7, 153.9, 143.9, 132.8, 129.3, 126.1, 119.4, 113.3, 110.4, 26.6, 25.6, 20.8
HRMS (-ESI): Calculated: 320.0331 ($C_{15}H_{11}ClNO_5$). Observed: 320.0326

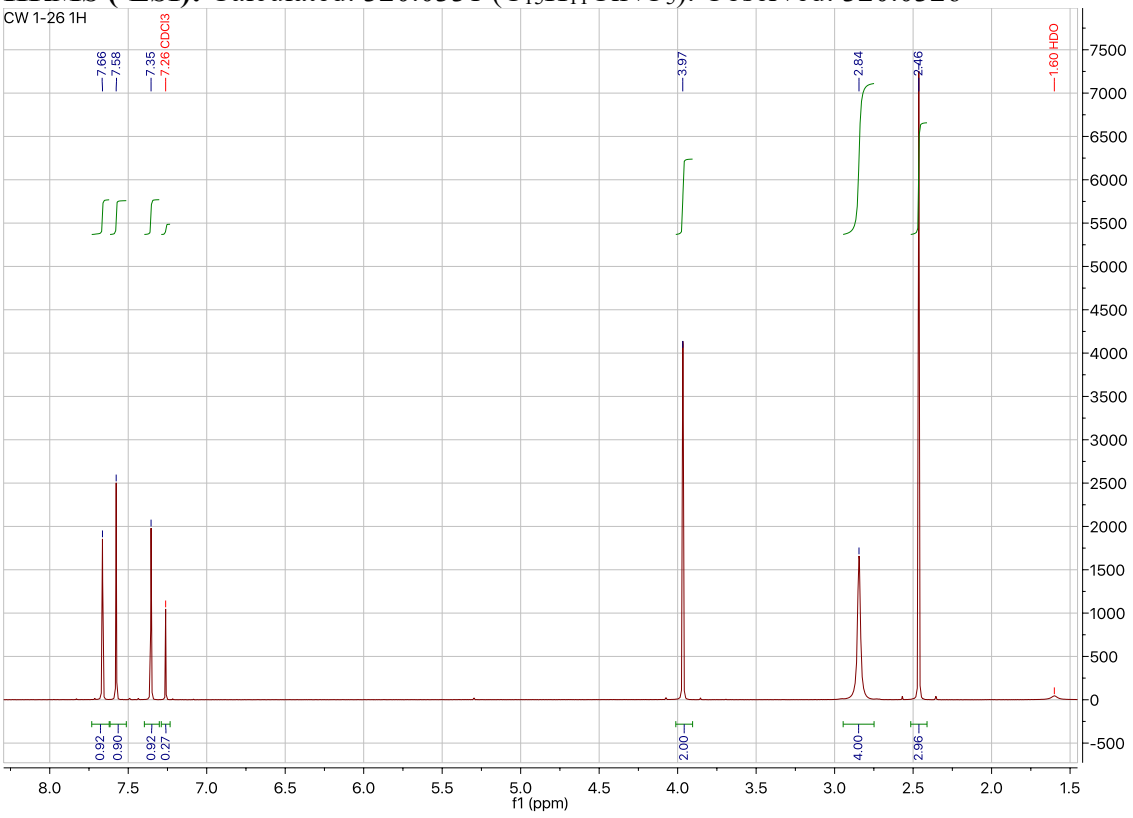

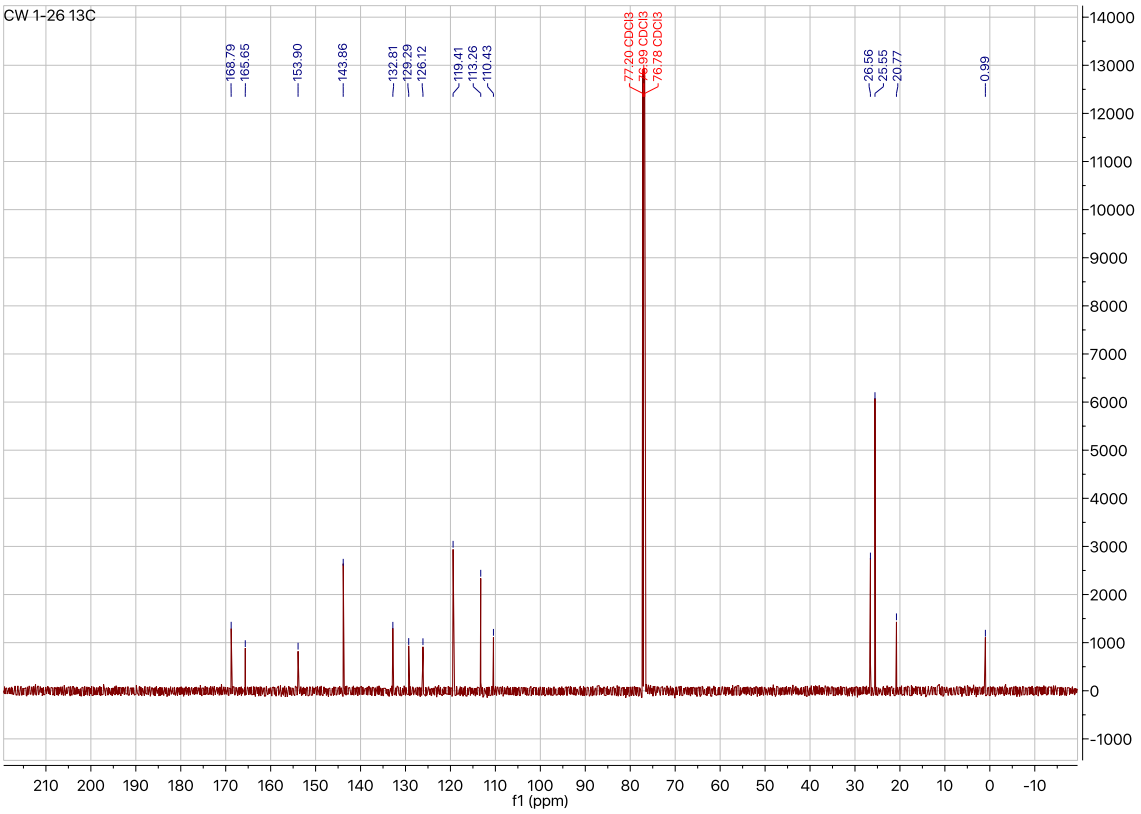

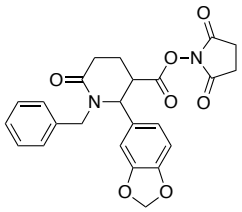

Synthesis of 2,5-dioxopyrrolidin-1-yl 2-(benzo[*d*][1,3]dioxol-5-yl)-1-benzyl-6-oxopiperidine-3-carboxylate, CW 1-33: 51.5 mg of 2-(1,3-Benzodioxol-5-yl)-1-benzyl-6-oxo-3-piperidinecarboxylic acid (146 µmol, Matrix scientific) were dissolved in 7.5 mL of anhydrous DCM. 1.4 equivalents of NHS (23.5 mg, 204 µM, Sigma) and EDC-HCl (39.1 mg, 204 µM, Acros) were added and the mixture stirred overnight under nitrogen. TLC (EtOAc) of the reaction showed > 90% conversion after 14 hours. The mixture was filtered, concentrated and applied directly to a silica gel column and purified with a mobile phase of EtOAc. 31.0 mg were recovered (47%).

^{1}H NMR (600MHz, $CDCl_3$): δ 7.27-7.23 (m, 3H), 7.13 (d, *J* = 6.9 Hz, 2H), 6.81 (d, *J* = 7.8 Hz, 1H), 6.67-6.21 (m, 2H), 6.00 (s, 2H), 5.51 (d, *J* = 14.9 Hz, 1H), 4.75 (d, *J* = 4.4 Hz, 1H), 3.49 (d, *J* = 14.8 Hz, 1H), 3.10 (dt, *J* = 6.4, 4.2 Hz, 1H), 2.84-2.78 (m, 5H), 2.67 (dt, *J* = 18.4, 5.7 Hz, 1H), 2.28-2.14 (m, 2H)

^{13}C NMR (125MHz, $CDCl_3$): δ 169.3, 168.7, 167.7, 148.7, 147.9, 136.3, 132.7, 128.8, 128.5, 127.5, 120.7, 108.8, 107.1, 101.6, 60.2, 47.9, 45.1, 29.8, 25.7, 20.7

HRMS (+ESI): Calculated: 451.1500 ($C_{24}H_{23}O_7N_2$). Observed: 451.1500

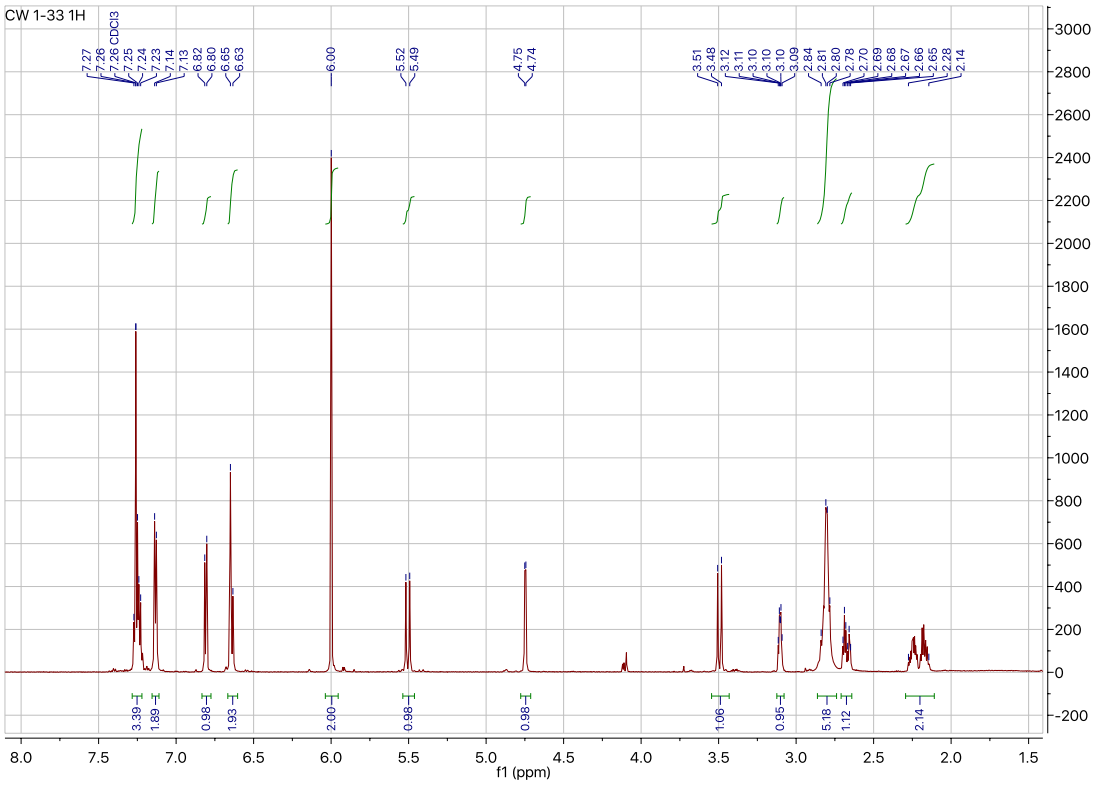

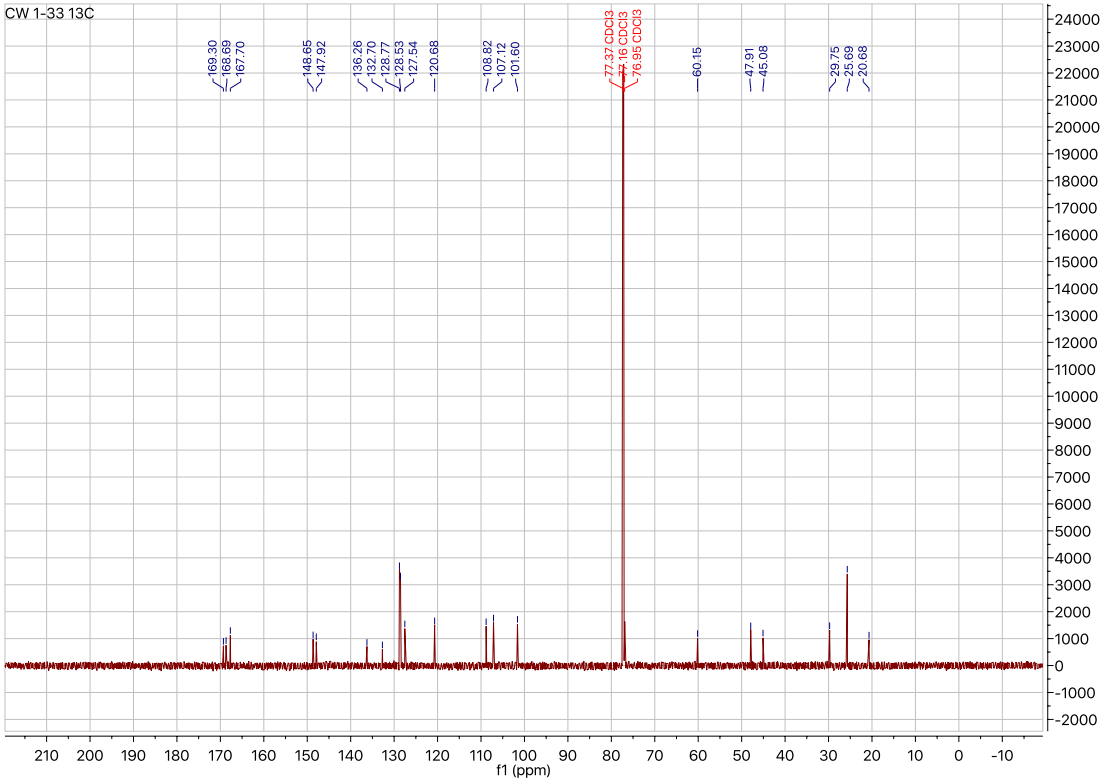

A.2 Supplemental Tables

Please see supporting data for full tables

Table A.2.1-12:
Amino acid reactivity of NHS-ester-alkyne in mouse liver proteome. Mouse liver proteomes were labeled with NHS-ester-alkyne (500 or 100 μM), followed by appendage of biotin-azide tags bearing an isotopically light (for 500 μM) or heavy (for 100 μM) tags and a TEV recognition sequence, followed by mixing heavy or light proteomes in 1:1 ratio, avidin-enrichment of probe-labeled proteins, digestion of enriched proteins by trypsin, and isolation of release of probe-modified tryptic peptides by TEV protease for subsequent LC-LC/MS/MS analysis. Reported in **Tables A.2.1, 3, 5, 7, 9,** and **11** are probe-modified peptides separated by amino acid reactivity, the specific amino acids labeled, the light to heavy isotopic ratios, Uniprot identification numbers, and protein designations. Only peptides that were present in 2 out of 4 biological replicates are reported here. Ratios shown are average ratios from the biological replicates. Reported in **Tables A.2.2, 4, 6, 8, 10,** and **12** are known annotations from probe-modified peptides based on the Uniprot database.

Table A.2.13:
Lysine-reactivity of the Dichlorotriazine-alkyne probe in mouse liver proteomes. Mouse liver proteomes were labeled with dichlorotriazine-alkyne (500 or 100 μM), followed by appendage of biotin-azide tags bearing an isotopically light (for 500 μM) or heavy (for 100 μM) tags and a TEV recognition sequence, followed by mixing heavy or light proteomes in 1:1 ratio, avidin-enrichment of probe-labeled proteins, digestion of enriched proteins by trypsin, and isolation of release of probe-modified tryptic peptides by TEV protease for subsequent LC-LC/MS/MS analysis. Only peptides that were present in 2 out of 3 biological replicates are reported here. Ratios shown are average ratios from the biological replicates.

Table A.2.14-15:
IsoTOP-ABPP analysis of CW 1-26 (**A.2.14**) and CW 1-33 (**A.2.15**) in mouse liver proteomes. DMSO vehicle or CW 1-26 (100 μM) or CW 1-33 (100 μM) were pre-treated in mouse liver proteomes for 30 min prior to labeling of proteomes with NHS-ester-alkyne (500 μM) for 1 h at room temperature, followed by appendage of light (for vehicle-treated control) or heavy (for fragment-treated) biotin-TEV-azide tags, followed by the isoTOP-ABPP procedure. Shown are the probe-modified peptides identified, the isotopic light to heavy ratios, sites of probe-modification, uniprot IDs, and protein designations. Only peptides that were present in 2 out of 3 biological replicates are reported here. Ratios shown are average ratios from the biological replicates.

A.3 Supplemental Figures

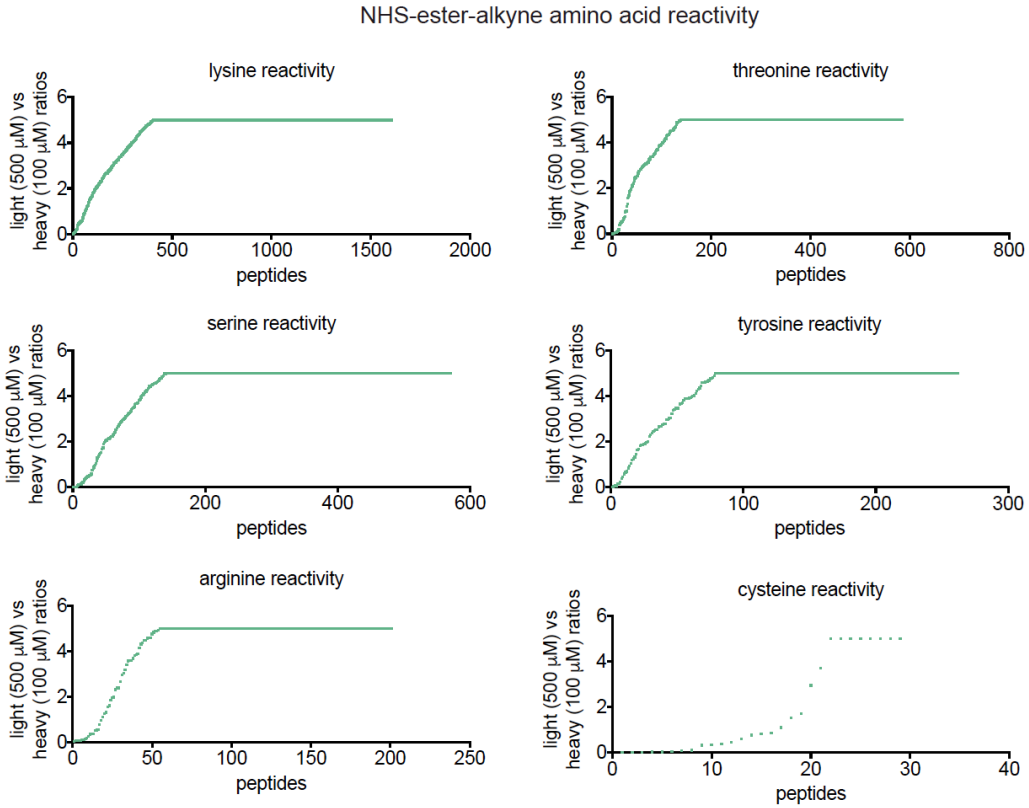

Figure A.3.1 NHS-ester-alkyne amino acid reactivity. We labeled mouse liver proteomes with 500 versus 100 µM NHS-ester-alkyne probe, followed by CuAAC-mediated conjugation of an isotopically light (for 500 µM) or heavy (for 100 µM) biotin-azide handles bearing a TEV protease recognition sequence, followed by isoTOP-ABPP analysis of isolated probe-modified tryptic peptides. Shown are the ratios for the individual peptides identified categorized by amino acid reactivity. A light to heavy isotopic ratio of 5 indicates a site that is not hyper-reactive, versus an isotopic ratio of <2 which can be considered hyper-reactive. Data shown are average ratios for probe-modified peptides that were found in at least two out of three biological replicates. Those ratios that were >5 are just shown as having a ratio of 5. Raw data for these plots can be found in **Table S1.**

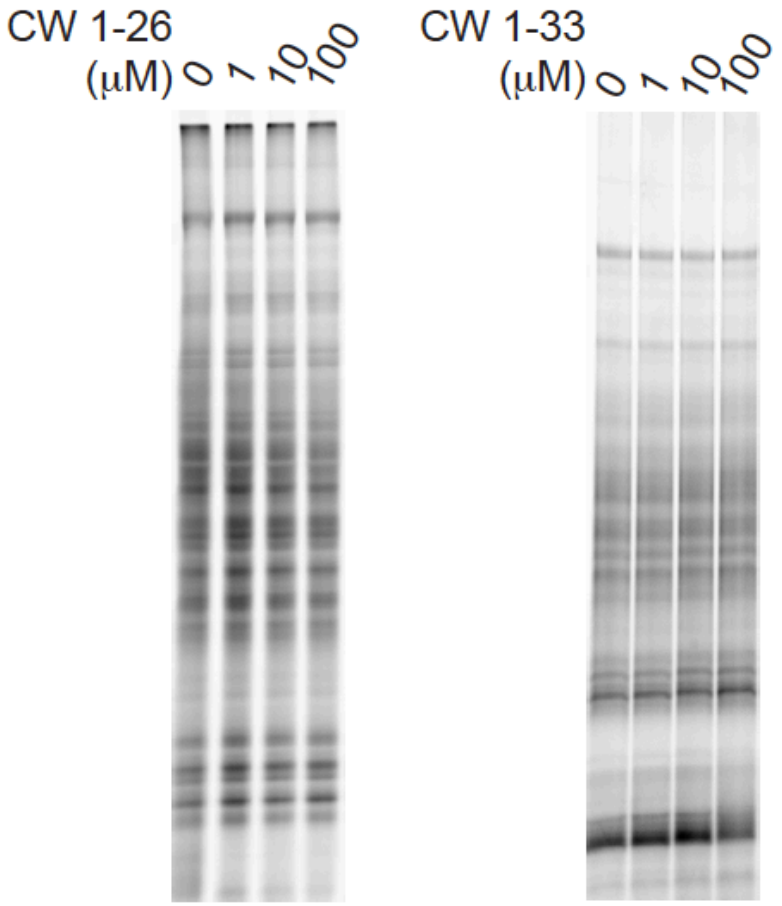

Figure A.3.2 CW 1-26 and CW 1-33 competition against NHS-ester-alkyne reactivity in mouse liver proteomes. DMSO vehicle or CW 1-26 or CW 1-33 were pre-incubated for 30 min with mouse liver proteomes prior to labeling with NHS-ester-alkyne (100 μM) for 30 min. Rhodamine-azide was then appended to probe-labeled proteins and proteins were separated by SDS/PAGE and NHS-ester-alkyne reactivity was assessed by in-gel fluorescence. Shown is a representative grey-scale gel.

Appendix B

B.1 Supplemental Methods

B.1.1 General synthetic methods

Chemicals and reagents were purchased from major commercial suppliers and used without further purification. Reactions were performed under a nitrogen atmosphere unless otherwise noted. Silica gel flash column chromatography was performed using EMD or Sigma Aldrich silica gel 60 (230-400 mesh). Proton and carbon nuclear magnetic resonance (^{1}H NMR and ^{13}C NMR) data was acquired on a Bruker AVB 400, AVQ 400, or AV 600 spectrometer at the University of California, Berkeley. High resolution mass spectrum were obtained from the QB3 mass spectrometry facility at the University of California, Berkeley using positive or negative electrospray ionization (+ESI or -ESI). Yields are reported as a single run.

B.1.2 General Procedure A

The amine (1 eq.) was dissolved in DCM (5 mL/mmol) and cooled to 0ºC. To the solution was added acryloyl chloride (1.2 eq.) followed by triethylamine (1.2 eq.). The solution was warmed to room temperature and stirred overnight. The solution was then washed with brine and the crude product was purified by silica gel chromatography (and recrystallization if necessary) to afford the corresponding acrylamide.

B.1.3 General Procedure B

The amine (1 eq.) was dissolved in DCM (5 mL/mmol) and cooled to 0ºC. To the solution was added chloroacetyl chloride (1.2 eq.) followed by triethylamine (1.2 eq.). The solution was warmed to room temperature and stirred overnight. The solution was then washed with brine and the crude product was purified by silica gel chromatography (and recrystallization if necessary) to afford the corresponding chloroacetamide.

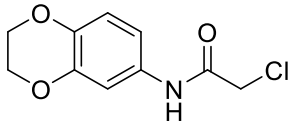

2-Chloro-N-(2,3-dihydrobenzo[b][1,4]dioxin-6-yl)acetamide (DKM 2-90)
Following **General Procedure B** starting from 1,4-benzodioxan-6-amine (1.51 g, 10 mmol) product was obtained after silica gel chromatography (40% ethyl acetate in hexanes) in 70% yield as an off-white solid (1.59 g).

^{1}H NMR (400MHz, $CDCl_3$): δ 8.11 (s, 1H), 7.18 (d, *J* = 2.4 Hz, 1H), 6.92 (dd, *J* = 2.4, 8.7 Hz, 1H), 6.83 (d, *J* = 8.7 Hz, 1H), 4.25 (s, 4H), 4.17 (s, 2H).

^{13}C NMR (100MHz, $CDCl_3$): δ 163.8, 143.7, 141.3, 130.4, 117.5, 114.0, 110.2, 64.5, 64.4, 43.0.

HRMS (+ESI): Calculated: 228.0422 ($C_{10}H_{11}ClNO_3$). Observed: 228.0421.

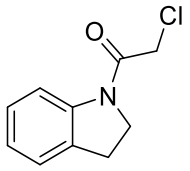

2-chloro-1-(indolin-1-yl)ethan-1-one (DKM 2-79)
Following **General Procedure B** starting from indoline (331 mg, 2.8 mmol) product was obtained after silica gel chromatography (0% to 20% ethyl acetate in hexanes) in 51% yield as a pale brown solid (278 mg).

^{1}H NMR (400MHz, $CDCl_3$): δ 8.17 (d, *J* = 8.0 Hz, 1H), 7.20-7.16 (m, 2H), 7.04 (t, *J* = 7.4 Hz, 1H), 4.09 (s, 2H), 4.05 (t, *J* = 8.4 Hz, 2H), 3.17 (t, *J* = 8.4 Hz, 2H).

^{13}C NMR (100MHz, $CDCl_3$): δ 164.0, 142.4, 131.3, 127.6, 124.7, 124.5, 117.1, 47.7, 43.02, 28.1.

HRMS (+ESI): Calculated: 196.0524 ($C_{10}H_{11}ClNO$). Observed: 196.0523.

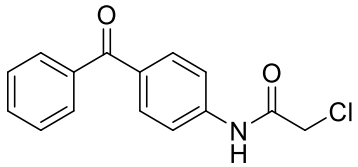

***N*-(4-Benzoylphenyl)-2-chloroacetamide (DKM 3-22)**
Following **General Procedure B** starting from 4-aminobenzophenone (590 mg, 3.0 mmol) product was obtained after silica gel chromatography (30% to 50% ethyl acetate in hexanes) in 83% yield as a light brown solid (679 mg).

^{1}H NMR (400MHz, $CDCl_3$): δ 8.48 (s, 1H), 7.85-7.83 (m, 2H), 7.78-7.76 (m, 2H), 7.71-7.68 (m, 2H), 7.61-7.57 (m, 1H), 7.50-7.46 (m, 2H), 4.22 (s, 2H).

^{13}C NMR (100MHz, $CDCl_3$): δ 195.7, 164.2, 140., 137.7, 134.1, 132.5, 131.7, 130.0, 128.5, 119.3, 43.0.

HRMS (-ESI): Calculated: 272.0484 ($C_{15}H_{11}NO_2Cl$). Observed: 272.0482.

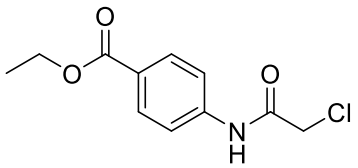

Ethyl 4-(2-chloroacetamido)benzoate (TRH 1-17)
Following **General Procedure B** starting from benzocaine (498 mg, 3.0 mmol) product was obtained after silica gel chromatography (2% to 20% ethyl acetate in hexanes) in 68% yield as a white solid (494 mg).

^{1}H NMR (400MHz, $CDCl_3$): δ 8.67 (s, 1H), 7.98 (d, *J* = 8.0 Hz, 2H), 7.62 (d, *J* = 8.0 Hz, 2H), 4.33 (q, *J* = 8.0 Hz, 2H), 4.15 (s, 2H), 1.34 (t, *J* = 6.0 Hz, 3H).

^{13}C NMR (100MHz, $CDCl_3$): δ 166.1, 164.5, 141.0, 130.7, 126.7, 119.3, 61.1, 43.0, 14.3.

HRMS (-ESI): Calculated: 240.0433 ($C_{11}H_{11}NO_3Cl$). Observed: 240.0430.

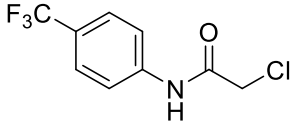

2-Chloro-*N*-(4-(trifluoromethyl)phenyl)acetamide (TRH 1-51)
Following **General Procedure B** starting from 4-(trifluoromethyl)aniline (346 mg, 2.0 mmol) product was obtained after silica gel chromatography (10% to 30% ethyl acetate in hexanes) in 61% yield as a white solid (309 mg).

^{1}H NMR (400 MHz, MeOD): δ 7.77 (d, *J* = 8.3 Hz, 2H), 7.61 (d, *J* = 8.3 Hz, 2H), 4.20 (s, 2H).

^{13}C NMR (100 MHz, MeOD): δ 167.7, 162.4, 142.9, 127.14, 127.10, 127.06, 127.02, 124.3, 120.9, 44.0.

HRMS (-ESI): Calculated: 236.0095 ($C_9H_6NOClF_3$). Observed: 236.0094.

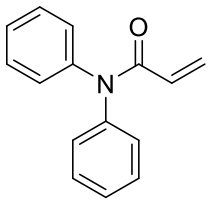

N,N-diphenylacrylamide (DKM 3-70)
A solution of diphenylamine (347 mg, 2.1 mmol) in DCM (10 mL) was cooled to 0 ºC. To the solution was added acryloyl chloride (222 mg, 2.5 mmol) followed by triethylamine (279 mg, 2.8 mmol). The solution was allowed to warm to room temperature and stirred overnight. The solution was washed with brine and citric acid and the crude product was purified via silica gel chromatography (20% to 60% ethyl acetate in hexanes) to afford the product in 24% yield as a dark yellow oil (112 mg).

^{1}H NMR (400MHz, $CDCl_3$): δ 7.43-7.28 (m, 10H), 6.52 (dd, *J* = 2.0, 16.8 Hz, 1H), 6.25 (dd, *J* = 10.2, 16.8 Hz, 1H), 5.67 (dd, *J* = 1.8, 10.2 Hz, 1H).

^{13}C NMR (100MHz, $CDCl_3$): δ 165.8, 142.6, 129.7, 129.3, 128.5, 127.0.

HRMS (+ESI): Calculated: 246.0889 ($C_{15}H_{13}NONa$). Observed: 246.0887.

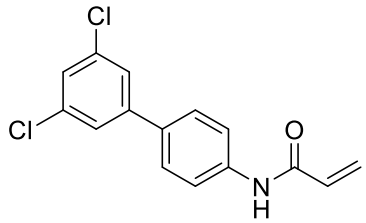

N-(3',5'-dichloro-[1,1'-biphenyl]-4-yl)acrylamide (DKM 3-3)
Following **General Procedure A** starting from 4-amino-3,5-dichlorobiphenyl (717 mg, 3.0 mmol), product was obtained after silica gel chromatography (20% to 45% ethyl acetate in hexanes) and recrystallization from toluene in 23% yield as a white solid (203 mg).

^{1}H NMR (600MHz, MeOD): δ 7.77 (d, *J* = 8.6 Hz, 2H), 7.59 (d, *J* = 8.6 Hz, 2H), 7.56 (d, *J* = 1.7 Hz, 2H), 7.37 (t, *J* = 1.7 Hz, 1H), 6.46 (dd, *J* = 9.9, 17.0 Hz, 1H), 6.39 (dd, *J* = 1.7, 17.0 Hz, 1H), 5.80 (dd, *J* = 1.7, 9.9 Hz, 1H).

^{13}C NMR (150MHz, MeOD): δ 166.2, 145.2, 140.4, 136.5, 135.2, 132.4, 128.5, 128.0, 127.7, 126.2, 121.7.

HRMS (-ESI): Calculated: 290.0145 ($C_{15}H_{110}NOCl_2$). Observed: 290.0143.

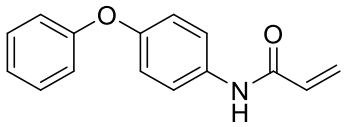

N-(4-phenoxyphenyl)acrylamide (DKM 2-119)
Following **General Procedure A** starting from 4-phenoxyaniline (571 mg, 3.1 mmol), product was obtained after silica gel chromatography (10% to 30% ethyl acetate in hexanes) in 69% yield as a white solid (512 mg).

^{1}H NMR (400MHz, $CDCl_3$): δ 8.17 (s, 1H), 7.55 (d, *J* = 8.9 Hz, 2H), 7.33-7.29 (m, 2H), 7.08 (t, *J* = 7.4 Hz, 1H), 6.98-6.94 (m, 4H), 6.42 (dd, *J* = 1.4, 16.9 Hz, 1H), 6.31 (dd, *J* = 10.0, 16.9 Hz, 1H), 5.73 (dd, *J* = 1.4, 10.0 Hz, 1H).

^{13}C NMR (100MHz, $CDCl_3$): δ 16.0, 157.5, 153.8, 13.4, 131.2, 129., 12.8, 123.3, 122.1, 119.6, 118.6.

HRMS (+ESI): Calculated: 240.1019 ($C_{15}H_{14}NO_2$). Observed: 240.1015.

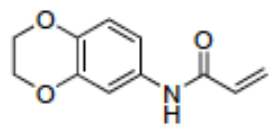

N-(2,3-dihydrobenzo[b][1,4]dioxin-6-yl)acrylamide (DKM 2-87)
Following **General Procedure A** starting from 1,4-benzodioxan-6-amine (462 mg, 3.1 mmol), product was obtained after silica gel chromatography (40% ethyl acetate in hexanes) in 38% yield as a light yellow solid (239 mg).

^{1}H NMR (400MHz, $(CD_3)_2SO$): δ 9.97 (s, 1H), 7.33 (d, *J* = 2.4 Hz, 1H), 7.03 (dd, *J* = 2.4, 8.7 Hz, 1H), 6.79 (d, *J* = 8.7 Hz, 1H), 6.38 (dd, *J* = 10.0, 17.0, 1H), 6.22 (dd, *J* = 2.1, 17.0 Hz, 1H), 5.71 (dd, *J* = 2.1, 10.0 Hz, 1H), 4.23-4.18 (m, 4H).

^{13}C NMR (100MHz, $(CD_3)_2SO$): δ 162.7, 142.9, 139.5, 132.7, 131.9, 126.4, 116.8, 112.5, 108.4, 64.2, 63.9.

HRMS (+ESI): Calculated: 206.0812 ($C_{11}H_{12}NO_3$). Observed: 206.0807.

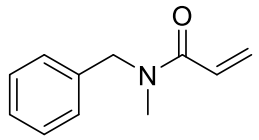

N-((tetrahydrofuran-2-yl)methyl)acrylamide (DKM 3-15)
Following **General Procedure A** starting from tetrahydrofurfurylamine (294 mg, 2.9 mmol), product was obtained after silica gel chromatography (20% to 70% ethyl acetate in hexanes) in 55% yield as a pale yellow oil (246 mg).

^{1}H NMR (400MHz, $CDCl_3$): 6.48 (s, 1H), 6.20 (dd, *J* = 1.7, 17.0 Hz, 1H), 6.07 (dd, *J* = 10.1, 17.0 Hz, 1H), 5.54 (dd, *J* = 1.7, 10.1 Hz, 1H), 3.96-3.90 (m, 1H), 3.80-3.75 (m, 1H), 3.70-3.64 (m, 1H), 3.58-3.52 (m, 1H), 3.17-3.11 (m, 1H), 1.95-1.87 (m, 1H), 1.86-1.78 (m, 2H), 1.53-1.44 (m, 1H).

^{13}C NMR (100MHz, $CDCl_3$): δ 165.7, 130.8, 126.3, 77.7, 68.0, 43.2, 28.7, 25.7.

HRMS (+ESI): Calculated: 156.1019 ($C_8H_{14}NO_2$). Observed: 156.1017.

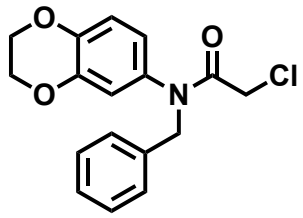

***N*-benzyl-2-chloro-*N*-(2,3-dihydrobenzo[*b*][1,4]dioxin-6-yl)acetamide (JNS 1-40)**
A solution of DKM 2-90 (1 g, 4.39 mmol) and sodium hydride (0.7 g 60% dispersion in mineral oil, 17.56 mmol, 4 eq.) in THF (50 mL) was allowed to stir at 0 °C for 15 min, after which benzyl bromide (2.1 mL, 17.56 mmol, 4 eq.) was added. After 3 hr at 0 °C, the reaction was quenched with $NaHCO_3$ and diluted with EtOAc for extraction. The organic layer was subsequently washed with brine and dried over $MgSO_4$. The crude product was purified by silica gel chromatography (30% ethyl acetate in hexanes) to obtain the desired product in 55% yield as an off-white solid (770 mg).

^{1}H NMR (400MHz, $CDCl_3$): δ 7.26 (m, 5H), 6.79 (d, *J* =8.6 Hz, 1H), 6.56 (d, 2.5 Hz, 1H), 6.45 (dd, *J* =8.5 Hz, 2.5 Hz, 1H), 4.84 (s, 2H), 4.25 (s, 4H), 3.90 (s, 2H).

^{13}C NMR (100MHz, $CDCl_3$): δ 166.4, 144.0, 143.9, 136.7, 134.0, 129.0, 128.5, 127.7, 121.31, 118.0, 117.1, 64.3, 53.8, 42,2.

HRMS (+ESI): Calculated: 318.0891 ($C_{17}H_{17}ClNO_3$). Observed: 318.0898.

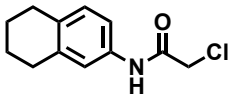

2-Chloro-N-(5,6,7,8-tetrahydronaphthalen-2-yl)acetamide (JNS 1-37)
Following **General Procedure B** starting from **1,2,3,4-tetrahydronaphthalen-2-amine** (1.472 g, 10.0 mmol) product was obtained after silica gel chromatography (30% ethyl acetate in hexanes) in 98% yield as an off-white solid (2.2 g).

^{1}H NMR (400MHz, $CDCl_3$): δ 8.17 (s, 1H), 7.23 (m, 2H), 7.03 (d, *J* = 8.1 Hz, 1H), 4.12 (s, 2H), 4.55 (s, 4H), 1.78 (s, 4H).

^{13}C NMR (100MHz, $CDCl_3$): δ 170.9, 163.8, 137.8, 134.3, 134.0, 129.4, 120.6, 117.6, 60.2, 53.4, 42.9, 30.7, 29.4, 28.8, 23.0, 20.8, 14.1.

HRMS (+ESI): Calculated: 224.0837($C_{12}H_{15}ClNO$). Observed: 224.0835.

B.2 Supplemental Tables
Please see supporting data for full tables
Tables B.2.1-12
IsoTOP-ABPP analysis of Withaferin A and DKM 2-90 targets in 231MFP breast cancer proteomes. We mapped the cysteine-reactivity of withaferin A and DKM 2-90 by pre-incubating withaferin A (10 μM) or DKM 2-90 (100 μM) for 30 min in 231MFP breast cancer cell proteomes, prior to labeling with the cysteine-reactive iodoacetamide-alkyne (IAyne) probe (100 μM, 30 min). Probe labeled proteins were then tagged with an isotopically light (for control) or heavy (for withaferin A- or DKM 2-90-treated) biotin-azide tag bearing a TEV protease recognition site by copper-catalyzed azide-alkyne cycloaddition. Control and treated proteomes were then mixed in a 1:1 ratio, probe labeled proteins were avidin-enriched and tryptically digested, probe-labeled tryptic peptides were avidin-enriched again, and released by TEV protease and analyzed by quantitative proteomic methods and light to heavy peptide ratios were quantified. Competitive isoTOP-ABPP analysis of withaferin A and DKM 2-90 cysteine-reactivity in 231MFP breast cancer cell proteomes. Light to heavy ratios of ~1 indicate peptides that were labeled by IAyne, but not bound by withaferin A or DKM 2-90. We designate light to heavy ratios of >10 as targets that were bound by withaferin A or DKM 2-90. **Table B.2.1** and **B.2.3** shows average light versus heavy ratios from those probe-modified peptides found in at least 2 out of 3 biological replicates. **Table B.2.1-6**. IsoTOP-ABPP analysis of withaferin A (10 μM), DKM 2-90 (100 μM), and JNS 1-40 (100 μM) treatment *in vitro* in 231MFP proteomes or *in situ* in 231MFP cells. For *in vitro* experiments, DMSO or compounds were pre-treated for 30 min prior to labeling with IAyne. For *in situ* experiments, cells were treated with DMSO or compounds for 4 hours and cell proteomes were subsequently labeled with IAyne.
Tables B.2.7-12. All peptides identified in isoTOP-ABPP experiments from Tabs 1-6.
Tables B.2.1-12 is associated with **Figs. 3.2, 3.4,** and **3.5** as well as **Figs. B.3.1** and **B.3.2.**

B.3 Supplemental Figures

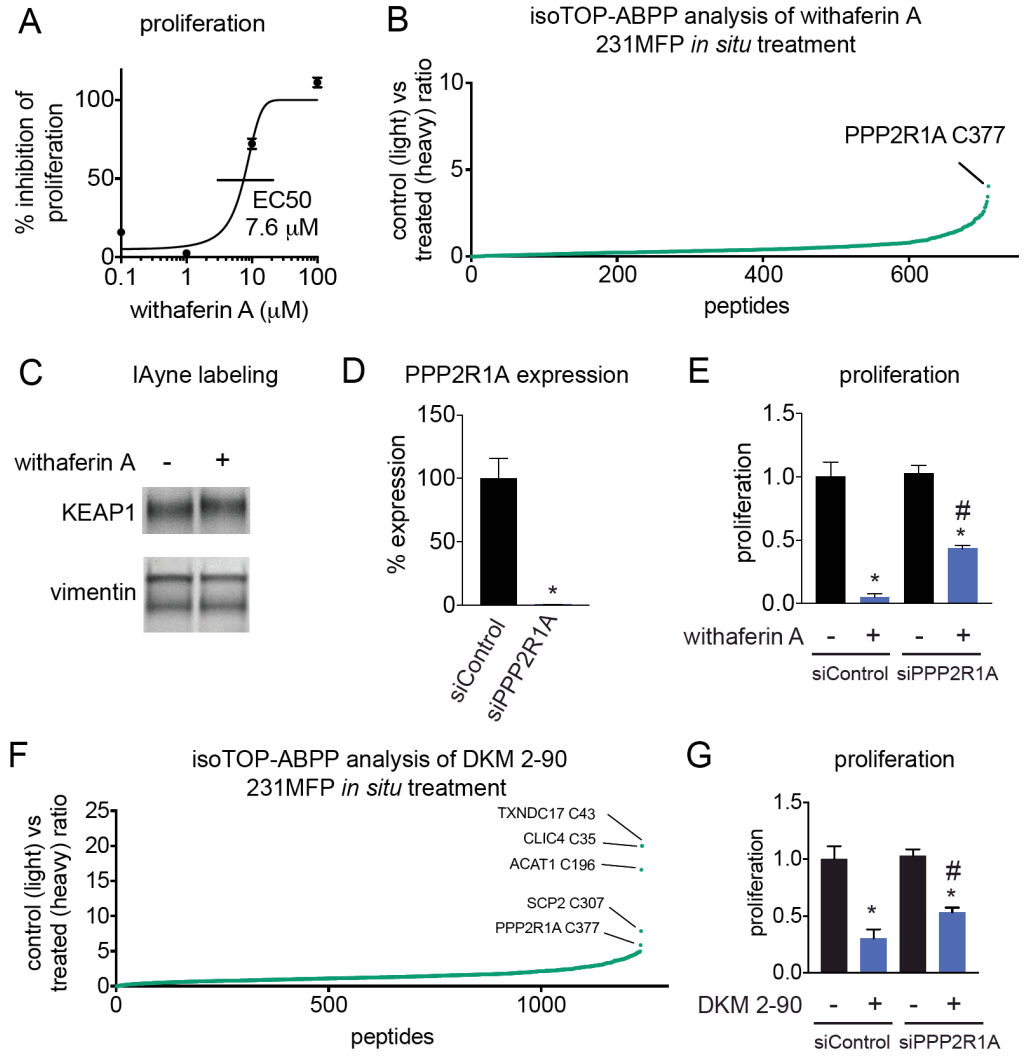

Figure B.3.1 Investigating the interactions of withaferin A and DKM 2-90. (A) Anti-proliferative dose-response of withaferin A in 231MFP cells. Cells were treated with DMSO or withaferin A for 48 h in serum-containing media and cell viability was assessed by Hoechst staining. **(B)** IsoTOP-ABPP analysis of withaferin A treatment in 231MFP cells. 231MFP cells were treated with DMSO or withaferin A (10 μM) for 4 h. Proteomes were subsequently labeled *ex situ* with IAyne for 1 h and subjected to the isoTOP-ABPP method. Light to heavy ratios of probe-modified peptides are shown. **(C)** Gel-based ABPP analysis of withaferin A competition against IAyne labeling of pure human KEAP1 and vimentin. Purified proteins were pre-treated with DMSO or withaferin A (10 μM) for 30 min at 37 °C before IAyne labeling (10 μM) for 30 min at room temperature. Probe labeled proteins were subsequently appended to rhodamine-azide by CuAAC and analyzed by SDS/PAGE and in-gel fluorescence. **(D)** PPP2R1A expression as assessed by qPCR. 231MFP cells were transfected with siControl or siPPP2R1A oligonucleotides and cells were harvested for qPCR analysis after 48 h. **(E)** 231MFP cell proliferation. 231MFP cells were transfected with siControl or siPPP2R1A oligonucleotides for 48 h and then cells were seeded and treated with either DMSO or withaferin A (10 μM) for an additional 48 h and cell viability was assessed by Hoechst staining. **(F)** IsoTOP-ABPP analysis of DKM 2-90 treatment in 231MFP cells. 231MFP cells were treated with DMSO or DKM 2-90 (100 μM) for 4 h. Proteomes were subsequently labeled *ex situ* with IAyne for 1 h and subjected to the isoTOP-ABPP method. Light to heavy ratios of probe-modified peptides are shown. **(G)** 231MFP cell proliferation. 231MFP cells were transfected with siControl or siPPP2R1A oligonucleotides for 48 h and then cells were seeded and treated with either DMSO or DKM 2-90 (100 μM) for an additional 48 h and cell viability was assessed by Hoechst staining. Data in **(A, D, E,** and **G)** is presented as mean ± sem, n=3-5/group. Significance

in **(D, E,** and **G)** is expressed as *p<0.05 compared to vehicle-treated siControl cells and #p<0.05 compared to withaferin A or DKM 2-90-treated siControl cells. **Figure B.3.1** is associated with **Figs. 3.1, 2, 3,** and **4.**

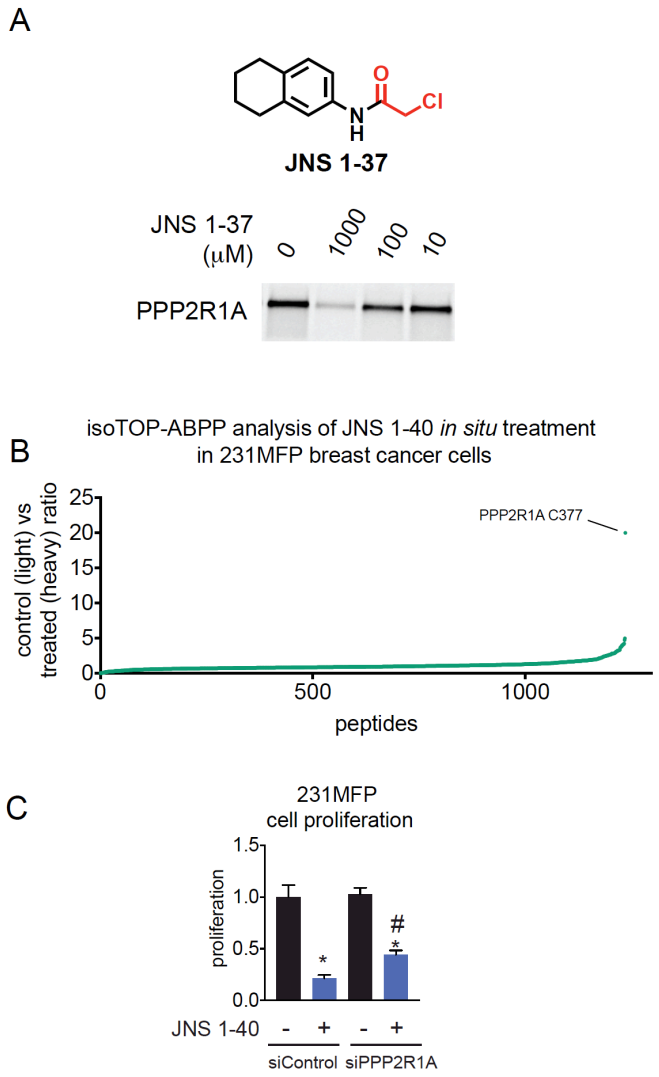

Figure B.3.2. Characterization of DKM 2-90 analogs JNS 1-37 and JNS 1-40. (A) Structure of JNS 1-37 and gel-based ABPP analysis of its potency against PPP2R1A. Reactive chloroacetamide is shown in red. Pure human PPP2R1A was pre-treated with DMSO or JNS 1-37 for 30 min at 37 ºC prior to IAyne labeling for 30 min at room temperature. Probe-labeled proteins were appended to rhodamine-azide by CuAAC and analyzed by SDS/PAGE and in-gel fluorescence. **(B)** IsoTOP-ABPP analysis of JNS 1-40 treatment in 231MFP cells. 231MFP cells were treated with DMSO or JNS 1-40 (100 μM) for 4 h. Proteomes were subsequently labeled *ex situ* with IAyne for 1 h and subjected to the isoTOP-ABPP method. Light to heavy ratios of probe-modified peptides are shown. **(C)** 231MFP cell proliferation. 231MFP cells were transfected with siControl or siPPP2R1A oligonucleotides for 48 h and then cells were seeded and treated with either DMSO or JNS 1-40 (100 μM) for an additional 48 h and cell viability was assessed by Hoechst staining. Data in **(C)** is presented as mean ± sem, n=5/group. Significance in **(C)** is expressed as *p<0.05 compared to vehicle-treated siControl cells and #p<0.05 compared to JNS 1-40-treated siControl cells. **Fig. B.3.2** is associated with **Fig. 3.5.**

Appendix C

C.1 Supplemental Methods

C.1.1 Synthesis and characterization of TRH 1-23 Analogs and CCW 28-3 Degrader

General synthetic methods
Chemicals and reagents were purchased from major commercial suppliers and used without further purification. Reactions were performed under a nitrogen atmosphere unless otherwise noted. Silica gel flash column chromatography was performed using EMD or Sigma Aldrich silica gel 60 (230-400 mesh). Proton and carbon nuclear magnetic resonance (^{1}H NMR and ^{13}C NMR) data was acquired on a Bruker AVB 400, AVQ 400, or AV 600 spectrometer at the University of California, Berkeley. High resolution mass spectrum were obtained from the QB3 mass spectrometry facility at the University of California, Berkeley using positive or negative electrospray ionization (+ESI or -ESI). Yields are reported as a single run.

General method for chloroacetamide synthesis
The amine (1 eq.) was dissolved in anhydrous DCM (2-10 mL) in a 20 mL scintillation vial. To the solution was added 2-chloroacetyl chloride (Sigma, 1.2 eq.) followed by triethylamine (Sigma, 1.2 eq.). The solution was stirred overnight under nitrogen. The reaction was monitored by TLC with ninhydrin staining. Upon reaction completion, the solvent was removed with rotary evaporation and the crude applied directly to a silica gel column for flash chromatography which gave the corresponding chloroacetamide.

2-chloro-N-(4-(4-(trifluoromethyl)phenoxy)phenyl)acetamide (CCW 1)
To a solution of 4-(4-(trifluoromethyl)phenoxy)aniline (AK Scientific, 63 mg, 0.25 mmol) in DCM 2-chloroacetyl chloride (Sigma, 34 mg, 0.30 mmol) and triethylamine (Sigma, 30.4 mg, 0.30 mmol) were added and the reaction stirred overnight. Upon reaction completion the crude was purified by silica gel chromatography (10-40% EtOAc/hexanes) to yield 65 mg (78%).
^{1}H NMR (400 MHz, $CDCl_3$): δ 8.25 (s, 1H), 7.63 – 7.51 (m, 4H), 7.12 – 6.99 (m, 4H), 4.22 (s, 2H).
HRMS: (-ESI): calcd. for: $C_{15}H_{10}O_2NF_3Cl$ = 328.0358, found: 327.0356

2-chloro-N-(4-(3-fluorophenoxy)phenyl)acetamide (CCW 2)
To a solution of 4-(3-fluorophenoxy)aniline (AK Scientific, 63 mg, 0.31 mmol) in DCM 2-chloroacetyl chloride (Sigma, 42 mg, 0.37 mmol) and triethylamine (Sigma, 38 mg, 0.37 mmol) were added and the reaction stirred overnight. Upon reaction completion the crude was purified by silica gel chromatography (10-40% EtOAc/hexanes) to yield 53 mg (61%).
^{1}H NMR (400 MHz, $CDCl_3$): δ 8.24 (s, 1H), 7.55 (dq, *J* = 10.0, 3.5, 2.4 Hz, 2H), 7.33 – 7.23 (m, 1H), 7.05 (dq, *J* = 10.1, 3.5, 2.6 Hz, 2H), 6.85 – 6.74 (m, 2H), 6.69 (dq, *J* = 10.2, 2.3 Hz, 1H), 4.21 (s, 2H).
^{13}C NMR (151 MHz, $CDCl_3$): δ 164.29, 163.75, 162.66, 158.85, 158.78, 153.31, 132.67, 130.51, 130.45, 121.95, 120.13, 113.71, 113.69, 109.98, 109.84, 105.92, 105.75, 77.19, 76.97, 76.76, 42.79.
HRMS: (-ESI): calcd. for: $C_{14}H_{10}O_2NFCl$ = 278.0390, found: 278.0389

2-chloro-N-(3-chloro-4-(4-chlorophenoxy)phenyl)acetamide (CCW 3)
To a solution of 3-chloro-4-(4-chlorophenoxy)aniline (Sigma, 64 mg, 0.25 mmol) in DCM 2-chloroacetyl chloride (Sigma, 34 mg, 0.30 mmol) and triethylamine (Sigma, 30.4 mg, 0.30 mmol) were added and the reaction stirred overnight. Upon reaction completion the crude was purified by silica gel chromatography (10-40% EtOAc/hexanes) to yield 69 mg (83%).
^{1}H NMR (400 MHz, $CDCl_3$): δ 8.28 (s, 1H), 7.83 (d, *J* = 2.6 Hz, 1H), 7.44 (dd, *J* = 8.8, 2.6 Hz, 1H), 7.36 – 7.28 (m, 3H), 7.05 (d, *J* = 8.8 Hz, 1H), 6.95 – 6.89 (m, 2H), 4.25 (s, 2H).
^{13}C NMR (151 MHz, $CDCl_3$): δ 163.85, 155.67, 148.97, 133.57, 129.72, 128.30, 126.60, 122.59, 121.48, 119.87, 118.65, 77.20, 76.98, 76.77, 42.73.
HRMS: (-ESI): calcd. for: $C_{14}H_9O_2NCl$ = 327.9704, found: 327.9702

2-chloro-N-(4-(4-methoxyphenoxy)phenyl)acetamide (CCW 5)
To a solution of 4-(4-methoxyphenoxy)aniline HCl (Astatech, 63 mg, 0.25 mmol) in DCM 2-chloroacetyl chloride (Sigma, 34 mg, 0.30 mmol) and triethylamine (Sigma, 60.8 mg, 0.60 mmol) were added and the reaction stirred overnight. Upon reaction completion the crude was purified by silica gel chromatography (10-40% EtOAc/hexanes) to yield 69 mg (95%).
^{1}H NMR (400 MHz, $CDCl_3$): δ 8.18 (s, 1H), 7.49 – 7.42 (m, 2H), 7.00 – 6.84 (m, 6H), 4.19 (s, 2H), 3.80 (s, 3H).
^{13}C NMR (151 MHz, $CDCl_3$): δ 163.67, 155.92, 155.72, 150.11, 131.22, 121.95, 120.57, 118.14, 114.87, 77.18, 76.97, 76.76, 55.63, 42.79.
HRMS: (-ESI): calcd. for: $C_{15}H_{13}O_3NCl$ = 290.0589, found: 290.0587

2-chloro-N-(4-(4-nitrophenoxy)phenyl)acetamide (CCW 6)
To a solution of 4-(4-nitrophenoxy)aniline (Sigma, 50 mg, 0.22 mmol) in DCM 2-chloroacetyl chloride (Sigma, 29 mg, 0.26 mmol) and triethylamine (Sigma, 26 mg, 0.26 mmol) were added and the reaction stirred overnight. Upon reaction completion the crude was purified by silica gel chromatography (10-40% EtOAc/hexanes) to yield 62.5 mg (93%).
^{1}H NMR (400 MHz, $CDCl_3$): δ 8.29 (s, 1H), 8.25 – 8.16 (m, 2H), 7.67 – 7.59 (m, 2H), 7.14 – 7.07 (m, 2H), 7.05 – 6.96 (m, 2H), 4.22 (s, 2H).
^{13}C NMR (101 MHz, $CDCl_3$): δ 163.93, 163.27, 151.63, 142.77, 133.98, 126.01, 122.18, 121.26, 117.01, 77.36, 77.04, 76.73, 42.85.
HRMS: (+ESI): calcd. for: $C_{14}H_{10}O_4N_2Cl$ = 305.0335, found: 305.0332

2-chloro-N-(4-(naphthalen-2-yloxy)phenyl)acetamide (CCW 7)
To a solution of 2-(4-Aminophenoxy)naphthalene (TCI, 118 mg, 0.50 mmol) in DCM 2-chloroacetyl chloride (Sigma, 67.8 mg, 0.60 mmol) and triethylamine (Sigma, 60.8 mg, 0.60 mmol) were added and the reaction stirred overnight. Upon reaction completion the crude was purified by silica gel chromatography (10-40% EtOAc/hexanes) to yield 111 mg (71%).
^{1}H NMR (400 MHz, $CDCl_3$): δ 8.25 (s, 1H), 7.83 (dt, *J* = 7.8, 3.3 Hz, 2H), 7.69 (d, *J* = 8.1 Hz, 1H), 7.57 – 7.50 (m, 2H), 7.49 – 7.37 (m, 2H), 7.31 – 7.22 (m, 2H), 7.12 – 7.03 (m, 2H), 4.21 (s, 2H), .
^{13}C NMR (101 MHz, $CDCl_3$): δ 163.86, 155.13, 154.31, 134.30, 132.22, 130.19, 129.99, 127.77, 127.14, 126.63, 124.80, 122.10, 119.84, 119.76, 113.84, 77.39, 77.07, 76.75, 42.89.
HRMS: (+ESI): calcd. for: $C_{18}H_{15}O_2NCl$ = 312.0786, found: 312.0785

2-chloro-N-(4-(3,5-dimethylphenoxy)phenyl)acetamide (CCW 8)

To a solution of 4-(3,5-dimethylphenoxy)aniline (Enamine, 107 mg, 0.50 mmol) in DCM 2-chloroacetyl chloride (Sigma, 67.8 mg, 0.60 mmol) and triethylamine (Sigma, 60.8 mg, 0.60 mmol) were added and the reaction stirred overnight. Upon reaction completion the crude was purified by silica gel chromatography (10-40% EtOAc/hexanes) to yield 60 mg (41%).
^{1}H NMR (400 MHz, $CDCl_3$): δ 8.22 (s, 1H), 7.53 – 7.46 (m, 2H), 7.03 – 6.96 (m, 2H), 6.74 (s, 1H), 6.61 (s, 2H), 4.20 (s, 2H), 2.28 (s, 6H).
^{13}C NMR (101 MHz, $CDCl_3$): δ 163.80, 157.21, 154.61, 139.67, 131.79, 125.09, 121.98, 119.55, 116.36, 77.37, 77.06, 76.74, 42.87, 21.33.
HRMS: (+ESI): calcd. for: $C_{18\backslash 6}H_{17}O_2NCl$ = 290.0942, found: 290.0941

N-benzyl-4-(4-methoxyphenoxy)aniline (CCW 14)
4-(4-methoxyphenoxy)aniline (Astatech, 108 mg, 0.50 mmol) was dissolved in anhydrous DCM (5 mL) in a 20 mL scintillation vial. Benzaldehyde (Alfa Aesar, 53 mg, 0.50 mmol) was added and the solution stirred for 2 h under nitrogen. Sodium triacetoxyborohydride (Sigma, 159 mg, 0.75 mmol) was added in small aliquots and the reaction stirred overnight. TLC (20% EtOAc/hexanes) showed full conversion of starting materials. The solution was washed with saturated sodium bicarbonate and, followed by brine. The aqueous fractions were combined, extracted with 3x5 mL EtOAc and all organic fractions combined, concentrated and purified on a silica gel column (10-40% EtOAc/hexanes) to give 89.7 mg (58.8%)
1H NMR (400 MHz, $CDCl_3$): δ 7.42 – 7.33 (m, 4H), 7.32 – 7.27 (m, 1H), 6.94 – 6.81 (m, 6H), 6.64 – 6.59 (m, 2H), 4.31 (s, 2H), 3.79 (s, 3H).
HRMS: (+ESI): calcd. for: $C_{20}H_{20}O_2N_1$ = 306.1489, found: 307.1481.

N-benzyl-2-chloro-N-(4-(4-methoxyphenoxy)phenyl)acetamide (CCW 16)
To a solution of N-benzyl-4-(4-methoxyphenoxy)aniline **(CCW 14)** (25 mg, 0.081 mmol) in DCM 2-chloroacetyl chloride (Sigma, 11 mg, 0.097 mmol) and triethylamine (Sigma, 9.8 mg, 0.097 mmol) were added and the reaction stirred overnight. Upon reaction completion the crude was purified by silica gel chromatography (10-40% EtOAc/hexanes) to yield 26 mg (84%)
^{1}H NMR (400 MHz, $CDCl_3$): δ 7.26 (s, 3H), 7.20 (dd, *J* = 7.3, 2.3 Hz, 2H), 7.01 – 6.96 (m, 2H), 6.93 – 6.82 (m, 6H), 4.86 (s, 2H), 3.87 (s, 2H), 3.81 (s, 3H).
^{13}C NMR (101 MHz, $CDCl_3$): δ 166.45, 158.95, 156.54, 148.89, 136.63, 134.71, 129.54, 129.03, 128.51, 127.71, 121.47, 117.82, 115.07, 77.36, 77.25, 77.05, 76.73, 55.69, 53.85, 42.09.
HRMS: (+ESI): calcd. for: $C_{22}H_{21}O_3NCl$ = 382.1204, found: 307.1199.

2-chloro-N-(4-(4-(hydroxymethyl)phenoxy)phenyl)acetamide (JIK 1-36)
To a solution of (4-(4-aminophenoxy)phenyl)methanol (Sigma, 54.8 mg, 0.25 mmol) in DCM 2-choloracetyl chloride (Sigma, 34 mg, 0.30 mmol) and triethylamine (Sigma, 30.4 mg, 0.30 mmol) were added and the reaction stirred overnight. Upon reaction completion the crude was purified by silica gel chromatography (10-40% EtOAc/hexanes) to yield 55 mg (74%).
^{1}H NMR (400 MHz, $CDCl_3$): δ 8.21 (s, 1H), 7.55 – 7.48 (m, 2H), 7.34 (d, *J* = 8.4 Hz, 2H), 7.05 – 6.96 (m, 4H), 4.67 (s, 2H), 4.20 (s, 2H). ^{13}C NMR (151 MHz, $CDCl_3$) δ 163.70, 156.77, 154.32, 135.82, 132.01, 128.68, 121.93, 119.46, 118.71, 64.85, 42.79.
HRMS: (-ESI): calc'd for $C_{15}H_{10}ClF_3NO_2$ = 328.0352; found 328.0358.

2-chloro-N-(4-(3-(trifluoromethyl)phenoxy)phenyl)acetamide (JIK 1-37)

To a solution of (4-(3-trifluoromethyl)phenyl)aniline (Sigma, 64.5 mg, 0.25 mmol) in DCM 2-choloracetyl chloride (Sigma, 34 mg, 0.30 mmol) and triethylamine (Sigma, 30.4 mg, 0.30 mmol) were added and the reaction stirred overnight. Upon reaction completion the crude was purified by silica gel chromatography (10-40% EtOAc/hexanes) to yield 80 mg (95%).
^{1}H NMR (400 MHz, $CDCl_3$): δ 8.26 (s, 1H), 7.56 (d, *J* = 8.8 Hz, 2H), 7.44 (t, *J* = 7.9 Hz, 1H), 7.34 (d, *J* = 7.7 Hz, 1H), 7.22 (s, 1H), 7.15 (d, *J* = 8.1 Hz, 1H), 7.04 (d, *J* = 8.8 Hz, 2H), 4.21 (s, 2H).^{13}C NMR (151 MHz, $CDCl_3$) δ 163.76, 157.81, 153.12, 132.85, 130.30, 124.51, 122.71, 122.04, 121.31, 120.10, 119.69, 115.02, 42.78.
HRMS: (-ESI): calc'd for $C_{15}H_{13}ClNO_3$ = 290.0585; found 290.0589.

***N*-benzyl-4-(4-(prop-2-yn-1-yloxy)phenoxy)aniline (CCW 35)**
To a stirring solution of 4-(4-(benzylamino)phenoxy)phenol **(CCW 22)** (100 mg, 0.34 mmol) in acetonitrile, propargyl bromide (Sigma, 80% wt. in toluene, 53 mg, 0.45 mmol) and potassium carbonate (142 mg, 1.03 mmol) were added. The reaction was heated to reflux overnight. The reaction was concentrated, redissolved in EtOAc, filtered, and the filtrate purified by silica gel chromatography (10-40% EtOAc/hexanes) to yield 54 mg (47 %).
^{1}H NMR (400 MHz, $CDCl_3$): δ 7.42 – 7.32 (m, 4H), 7.32 – 7.24 (m, 1H), 6.94 – 6.83 (m, 6H), 6.67 – 6.59 (m, 2H), 4.65 (d, *J* = 2.4 Hz, 2H), 4.31 (s, 2H), 2.51 (t, *J* = 2.4 Hz, 1H).
HRMS: (+ESI): calcd. for: $C_{22}H_{20}O_2N$ = 330.1489, found: 330.1489.

***N*-benzyl-2-chloro-*N*-(4-(4-(prop-2-yn-1-yloxy)phenoxy)phenyl)acetamide (CCW 36)**
To a solution of *N*-benzyl-4-(4-(prop-2-yn-1-yloxy)phenoxy)aniline **(CCW 35)** (48 mg, 0.15 mmol) in DCM, 2-choloracetyl chloride (Sigma, 20 mg, 0.18 mmol) and triethylamine (Sigma, 17.7 mg, 0.18 mmol) were added and the reaction stirred overnight. Upon reaction completion the crude was purified by silica gel chromatography (10-40% EtOAc/hexanes) to yield 45 mg (76%).
^{1}H NMR (400 MHz, $CDCl_3$): δ 7.32 – 7.16 (m, 5H), 7.03 – 6.96 (m, 4H), 6.94 – 6.83 (m, 4H), 4.86 (s, 2H), 4.69 (d, *J* = 2.4 Hz, 2H), 3.87 (s, 2H), 2.54 (t, *J* = 2.4 Hz, 1H).
^{13}C NMR (151 MHz, $CDCl_3$): δ 166.38, 158.63, 154.36, 149.71, 136.57, 134.86, 129.54, 128.97, 128.47, 127.67, 121.27, 118.01, 116.27, 78.40, 77.21, 77.00, 76.79, 75.66, 56.30, 53.79, 42.01.
HRMS: (+ESI): calcd. for: $C_{24}H_{21}O_3NCl$ = 406.1204, found: 406.1202.

C.1.2 CCW 16 + JQ1 bifunctional degrader synthesis and scheme (CCW 28-3)

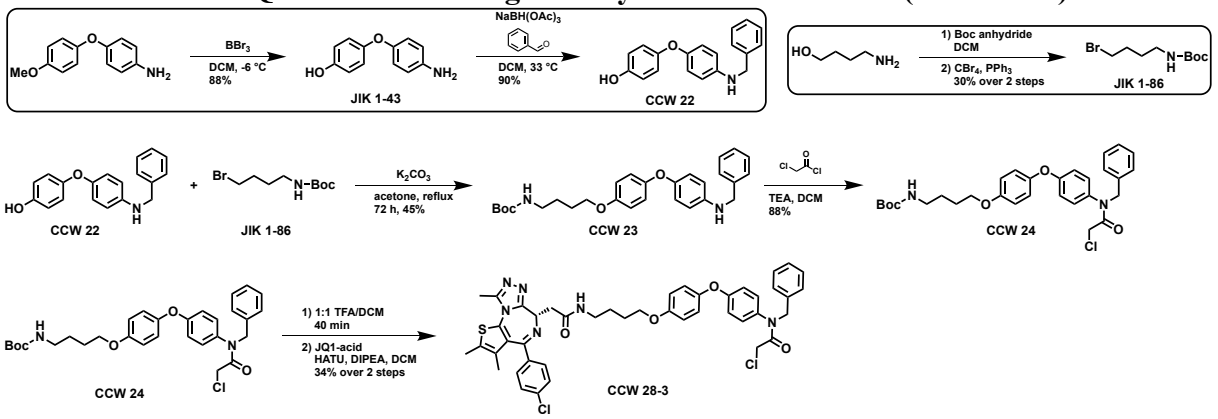

***tert*-butyl (4-bromobutyl)carbamate (JIK 1-86)**
4-amino-1-butanol (TCI; 5.0 g, 56.0 mmol) was dissolved in dry DCM (22mL). To the solution di-tert-butyl dicarbonate (Chem-Impex Int'l Inc.; 17.3 g, 79.4 mmol) was added. The reaction was stirred at room temperature for 3 hours and was monitored by TLC (developed in 100% EtOAc, visualized by ninhydrin). Upon completion, the solvent was removed by rotary evaporation. The crude was partially purified by silica gel chromatography (55 to 100% EtOAc in hexanes) to remove baseline impurity; eluent from column was carried forward to next reaction. DCM (22 mL, dry) was added to column eluent and the solution was cooled to 0°C. To the solution carbon tetrabromide (Aldrich; 23.9 g, 72.0 mmol) was added and dissolved, followed by triphenylphosphine (Sigma Aldrich; 22.3 g, 84.9 mmol). Reaction was stirred for 1hr, then allowed to warm to room temperature and run overnight. After 24 hours, solvent was removed by rotary evaporation. The crude was purified by silica gel chromatography (2-15% EtOAc in hexanes) to afford 4.1 g of product as a pale yellow oil (29.6% yield over two reactions).
^{1}H NMR (400 MHz, $CDCl_3$): δ 4.55 (s, 1H), 3.42 (t, *J* = 6.7 Hz, 2H), 3.15 (q, *J* = 6.8 Hz, 2H), 1.93 – 1.83 (m, 2H), 1.63 (m, 1H), 1.43 (s, 10H).

4-(4-aminophenoxy)phenol (JIK 1-43)
4-(4-methoxyphenoxy)aniline (AstaTech; 2.5g, 11.6 mmol) was dissolved in DCM (40 mL) at -6°C. Boron tribromide (Acros; 34.8 mL, 1M in DCM, 34.8 mmol) was added dropwise over the course of 3 hours, monitored by TLC (40% EtOAc/Hex, $KMnO_4$). Upon completion, solution was quenched with 1 volume of sodium bicarbonate. Biphasic mixture was refrigerated overnight and product crystallized out and was removed by filtration. The aqueous layer was neutralized with NaOH, and back extracted with 3x25mL EtOAc. The combined organic layers were dried with $MgSO_4$ and condensed. Yielded 2.33 g (88%) product as a tan solid which required no further purification.
^{1}H NMR (400 MHz, Methanol-d_4): δ 5.22 – 5.09 (m, 8H), 1.73 (p, *J* = 1.6 Hz, 3H).
HRMS: (+ESI): calc'd for $C_{12}H_{12}NO_2$ = 202.0863; found 202.0860.

4-(4-(benzylamino)phenoxy)phenol (CCW 22)
4-(4-aminophenoxy)phenol **(JIK 1-43)** (604 mg, 3.0 mmol) was dissolved in anhydrous DCM (50mL) at 33 C to aid solubility, benzaldehyde (Alfa Aesar, 240 mg, 3.0 mmol) was added and the reaction stirred for two hours under nitrogen. Sodium triacetoxyborohydride (Sigma, 952 mg, 4.5 mmol) was added and the reaction stirred overnight. The mixture was concentrated and applied directly to a silica column for flash chromatography, yielding 787 mg (90%).
^{1}H NMR (400 MHz, $CDCl_3$): δ 7.41 – 7.24 (m, 5H), 6.89 – 6.80 (m, 4H), 6.78 – 6.71 (m, 2H), 6.65 – 6.58 (m, 2H), 4.31 (s, 2H).

tert-butyl (4-(4-(4-(benzylamino)phenoxy)phenoxy)butyl)carbamate (CCW 23)
4-(4-(benzylamino)phenoxy)phenol **(CCW 22)** (450 mg, 1.55 mmol) and *tert*-butyl (4-bromobutyl)carbamate **(JIK 1-86)** (585 mg, 2.32 mmol) were dissolved in acetone (20 mL). Potassium carbonate (642 mg, 4.65 mmol) was added and the solution brought to reflux and stirred for 72 h. The mixture was concentrated and applied directly to a silica column for flash chromatography (10-30 % EtOAc/hexanes), yielding 325 mg (45.3%)

^{1}H NMR (400 MHz, $CDCl_3$): δ 7.41 – 7.27 (m, 5H), 6.91 – 6.77 (m, 6H), 6.60 (d, J = 8.8 Hz, 2H), 4.62 (s, 1H), 4.30 (s, 2H), 3.93 (t, J = 6.2 Hz, 2H), 3.19 (q, J = 6.4 Hz, 2H), 1.83 – 1.74 (m, 2H), 1.66 (p, J = 7.1 Hz, 2H), 1.44 (s, 9H).
HRMS: (+ESI): calc'd for $C_{28}H_{35}O_4N_2$ = 463.2591; found 462.2583.

tert-butyl (4-(4-(4-(N-benzyl-2-chloroacetamido)phenoxy)phenoxy)butyl)carbamate (CCW 24)
To a solution of **CCW 23** (200 mg, 0.43 mmol) in DCM (10 mL). 2-choloracetyl chloride (Sigma, 59 mg, 0.52 mmol) and triethylamine (Sigma, 53 mg, 0.52 mmol) were added and the reaction stirred overnight. Upon reaction completion the crude was purified by silica gel chromatography (20-60% EtOAc/hexanes) to yield 232 mg (87.6%).
^{1}H NMR (400 MHz, $CDCl_3$): δ 7.29 (d, *J* = 4.8 Hz, 2H), 7.20 (dd, *J* = 7.2, 2.2 Hz, 3H), 6.97 (d, *J* = 9.0 Hz, 2H), 6.93 – 6.83 (m, 6H), 4.86 (s, 2H), 4.61 (s, 1H), 3.96 (t, *J* = 6.2 Hz, 2H), 3.87 (s, 2H), 3.20 (q, *J* = 6.4 Hz, 2H), 1.87 – 1.77 (m, 2H), 1.68 (p, *J* = 7.1 Hz, 2H), 1.45 (s, 9H).

(S)-2-(4-(4-chlorophenyl)-2,3,9-trimethyl-6H-thieno[3,2-f][1,2,4]triazolo[4,3-a][1,4]diazepin-6-yl)acetic acid (JQ1-acid)
tert-butyl (S)-2-(4-(4-chlorophenyl)-2,3,9-trimethyl-6H-thieno[3,2-f][1,2,4]triazolo[4,3-a][1,4]diazepin-6-yl)acetate (**JQ1**) was prepared based on previous procedures [1]. JQ1 (eNovation Chemicals, 204 mg, 0.446 mmol) was dissolved in formic acid (3mL) and stirred at 45 °C overnight. The mixture was diluted with DCM and solvent removed *in vacuo.* The resulting yellow oil was redissolved in 3 mL DCL and evaporated to dryness repeated until the process gave a fine yellow-brown solid: 178 mg (99.8%). No further purification was necessary.
1H NMR (400 MHz, $CDCl_3$): δ 7.46 – 7.40 (m, 2H), 7.34 (d, J = 8.7 Hz, 2H), 4.59 (t, J = 6.8 Hz, 1H), 3.75 – 3.55 (m, 2H), 2.68 (s, 3H), 2.41 (s, 3H), 1.74 – 1.65 (m, 3H).
HRMS: (-ESI): calcd. for $C_{19}H_{16}O_2N_4ClS$ = 399.0688; found 399.0683.

(S)-N-benzyl-2-chloro-N-(4-(4-(4-(2-(4-(4-chlorophenyl)-2,3,9-trimethyl-6H-thieno[3,2-f][1,2,4]triazolo[4,3-a][1,4]diazepin-6-yl)acetamido)butoxy)phenoxy)phenyl)acetamide (CCW-28-3)
CCW 24 (175 mg, 0.325 mmol) was deprotected in 1:1 DCM/TFA (5mL) by adding trifluoroacetic acid (Sigma-Aldrich) slowly over 20 min followed by stirring for an additional 20 min. TLC showed full conversion to amine and the solvent was removed *in vacuo,* and chases three times with 3mL DCM to remove excess TFA. The deprotected crude was used without further purification for amide coupling.
The resulting TFA salt was dissolved in 8 mL DCM, **JQ1-acid** (180 mg, 0.390 mmol), 1-[Bis(dimethylamino)methylene]-1H-1,2,3-triazolo[4,5-b]pyridinium 3-oxid hexafluorophosphate (HATU) (Small Molecules Inc., 201.5 mg, 0.530 mmol), and N,N-Diisopropylethylamine (DIPEA) (Sigma-Aldrich, 168 mg, 1.30 mmol). Stirred overnight and monitored by TLC (5% MeOH in DCM, 100% EtOAc). Crude concentrated and applied direct to a silica column for flash chromatography (1-5% MeOH/DCM). The eluted fractions were insufficiently pure and those containing product were combined, concentrated and purified again by flash silica chromatography (100-0% EtOAc/DCM followed by 0-5% MeOH/DCM) to afford 91.4 mg (34.2%).
^{1}H NMR (600 MHz, $CDCl_3$): δ 7.36 (dd, *J* = 50.3, 8.3 Hz, 4H), 7.26 (s, 2H), 7.22 – 7.18 (m, 2H), 6.99 – 6.95 (m, 2H), 6.92 – 6.83 (m, 6H), 6.59 (d, *J* = 6.1 Hz, 1H), 4.86 (s, 2H), 4.62 (dd, *J*

= 7.9, 6.1 Hz, 1H), 3.96 (t, *J* = 6.2 Hz, 2H), 3.87 (s, 2H), 3.57 (dd, *J* = 14.1, 7.9 Hz, 1H), 3.42 (dq, *J* = 13.3, 6.7 Hz, 1H), 3.32 (ddd, *J* = 13.2, 11.4, 6.2 Hz, 2H), 2.67 (s, 3H), 2.40 (s, 3H), 1.82 (td, *J* = 13.8, 13.2, 6.9 Hz, 2H), 1.74 (p, *J* = 6.8 Hz, 2H), 1.67 (s, 3H).
^{13}C NMR (151 MHz, $CDCl_3$): δ 170.46, 166.38, 163.87, 158.90, 155.84, 155.63, 149.84, 148.82, 136.79, 136.58, 136.56, 134.65, 132.10, 130.87, 130.82, 130.42, 129.76, 129.46, 128.97, 128.69, 128.44, 127.63, 121.39, 117.78, 115.64, 67.84, 54.53, 53.78, 42.01, 39.60, 39.20, 29.65, 26.59, 26.26, 14.32, 13.04, 11.78.
HRMS: (+ESI): calcd. for $C_{44}H_{43}Cl_2N_6O_4S$ = 821.2438; found 821.2426.

Supporting References

1) Zengerle, M.; Chan, K.-H.; Ciulli, A. Selective Small Molecule Induced Degradation of the BET Bromodomain Protein BRD4. *ACS Chem. Biol.* **2015**, *10* (8), 1770–1777

C.2 Supplemental Tables

Please see supporting data for full tables **C.2.2, C.2.3**

Table C.2.1.

Structures of covalent ligands screened against RNF4

Name	Compound Structure	Name	Compound Structure
DKM 2-31		DKM 3-41	
DKM 2-32		DKM 3-42	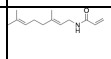
DKM 2-33		DKM 3-43	
DKM 2-34		DKM 3-70	
DKM 2-37	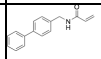	TRH 1-12	
DKM 2-39		TRH 1-13	
DKM 2-40		TRH 1-17	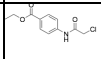
DKM 2-42		TRH 1-19	
DKM 2-43		TRH 1-20	
DKM 2-47		TRH 1-23	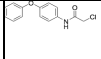
DKM 2-48		TRH 1-27	
DKM 2-49		TRH 1-32	
DKM 2-50		TRH 1-50	
DKM 2-52		TRH 1-51	
DKM 2-58		TRH 1-53	
DKM 2-59		TRH 1-54	
DKM 2-60		TRH 1-55	
DKM 2-62		TRH 1-56	
DKM 2-67		TRH 1-57	
DKM 2-71		TRH 1-58	
DKM 2-72		TRH 1-59	
DKM 2-76		TRH 1-60	
DKM 2-79		TRH 1-65	
DKM 2-80		TRH 1-68	
DKM 2-83		TRH 1-70	
DKM 2-84		TRH 1-74	
DKM 2-85		TRH 1-149	
DKM 2-86		YP 1-26	
DKM 2-87		TRH 1-115	
DKM 2-90		TRH 1-129	
DKM 2-91		IGA 1-12	
DKM 2-93		IGA 1-14	
DKM 2-94		IGA 1-15	
DKM 2-95	(Two rotamers in equal amounts)	TRH 1-143	
DKM 2-97		TRH 1-145	
DKM 2-98		YP 1-1	
DKM 2-100		YP 1-16	
DKM 2-101		YP 1-18	
DKM 2-102		YP1-19	
DKM 2-103		IGA 1-26	
DKM 2-106		YP 1-22	
DKM 2-107		YP 1-23	
DKM 2-108		YP 1-24	
DKM 2-109		YP 1-25	

DKM 2-110		TRH 1-152	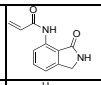
DKM 2-111		TRH 1-156	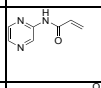
DKM 2-113		TRH 1-160	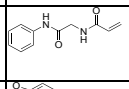
DKM 2-114		TRH 1-78	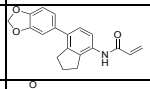
DKM 2-116		TRH 1-133	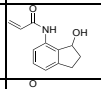
DKM 2-117	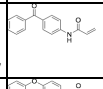	TRH 1-134	
DKM 2-119	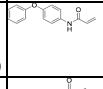	TRH 1-135	
DKM 2-120		TRH 1-155	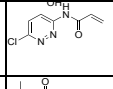
DKM 3-3	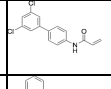	TRH 1-167	
DKM 3-4		YP 1-36	
DKM 3-5		TRH 1-170	
DKM 3-7		TRH 1-176	
DKM 3-8		YP 1-38	
DKM 3-9		TRH 1-162	
DKM 3-10		TRH 1-178	
DKM 3-11		YP 1-42	
DKM 3-12		YP 1-44	
DKM 3-13		TRH 1-140	
DKM 3-15		YP 1-31	
DKM 3-16		TRH 1-163	
DKM 3-22		TRH 1-168	
DKM 3-29		TRH 1-171	

DKM 3-30		YP 1-37	
DKM 3-31		TRH 1-177	
DKM 3-32		YP 1-39	
DKM 3-36		TRH 1-179	
		YP 1-40	

Table C.2.2.
TMT-based quantitative proteomic analysis of CCW 28-3 in 231MFP breast cancer cells *in situ*. 231MFP cells were treated with DMSO vehicle or CCW 28-3 (1 μM) *in situ* for 3 h, and proteomes were subjected to TMT-based quantitative proteomic analysis to determine changes in protein expression. Data in table show proteins identified and quantified in TMT proteomic experiments and the CCW 28-3/DMSO ratios. Data is from 3 biological replicates.

Table C.2.3.
IsoTOP-ABPP analysis of CCW 28-3 in 231MFP breast cancer cells *in situ*. 231MFP cells were treated with DMSO vehicle or CCW 28-3 (10 μM) *in situ* for 1 h prior to labeling of proteomes *in vitro* with IA-alkyne (100 μM) for 1h. Isotopically light (for DMSO-treated) or heavy (for compound-treated) TEV protease-cleavable biotin-azide tag were appended by CuAAC for isoTOP-ABPP analysis. Only probe-modified peptides that were present in two out of three biological replicates were interpreted. For those ratios >3, we only interpreted those peptides that were present in all biological replicates where all replicate ratios were >3. For those ratios >4, we only interpreted those peptides that were present in all biological replicates where all replicate ratios were >4. MS1 peak shape qualities were manually curated to confirm good peak quality for all replicates. Data in table shows probe-modified peptide identified, the site of modification, the light to heavy probe-modified peptide ratio, and the protein identification. Data is from 3 biological replicates.

C.3 Supplemental Figures

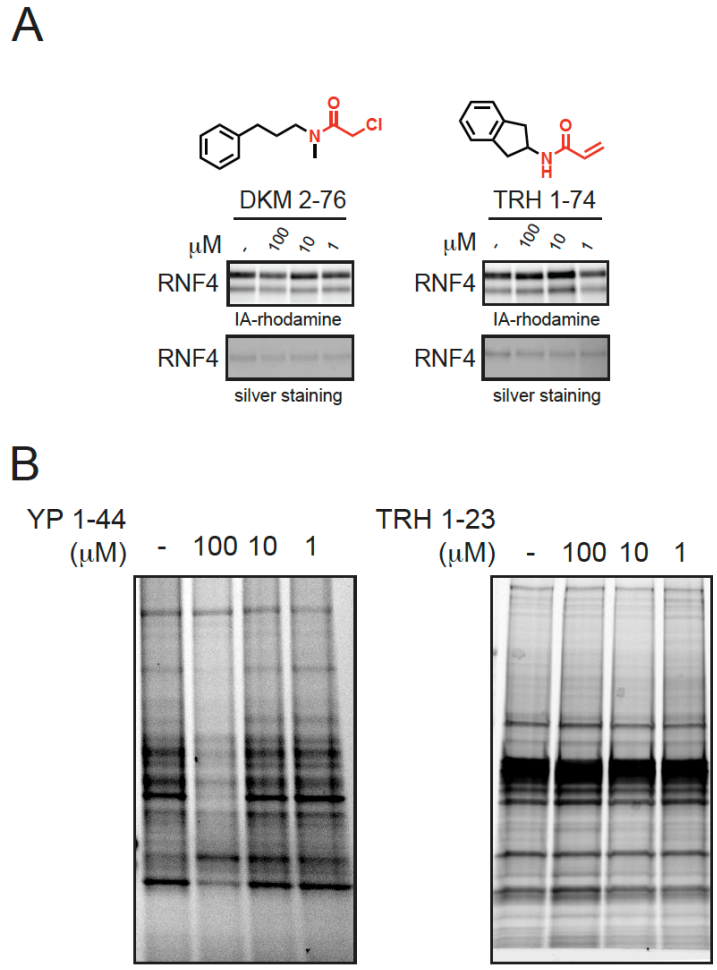

Figure C.3.1. Non-reproducible hits against RNF4 and general assessment of proteome-wide selectivity of RNF4 hits by gel-based ABPP. **(A)** Gel-based ABPP analysis of DKM 2-76 and TRH 1-74 against IA-rhodamine labeling of RNF4. Covalent ligands were pre-incubated with pure RNF4 protein for 30 min prior to IA-rhodamine labeling (250 nM) for 1 h. Proteins were subjected to SDS/PAGE and visualized by in-gel fluorescence. **(B)** Gel-based ABPP screen of RNF4 hits YP 1-44 and TRH 1-23 against IA-rhodamine labeling in 231MFP breast cancer cell proteomes. YP 1-44 and TRH 1-23 were pre-incubated with proteome for 30 min prior to IA-rhodamine labeling (250 nM) for 1 h. Proteins were subjected to SDS/PAGE and visualized by in-gel fluorescence.

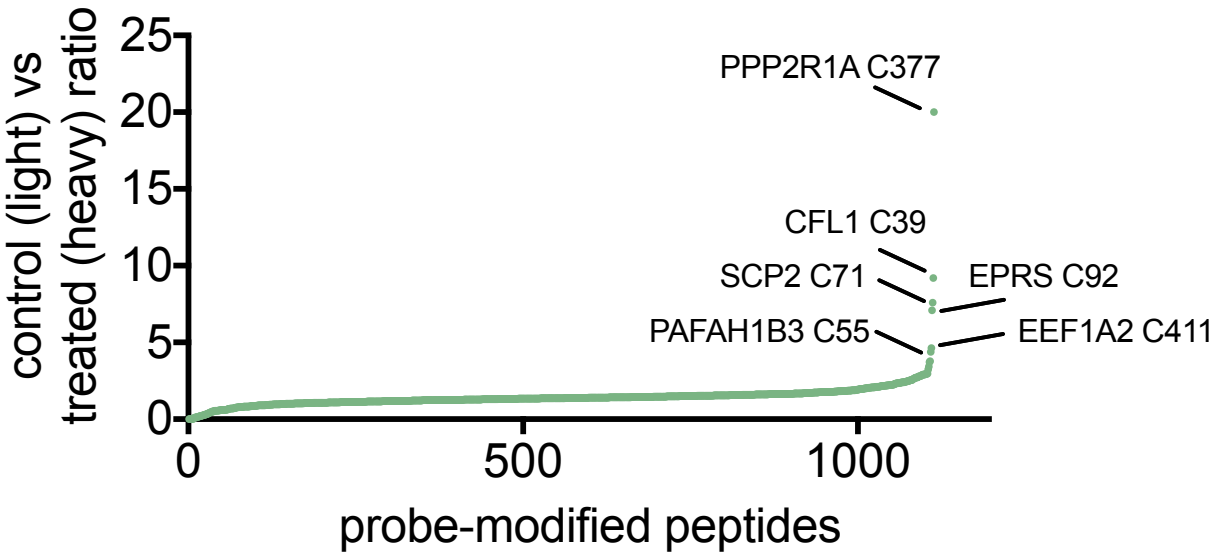

Figure C.3.2. isoTOP-ABPP analysis of CCW 28-3 in 231MFP breast cancer cells *in situ*. 231MFP cells were treated with DMSO vehicle or CCW 28-3 (10 μM) *in situ* for 1 h prior to labeling of proteomes *in vitro* with IA-alkyne (100 μM) for 1h. Isotopically light (for DMSO-treated) or heavy (for compound-treated) TEV protease-cleavable biotin-azide tag were appended by CuAAC for isoTOP-ABPP analysis. Data is for three biological replicates. Raw proteomic data is in **Table C.2.3**.

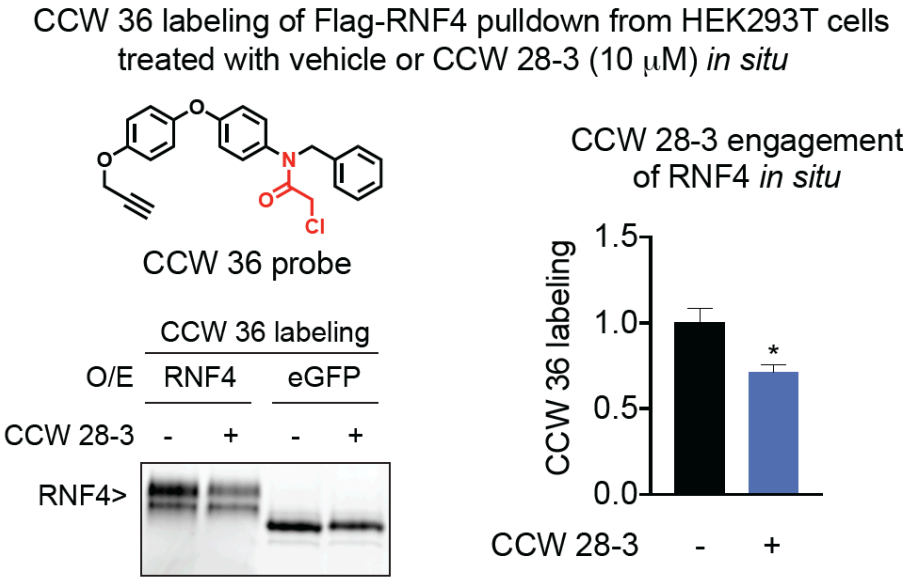

Figure C.3.3. Degree of CCW 28-3 engagement of RNF4 *in situ* in HEK293T cells. HEK293T cells were transiently transfected with a Flag-tagged GFP (eGFP) or a Flag-tagged RNF4 and treated with DMSO vehicle or CCW 28-3 (10 μM) for 1.5 h after which cells were harvested and eGFP and RNF4 were pulled down with anti-Flag beads after which pulled down proteins were labeled with CCW 36 (1 μM), an alkyne functionalized probe based on CCW 16, for 30 min, followed by appendage of rhodamine-azide by CuAAC. Resulting reactions were subjected to SDS/PAGE and in-gel fluorescence. In-gel fluorescence was quantified, normalized to the respective eGFP groups and normalized to the vehicle-treated control. Gel shown is a representative of n=3. Bar graphs are average ± sem, n=3/group. Significance is expressed as *$p<0.05$ compared to vehicle-treated controls.

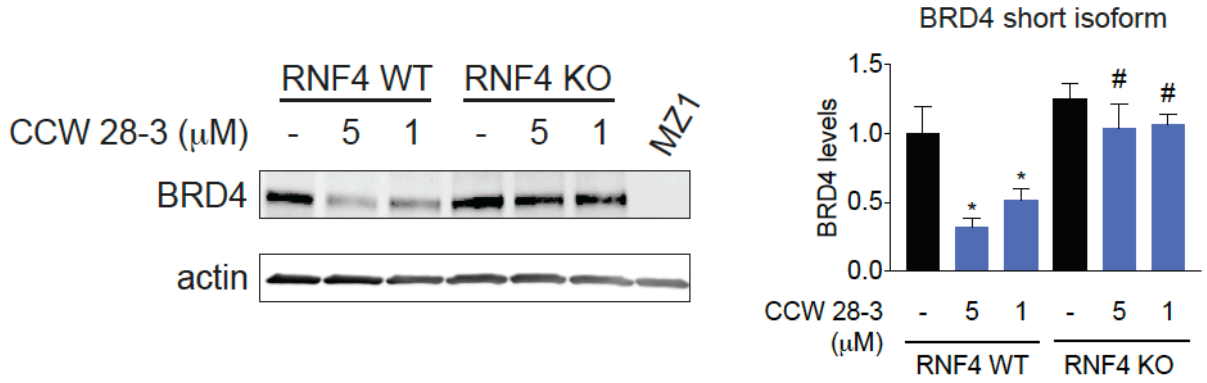

Figure C.3.4. CCW 28-3 tested at lower concentrations in RNF4 wild-type and knockout Hela cells. RNF4 wild-type and knockout Hela cells were treated with DMSO vehicle or CCW 28-3 (5 or 1 μM) for 5 h and subjected to SDS/PAGE and Western blotting for BRD4 and GAPDH. Blots were quantified by densitometry. Data in are from representative gels from n=3. Bar graphs are average ± sem, n=3/group. Significance is expressed as *$p<0.05$ compared to vehicle-treated controls and #$p<0.05$ compared to CCW 28-3 treated wild-type cells.